Thermal behavior of submicrometer spherical particle formation by pulsed laser melting in liquid

Shota SAKAKI

2019

Thermal behavior of submicrometer spherical particle formation by pulsed laser melting in liquid

Shota SAKAKI

Division of Quantum Science and Engineering

Graduate School of Engineering

Hokkaido University

March 2019

Contents

Chapter 1

General Introduction

1. Laser Processing in Liquids

Over the past few decades, nanotechnology and nanoscience and their application in almost every field related to industry have rapidly advanced.[1–4] Both chemical and physical nanoparticle synthesis techniques have been studied because of the global demand for diverse nanoparticles. Chemical synthesis of nanoparticles, however, always requires extra procedures to eliminate excess surfactants and residual reactants and ultimately obtain stable and pure nanoparticles. Laser processing in liquids is a convenient and scalable physical method for synthesizing various ligand-free, stable, and pure nanoparticles of versatile materials.

In pulsed laser ablation in liquids (PLAL), nanoparticles are formed through an explosive interaction caused by high-energy-density laser irradiation onto a bulk target in liquid (Figure 1. 1).[5–9] When a laser pulse with an intense energy interacts with a target in a liquid, plasma is generated on the target surface.[10–12] This plasma contains ionic and atomic species originating from the materials in the target.[13] The duration of the plasma generation is in the range of nanoseconds to microseconds, depending on the surrounding environment and laser parameters.[14, 15] The cavitation bubble forms a sharp quasi-hemispherical phase boundary in the liquid. Soon after, this cavitation bubble undergoes periodic evolution of further expansion and shrinkage until its collapse, which can last from microseconds to milliseconds.[10–12] The condensation of a cluster from vaporized material in a specific environment of PLAL is thought to be the main nanoparticle formation mechanism.[16]

Nanoparticles synthesized by PLAL are fascinating materials for various applications.[17–22] A variety of size-controlled nanoparticles with high purity and a unique surface chemistry, both of which are properties highly relevant for industrial applications, is synthesized by PLAL. Upscaling PLAL

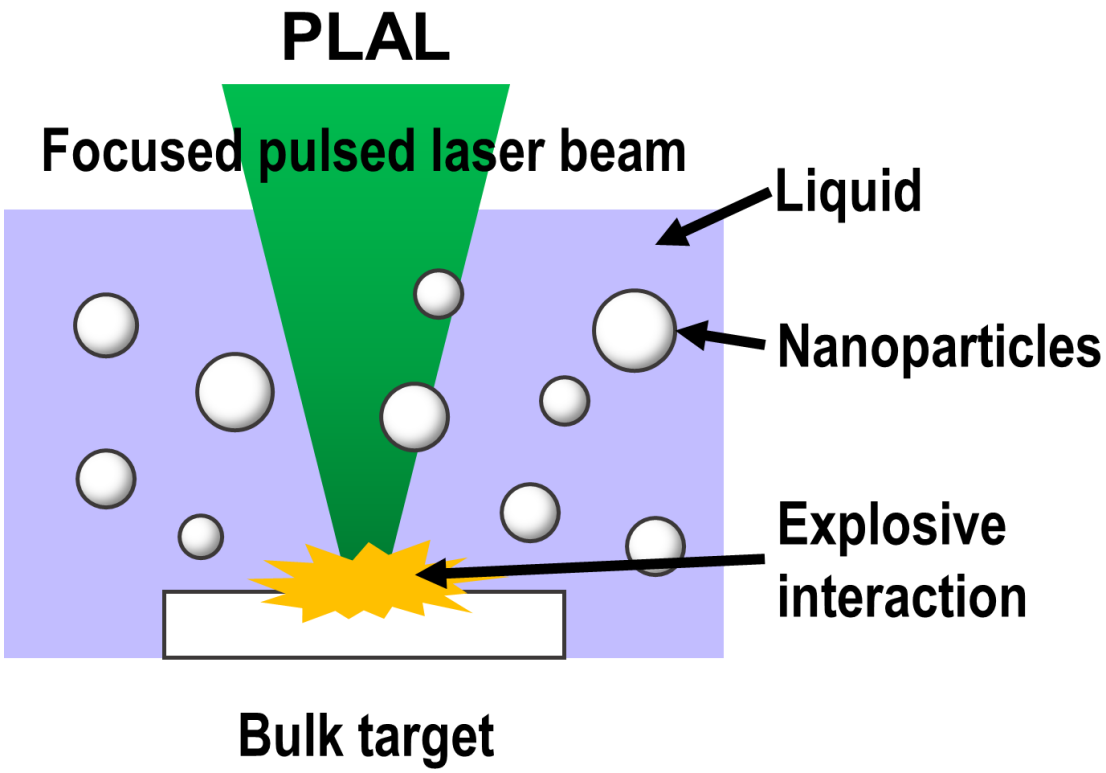

Figure 1. 1. Schematic drawing of nanoparticle synthesis by PLAL.

nanoparticle synthesis to the production of multiple grams per hour is essential for many applications. Recently, a model has been developed by Intartaglia et al. to predict productivity on the basis of ablation.[23] This model assumed that the ablation efficiency was proportional to the laser energy. Utilizing a novel laser system consisting of a 500 W, 10 MHz, 3 ps laser source that was fully synchronized with a polygon scanner reaching scanning speeds up to 500 m s^{-1}, Streubel et al. explored different strategies to increase the productivity of PLAL nanoparticle synthesis.[24] By employing a high scanning speed, laser-induced cavitation bubbles were spatially bypassed at high repetition rates, and continuous multigram ablation rates up to 4 g h^{-1} were demonstrated.[24]

2. Pulsed Laser Melting in Liquids (PLML)

Submicrometer spherical particles have been synthesized by subjecting raw colloidal nanoparticles dispersed in a liquid medium to pulsed laser irradiation (Figure 1. 2).[25–29] Referred to as PLML, in this process, raw nanoparticles are selectively heated to a temperature above the melting point and then melted by unfocused pulsed laser irradiation (Figure 1. 3). Raw nanoparticles are generally aggregated in liquid, and the aggregates merge into large submicrometer droplets. Subsequently, the formed droplets are quenched by the surrounding liquid to become nonporous, highly crystalline, submicrometer spherical particles. Using this technique, submicrometer spherical particles can be fabricated for various materials such as metals,[30, 31] oxides,[25] semiconductors,[32] and carbides.[33]

The particles obtained by PLML are unique in that they are spherical and crystalline.[34] These two features are generally incompatible because crystalline particles usually form a polyhedral shape with stable low-indexed crystalline faces. Submicrometer spherical particles used in commercial applications are limited to amorphous particles made of glass or polymer. Therefore, the material versatility of the particles obtained by PLML is an important advantage over other particle fabrication processes. In addition, submicrometer spherical particles synthesized by PLML are nonporous, which is not observed in spherical particles obtained by chemical methods. Furthermore, bimetallic alloy submicrometer spherical particles, which are

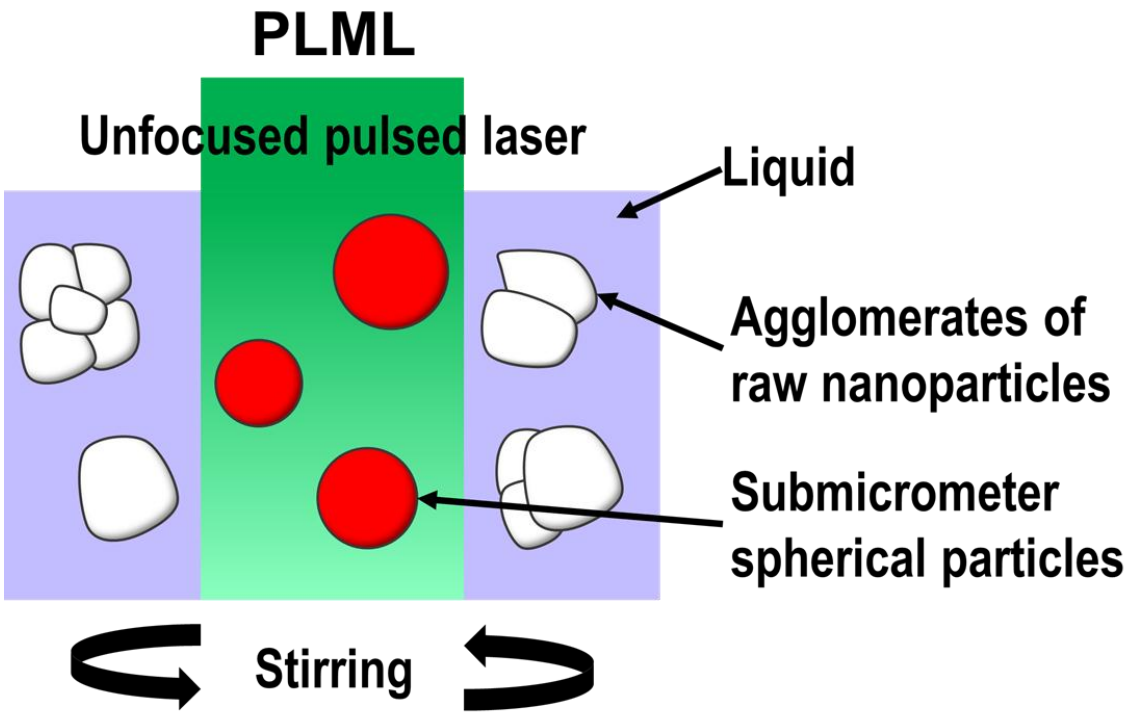

Figure 1. 2. Schematic drawing of the synthesis of submicrometer spherical particles by PLML.

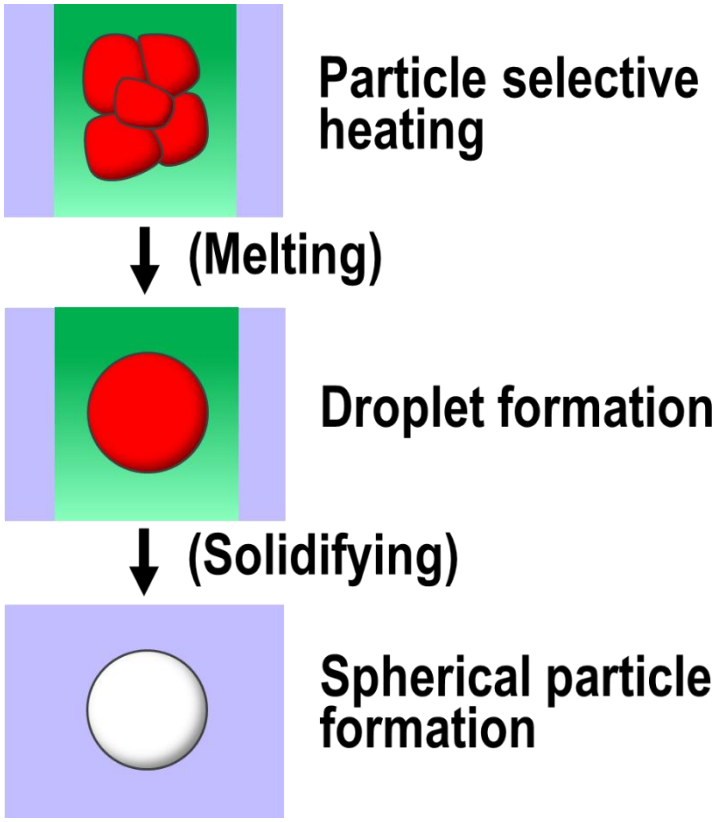

Figure 1. 3. Illustration of the formation of submicrometer spherical particles by PLML.

immiscible under equilibrium, can be formed by PLML.[35] The rapid cooling process of PLML leads to the formation of particles with unique features, such as submicrometer size, spherical shape, crystalline structure, nonporous nature, and nonequilibrium alloy phase.

In previous work, it was shown that the particle heating–melting–evaporation model can be successfully applied for many phenomena arising when colloidal nanoparticles interact with pulsed laser beams.[25–27] This model consists of two energy terms: (1) light energy absorbed by a particle and (2) thermal energy that induces phase transitions of a specific material. By equating these two terms (i.e., no heat loss), curves indicating the required laser fluence to induce the phase transition of a spherical particle versus particle diameter can be calculated. Despite the model's simplicity, the resulting phase diagram explains the size of the submicrometer spherical particles synthesized by PLML (Figure 1. 4).

3. Applications of Submicrometer Spherical Particles

In light of their unique features, various applications of nonporous crystalline submicrometer spherical particles have already been proposed and validated. In particular, optical applications of particles with sizes equivalent to the optical wavelength have been widely investigated, aiming for effective back reflectors in solar cells and for random lasing.[36, 37] In addition, the nonporous nature of these particles also leads to improved mechanical properties.[38, 39] Submicrometer spherical particles with high crystallinity are used in bulk materials such as lubricant oil additives to reduce the friction coefficient.[40] Such utilization of submicrometer spherical particles in bulk materials contributes to the miniaturization and weight lightening of devices.

Based on the results of fracture tests on various submicrometer spherical particles under applied compressive force, the fracture strength of the submicrometer spherical particles was found to be larger than that of the bulk material reported in the literature by about one order of magnitude.[41] Due to the single crystallinity of the particles, smaller particles have a higher fracture strength, exhibiting up to 10–40% of the calculated ideal tensile fracture strength based on the density functional theory. These results

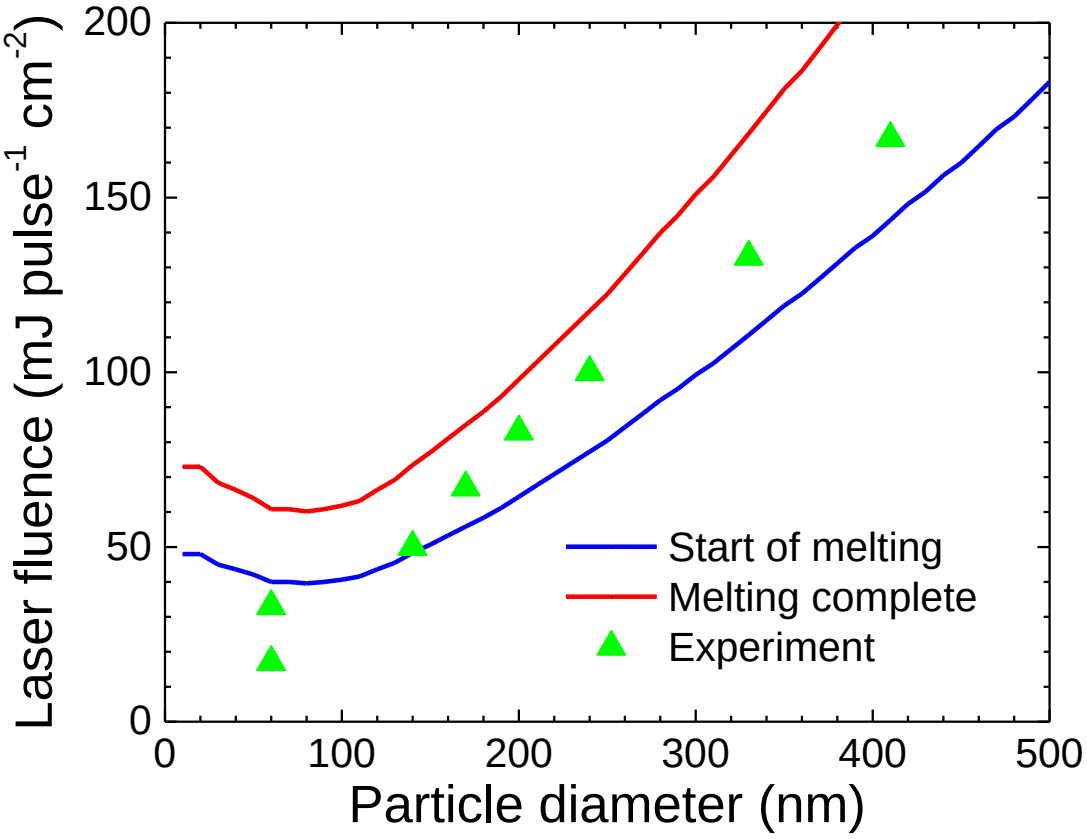

Figure 1. 4. Experimental results versus the phase diagram calculated using the particle heating–melting–evaporation model for ZnO spherical particles.

demonstrate that the particles have a high mechanical strength and, therefore, are promising for mechanical applications at the submicrometer length scale.

The synthesis of submicrometer spherical particles is difficult in both top-down approaches such as grinding techniques and bottom-up approaches such as chemical methods (Figure 1. 5). Recently, submicrometer particles were gradually synthesized by a top-down method based on an advanced grinding technique. However, the submicrometer particles synthesized by grinding often have an angular shape and an active surface caused by mechanical crashing. Particles synthesized by chemical approaches are generally below the submicrometer scale because conventional chemical synthesis methods involve or are based on a precursor reaction or ligand exchange, thus resulting in the formation of nanoparticles. PLML is an effective approach to obtain high-quality submicrometer spherical particles.

In order to fully exploit the unique features of PLML-fabricated particles (crystalline and spherical) in practice, a mass-production PLML technique is required. In previous PLML particle synthesis for batch-type irradiation, the production rate reached 7 mg h^{-1} under typical conditions.[42)] In order to achieve a high spheroidizing ratio of irradiated particles in the vessel, the PLML batch process requires a long irradiation time to compensate the extinction of suspended particles. Thus, to ensure that all particles suspended in the batch vessel are converted into spherical particles, the liquid in the vessel must be irradiated by an excessive number of laser pulses. By adopting the slit nozzle system that supports a continuous liquid film flow,, Ishikawa et al. improved the production rate of submicrometer spherical particles, achieving up to 195 mg h^{-1} using the same typical laser system.[43)] In order to further increase the production rate, employing a high-power laser source, which generally exhibits a high repetition rate, would be an effective approach.[24)]

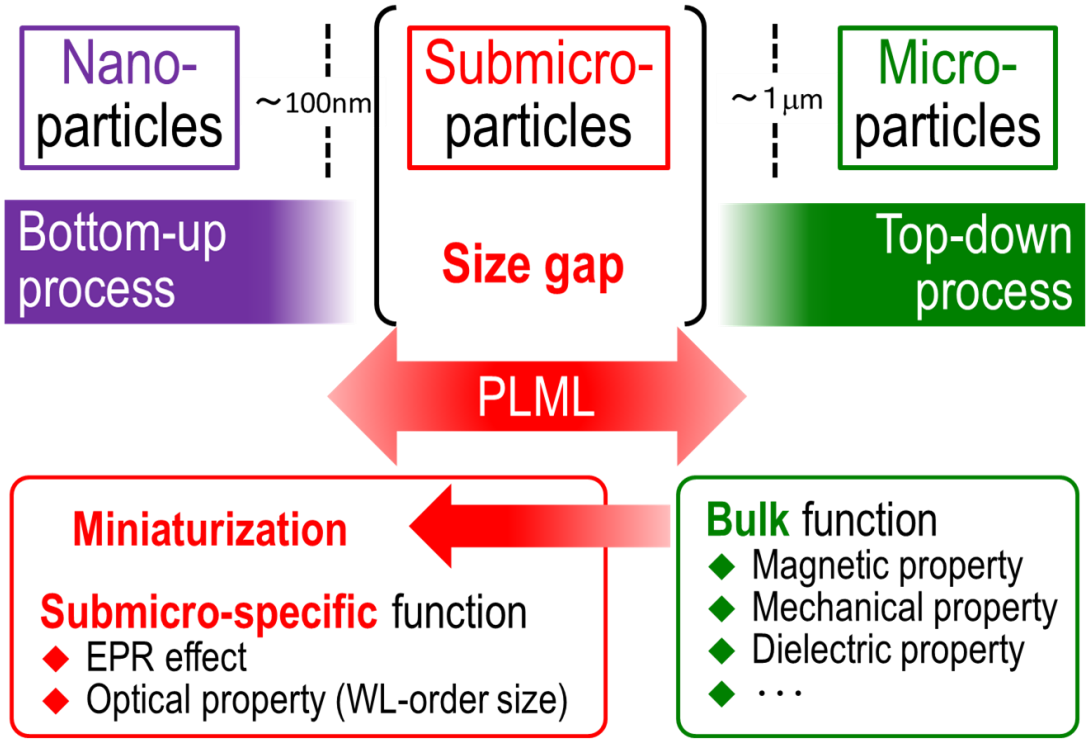

Figure 1. 5. Flowchart showing how PLML is situated among the synthesis processes for different-sized particles (top row) and the function of submicrometer spherical particles obtained by PLML (bottom row).

4. Thermal Behavior during Submicrometer Spherical Particles' Formation

The rapid cooling process of PLML is a significant factor in forming crystalline and spherical particles. These two features of the products are generally incompatible because crystalline particles are expected to be faceted (i.e., featuring a polyhedral shape with stable, low-indexed, crystal faces). The PLML cooling process is one of the fastest in thermal processing of materials because the specific surface area of submicrometer spherical particles is far larger than that of bulk materials.[27, 44)] It enables the formation of unique crystalline and spherical particles. The instantaneous heating process of PLML also has a significant effect on particle melting in liquids. Heat loss during PLML has been considered to be negligible because the heating rate by pulsed laser irradiation is much faster than the cooling rate.[26)] If the heating rate of particles irradiated with pulsed laser does not sufficiently exceed the cooling rate, the particles in the liquid will be poorly heated because nearly all heat energy would dissipate to the surrounding liquid from the particles during pulsed laser heating. Therefore, the heating rate of the particle, which depends on the pulse width of the pulsed laser, influences the formation of submicrometer spherical particles.

Submicrometer spherical particles interact strongly with light when the optical wavelength is close to the size of the particles.[36)] Depending on the optical properties of the material, the submicrometer particles absorb laser energy inhomogeneously.[45] In PLML, a homogeneous distribution of heat energy within the spherical particles is assumed because heat diffusion in the solid-state particle is much faster than heat transfer to the surrounding liquid from the particle. However, time is required to homogenize the heat distribution within the particle. Inhomogeneous heating leads to partial melting, evaporation, and ablation of the particle. Therefore, the heating duration during pulsed laser heating is important in synthesizing uniform and stable submicrometer spherical particles.

5. Outline of This Study

In PLML, the entire particle in the liquid is melted within a nanosecond-

scale heating and cooling process, resulting in submicrometer spherical particles. In order to form a submicrometer spherical particle via pulsed laser irradiation in a liquid, the laser fluence must be larger than the threshold for particle melting, but smaller than the threshold for laser ablation. When the laser fluence exceeds the threshold for laser ablation, nanoparticles are formed because of an explosive interaction between the particles and laser light. Therefore, the temperature of the whole particle is in the range of particle melting in the complicated nanosecond-scale heating and cooling process during the PLML synthesis of submicrometer spherical particles. However, the time evolution of the heating and cooling process during particle formation has never been considered in previous work. In this dissertation, the time-resolved thermal behavior of the submicrometer spherical particle formation is studied. The balance between the thermal diffusion within the particle and the thermal dissipation to the surrounding liquid from the particle should be considered to understand the particle formation mechanism.

In Chapter 2, submicrometer spherical particles are synthesized in a liquid using several tens of nanoseconds long laser pulses, and the particle temperature profile is calculated; the results are analyzed in terms of particle cooling. The experimental and computational results show that the heat energy of the particle is dissipated to the surrounding liquid by particle cooling, even during pulsed laser heating. Consequently, the authors reveal the submicrometer spherical particle formation conditions and mechanism for nanosecond- and nanometer-scale particle cooling in a liquid.

In Chapter 3, submicrometer spherical particles are fabricated via both picosecond and nanosecond laser irradiation under similar conditions to study the effect of picosecond laser irradiation. The laser fluence required for fabricating the submicrometer-size spherical particles by irradiation with a picosecond laser is lower than that with a nanosecond laser. This result suggests that the energy loss from the particles is lower for shorter laser pulse durations. Therefore, picosecond laser irradiation is an energy-efficient method for fabrication. Furthermore, the sizes of the obtained particles decrease as the pulse width decreases, which can be attributed to the decrease in the thermal diffusion length within the particle. This result suggests the possibility of size control of the submicrometer spherical particles by tuning the pulse width.

In Chapter 4, submicrometer spherical particles are synthesized by pulsed laser irradiation at a high pulse frequency. At 200 Hz or lower, laser irradiation at higher pulse frequencies is effective in reducing the irradiation time to treat almost all particles in the liquid. In comparison, at frequencies of 400 Hz or higher, nanoscale spherical particles form and the mass fraction of submicrometer spherical particles drastically decreases. This result suggests that consecutive laser pulse irradiation at 400 Hz or higher induces heat accumulation in the particles and suspension, thus resulting in further heating of the particles.

In Chapter 5, a burst-mode laser is used to control the increase in temperature of the particles irradiated with a picosecond pulsed laser by manipulating the burst pulse. Particles subjected to picosecond laser irradiation tend to be inhomogeneously heated. If the thermal diffusion length in the particles during ultrafast laser heating is smaller than the particle size, the inhomogeneous heating effect will form nanoparticles as a byproduct. Therefore, laser irradiation operated in burst mode is required to control the particle heating process to suppress byproduct formation through partial evaporation so that the synthesis of submicrometer spherical particles using a high-power, ultrafast laser system is enabled. Fewer nanoparticle byproducts form as the number of burst pulses is increased because the heat distribution within the particle is homogenized during the burst-pulse interval. Burst-pulse heating suppresses inhomogeneous particle heating and particle evaporation induced byproduct formation.

In Chapter 6, general conclusions are presented. The thermal diffusion within the particle and the thermal dissipation to the surrounding liquid from the particles on the picosecond to nanosecond timescales are summarized.

References

[1] J. Lee, S. Mahendra, and P. J. J. Alvarez, ACS Nano **4**, 3580 (2010).

[2] Z. Yang, J. Ren, Z. Zhang, X. Chen, G. Guan, L. Qiu, Y. Zhang, and H Peng, Chem. Rev. **115**, 5159 (2015).

[3] A. S. Arico, P. Bruce, B. Scrosati, J.-M. Tarascon, and W. V. Schalkwijk, Nat. Mater. **4**, 366 (2005).

[4] M.-C. Daniel, and D. Astruc, Chem. Rev. **104**, 293 (2004).

[5] P. P. Patil, D. M. Phase, S. A. Kulkarni, S. V. Ghaisas, S. K. Kulkarni, S. M. Kanetkar, S. B. Ogale, and V. G. Bhide, Phys. Rev. Lett. **58**, 238 (1987).

[6] J. Neddersen, G. Chumanov, and T. M. Cotton, Appl. Spectrosc. **47**, 1959 (1993).

[7] B. G. Ershov, E. Janata, and A. Henglein, J. Phys. Chem. **97**, 339 (1993).

[8] F. Mafuné, J. Kohno, Y. Takeda, and T. Kondow, J. Phys. Chem. B **104**, 9111 (2000).

[9] C. Liang, Y. Shimizu, M. Masuda, T. Sasaki, and N. Koshizaki, Chem. Mater. **16**, 963 (2004).

[10] T. Tsuji, D. H. Thang, Y. Okazaki, M. Nakanishi, Y. Tsuboi, and M. Tsuji, Appl. Surf. Sci. **254**, 5224 (2008).

[11] R. Tanabe, T. T. P. Nguyen, T. Sugiura, and Y. Ito, Appl. Surf. Sci. **351**, 327 (2015).

[12] K. Sasaki, and N. Takada, Pure Appl. Chem. **82**, 1317 (2010).

[13] T. E. Itina, J. Phys. Chem. C **115**, 5044 (2010).

[14] J. Lam, D. Amans, F. Chaput, M. Diouf, G. Ledoux, N. Mary, K. Masenelli-Varlot, V. Motto-Ros, and C. Dujardin, Phys. Chem. Chem. Phys. **16**, 963 (2014).

[15] K. K. Kim, M. Roy, H. Kwon, J. K. Song, and S. M. Park, J. Appl. Phys. **117**, 074302 (2015).

[16] C.-Y. Shih, C. Wu, M. V. Shugaev, and L. V. Zhigilei, J. Colloid Interface Sci. **489**, 3. (2017).

[17] H. Zeng, X. W. Du, S. C. Singh, S. A. Kulinich, S. Yang, J. He, and W. Cai, Adv. Funct. Mater. **22**, 1333 (2012).

[18] D. Tan, S. Zhou, J. Qiu, and N. Khusro, J. Photochem. Photobiol. C **17** 50 (2013).

[19] A. Tiwari, and A. Tiwari, Bioengineered Nanomaterials, CRC Press:

New York, pp 241−265 (2013).
[20] J. Zhang, M. Chaker, and D. Ma, J. Colloid Interface Sci. **489**, 138 (2017).
[21] C. Petridis, K. Savva, E. Kymakis, and E. Stratakis, J. Colloid Interface Sci., **489**, 28 (2017).
[22] S. V. Rao, G. K. Podagatlapalli, and S. Hamad, J. Nanosci. Nanotechnol. **14**, 1364 (2014).
[23] R. Intartaglia, K. Bagga, and F. Brandi, Opt. Express **22**, 3117 (2014).
[24] R. Streubel, S. Barcikowski, and B. Gökce, Opt. Lett. **41**, 1486 (2016).
[25] H. Wang, A. Pyatenko, K. Kawaguchi, X. Li, Z. Swiatkowska-Warkocka, and N. Koshizaki, Angew. Chem. Int. Ed. **49**, 6361 (2010).
[26] A. Pyatenko, H. Wang, N. Koshizaki, and T. Tsuji, Laser Photonics Rev. **7**, 596 (2013).
[27] A. Pyatenko, H. Wang, and N. Koshizaki, J. Phys. Chem. C **118**, 4495 (2014).
[28] T. Tsuji, Y. Higashi, M. Tsuji, Y. Ishikawa, and N. Koshizaki, Appl. Surf. Sci. **348**, 10 (2015).
[29] Z. Swiatkowska-Warkocka, A. Pyatenko, F. Krok, B. R. Jany, and M. Marszalek, Sci. Rep. **5**, 9849 (2015).
[30] T. Tsuji, T. Yahata, M. Yasutomo, K. Igawa, M. Tsuji, Y. Ishikawa, and N. Koshizaki, Phys. Chem. Chem. Phys. **15**, 3099, (2013).
[31] X. Li, N. Koshizaki, A. Pyatenko, Y. Shimizu, H. Wang, J. Liu, X. Wang, M. Gao, Z. Wang, and X. Zeng, Opt. Express **19**, 2847 (2011).
[32] X. Li, A. Pyatenko, Y. Shimizu, H. Wang, K. Koga, and N. Koshizaki, Langmuir, **27**, 5076 (2011).
[33] Y. Ishikawa, Y. Shimizu, T. Sasaki, and N. Koshizaki, Appl. Phys. Lett. 91, 161110 (2007).
[34] Y. Ishikawa, N. Koshizaki, A. Pyatenko, N. Saitoh, N. Yoshizawa, and Y. Shimizu, J. Phys. Chem. C **120**, 2439 (2016).
[35] Z. Swiatkowska-Warkocka, K. Koga, K. Kawaguchi, H. Wang, A. Pyatenko, and N. Koshizaki, RSC Adv. **3**, 79 (2013).
[36] H. Wang, M. Miyauchi, Y. Ishikawa, A. Pyatenko, N. Koshizaki, Y. Li, L. Li, X. Li, Y. Bando, and D. Golberg, J. Am. Chem. Soc. **133**, 19102 (2011).
[37] H. Fujiwara, R. Niyuki, Y. Ishikawa, N. Koshizaki, T. Tsuji, and K. Sasaki, Appl. Phys. Lett. **102**, 061110 (2013).

[38] J.-H. You, and K.-Y. Hsu, Chem. Eng. Res. Des. **88**, 1049 (2010).
[39] H. C. Zeng, Curr. Opin. Chem. Eng. **1**, 11 (2011).
[40] X. Hu, H. Gong, Y. Wang, Q. Chen, J. Zhang, S. Zheng, S. Yang, and B. Cao, J. Mater. Chem. **22**, 15947 (2012).
[41] M. Kondo, N. Shishido, S. Kamiya, A. Kubo, Y. Umeno, Y. Ishikawa, and N. Koshizaki, Part. Part. Syst. Charact. **35**, 1800061 (2018).
[42] H. Wang, N. Koshizaki, L. Li, L. Jia, K. Kawaguchi, X. Li, A. Pyatenko, Z. Swiatkowska-Warkocka, Y. Bando and D. Golberg, Adv. Mater. **23** 18651870 (2011).
[43] Y. Ishikawa and N. Koshizaki, Sci. Rep. **8**, 14208 (2018).
[44] Z. Swiatkowska-Warkocka, K. Koga, K. Kawaguchi, H. Wang, A. Pyatenko, and N. Koshizaki, RSC Adv. **3**, 79 (2013).
[45] S. Hashimoto, D. Werner, and T. Uwada, J. Photochem. Photobiol. C, **13**, 28 (2012).

Chapter 2

Pulse-width dependence of cooling effect on submicrometer ZnO spherical particle formation by pulsed laser melting in liquid

2. 1. Introduction

Over the past few decades, nanoparticle fabrication by pulsed laser irradiation with high fluence targeting material immersed in liquid (pulsed laser ablation in liquid) has been widely studied.[1–5)] In this method, nanoparticles are generated by an explosive interaction between bulk material and high-power laser light.

Recently, the synthesis of submicrometer spherical particles by irradiating particles dispersed in liquid with a nanosecond pulsed laser was reported.[6)] Particles dispersed in liquid are instantaneously heated over the melting point of the material when particles have adequate optical absorption of nanosecond pulsed laser light, whereas the dispersion medium is barely heated due to its optical transparency. The molten droplets are then quenched by the unheated surrounding liquid, maintaining the spherical shape of the droplets.[6–9)] The droplets of raw particles merge with adjacent droplets, which results in the growth of submicrometer spherical particles.[10, 11)] Through this rapid particle heating and cooling, submicrometer spherical particles are formed. This technique has been successfully applied to various

materials including metals, semiconductors, and oxides (e.g., Au, Ag, Si, ZnO, and TiO_2).[7, 8, 12–14)]

Pyatenko et al. developed a particle heating–melting–evaporation model that well explains the spherical particle formation conditions.[11, 15, 16)] In this model, all of the laser energy absorbed by a particle is assumed to be exclusively utilized for particle heating. A laser–fluence curve as a function of particle size for the phase transition from solid to liquid can then be obtained. This curve is quite useful to explain the submicrometer spherical particle formation mechanism and to predict the laser fluence required to obtain submicrometer spherical particles. The curve with a positive slope in the size range of several hundreds of nanometers suggests that the particle size increases with laser fluence.

The particle heating–melting–evaporation model considered particle cooling only by boiling conductive/convective heat transfer. This cooling rate is slow comparting with particle heating, and therefore cooling process was ignored in this model. However, heat dissipation by the liquid-phase surroundings is possibly considerable. Heated particles would be rapidly cooled by the liquid medium in the initial heating stage by laser pulse, and then heat dissipation from particles is disturbed by the vapor-phase surroundings generated by evaporation of surrounding liquid medium in the subsequent heating stage. We fabricated submicrometer spherical particles using a nanosecond pulsed laser with different pulse widths of 50 and 70 ns to study the pulse width effect on the products. If the laser fluence of a single laser pulse is the same, the pulse width should not affect submicrometer spherical particle formation according to the particle heating–melting–evaporation model without considering cooling effects of liquid-phase surroundings. However, in our experiments, the laser–fluence threshold for submicrometer spherical particle formation increased as the pulse width increased, which suggests the contribution of a cooling process during pulsed laser heating. Here we propose a new particle heating–cooling model to explain this experimental result. Based on this new model, we also calculate

time-dependent profiles of particle temperature, and computationally clarify the pulse-width dependence of the cooling effect. The calculation results are compared with experimental results to verify the validity of the developed particle heating–cooling model.

2. 2. Results and Discussion

2. 2. 1. Experimental results

In this study, colloidal ZnO particles were irradiated with a KrF excimer laser (Gigaphoton Inc., wavelength 248 nm, pulse frequency 100 Hz, pulse width 50 or 70 ns). Pulse shape was measured by biased silicon detector (Electro-Optics Technology Inc., ET-2020) (Figure 2. 1). Commercial ZnO powder (Sigma-Aldrich Co., LLC) was dispersed in de-ionized water with a ZnO concentration of 0.2 mg/ml. Then, 6 ml of the suspension in a glass vessel was irradiated for 8 min at various laser fluences with agitation by a magnetic stirrer. The laser beam was focused using a lens with a focal length of 500 mm to adjust the laser fluence (beam size 1.5 mm × 8.7 mm square). Part of the particles in suspension absorb laser energy and melt. By repeating this process with agitation for sufficient time, submicrometer spherical particles with homogeneous size distribution are formed.[9)] The quenching process is usually reported to require 10^{-6} to 10^{-4} s.[17–21)] This quenching time is much shorter than the interval between two consecutive laser pulses in this experiment. Therefore, no heat energy from a laser pulse is retained in the particle just before the subsequent laser pulse arrives, and particles can be regarded as independently interacting with each laser pulse. The suspension after laser irradiation was settled for a day to separate insufficiently treated raw particles and nanoparticle by-products from the produced submicrometer spherical particles. The precipitation in the glass vessel was dropped onto a Si substrate to observe the particle morphology

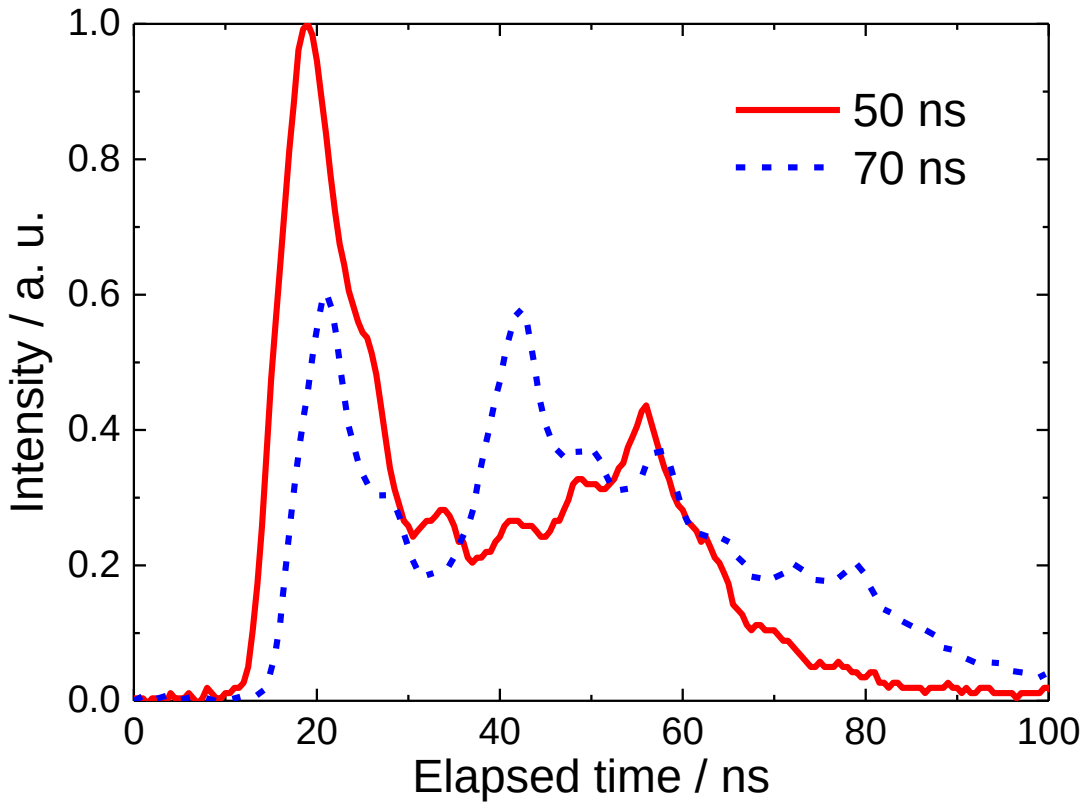

Figure 2. 1. Temporal pulse profile of a KrF excimer laser with a pulse width of 50 ns (red solid curve) or 70 ns (blue dashed curve).

using a field-emission scanning electron microscope (FE-SEM).

SEM images of raw ZnO particles and particles obtained by KrF excimer laser irradiation with different pulse widths at 81 mJ pulse^{-1} cm^{-2} are presented in Figures 2. 2(a), (b), and (c). Raw particles have non-spherical shapes with an average diameter of about 60 nm (Figure 2. 2(a)). At a pulse width of 50 ns, agglomerates of raw particles were melted, and submicrometer spherical particles with an average diameter of about 170 nm were formed (Figure 2. 2(b)). In contrast, at a pulse width of 70 ns, particles after laser irradiation were not spherical and were almost identical to the raw particles (Figure 2. 2(c)), though 81 mJ pulse^{-1} cm^{-2} is a sufficient laser fluence for agglomerates to melt based on the estimation by the particle heating–melting–evaporation model ignoring the pulse width effect. Pulsed lasers with short pulse widths would be efficient for pulsed laser melting in liquid because heating by longer pulses is supposed to cause larger heat dissipation.

Figures 2. 3(a) and (c) present the SEM images of the particles obtained after KrF excimer laser irradiation with different pulse widths at a larger laser fluence of 202 mJ pulse^{-1} cm^{-2}. For both pulse widths of 50 and 70 ns, submicrometer spherical particles were obtained. Additionally, the average size distribution histograms plotted by counting more than 200 particles are almost identical, regardless of pulse width (Figures 2. 3 (b) and (d)). At high laser fluence, the pulse width has little influence on the products obtained by pulsed laser melting in liquid.

The laser–fluence dependence of the average diameter and standard deviation of the obtained ZnO particles calculated from the SEM images are depicted in Figure 2. 4. The average diameter increases with laser fluence when the laser fluence exceeds the threshold for submicrometer spherical particle formation. In addition, the laser–fluence threshold increases with increasing pulse width. For the case of a KrF excimer laser with a pulse width of 50 ns, a laser fluence of 81 mJ pulse^{-1} cm^{-2} was the threshold, whereas a laser fluence of 101 mJ pulse^{-1} cm^{-2} was required for 70 ns. When the third

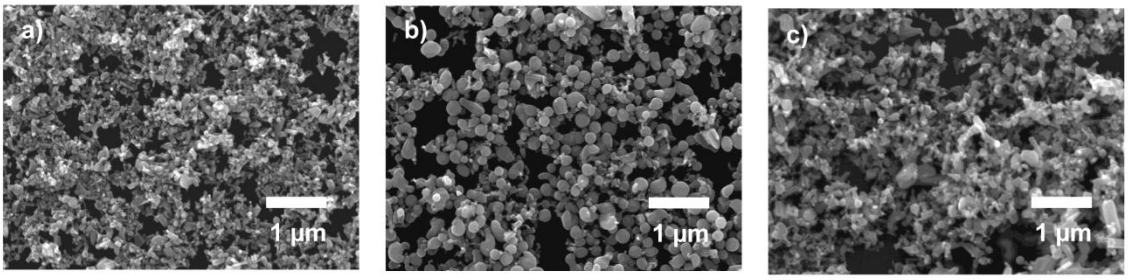

Figure 2. 2. SEM images of ZnO particles. Raw particles (a) and after KrF excimer laser irradiation at a laser fluence of 81 mJ pulse^{-1} cm^{-2} with a pulse width of 50 ns (b) or 70 ns (c).

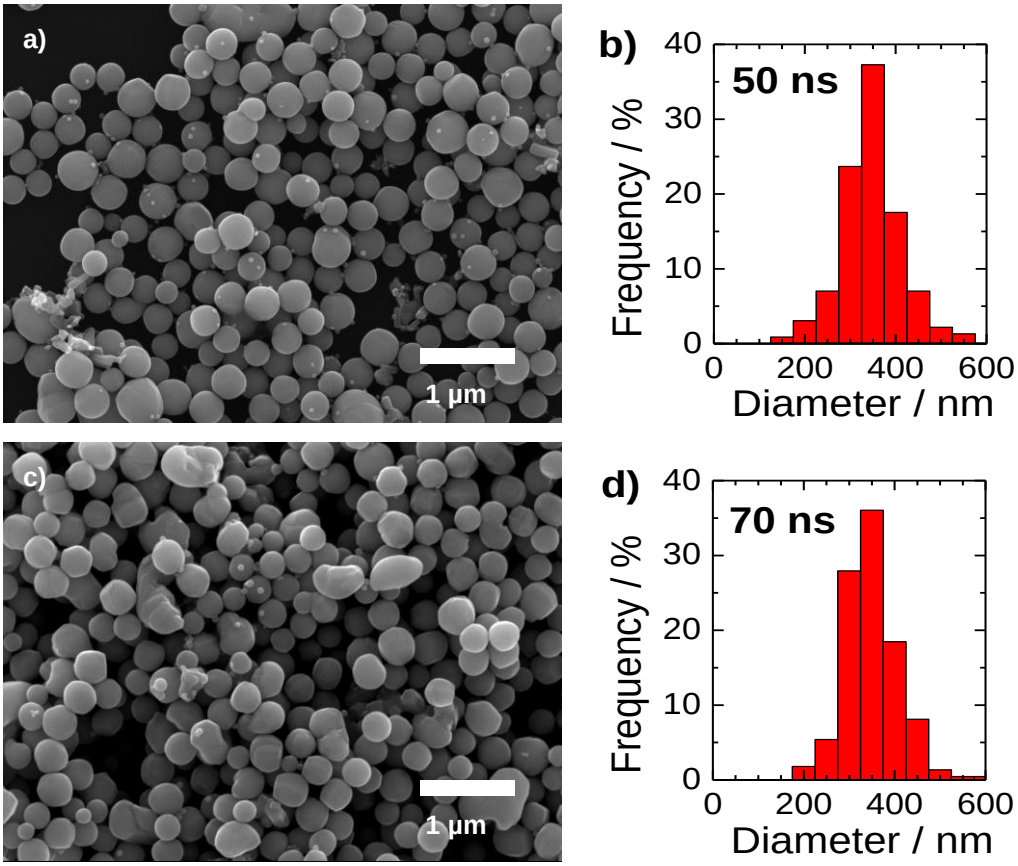

Figure 2. 3. SEM images of ZnO particles after KrF excimer laser irradiation at a laser fluence of 202 mJ pulse^{-1} cm^{-2} with a pulse width of (a) 50 ns or (c) 70 ns. The corresponding particle size distributions from (a) and (c) are shown in (b) and (d), and the average particle sizes are 327 nm and 323 nm, respectively.

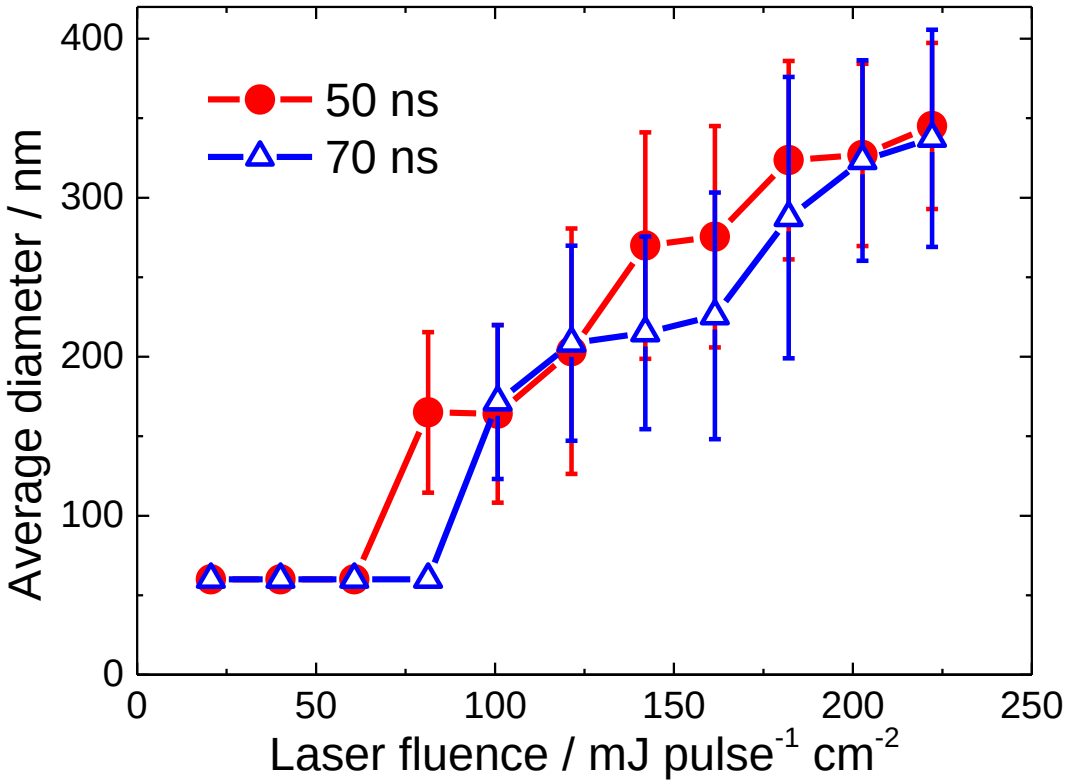

Figure 2. 4. Laser-fluence dependence of average particle diameter of ZnO particles obtained by nanosecond pulsed KrF excimer laser irradiation with a pulse width of 50 ns (red circles) or 70 ns (blue triangles).

harmonic of an Nd:YAG laser with a pulse width of 10 ns is used, the laser–fluence threshold is 67 mJ pulse^{-1} cm^{-2},[8] which is smaller than for the KrF excimer laser with pulse widths of 50 and 70 ns. The amount of laser energy absorbed by a particle from one pulse is almost the same regardless of the pulse width. This result suggests that the particles dissipate heat energy to the surrounding liquid during pulsed laser heating and the maximum heat energy accumulated in the particles decreases with increasing pulse width.

2. 2. 2. Particle heating–cooling model

The particle heating–melting–evaporation model could explain well the submicrometer spherical particle formation in our previous studies using a 10 ns pulse width Nd:YAG laser.[11, 16] However, particle cooling by the surrounding liquid, which might affect submicrometer spherical particle formation, was not considered to be significant in these studies. Here we take the cooling process into consideration and develop a new particle heating–cooling model describing the submicrometer spherical particle formation process. In this model, a homogeneous distribution of heat energy within a spherical particle and no volume change of the spherical particle during heating and cooling are assumed. The time required for submicrometer spherical particles to cool to room temperature is much shorter than 10 ms.[17–21] The calculations have been performed for a single pulse, because the pulse repetition rate of the laser used in these experiments is 100 Hz (pulse interval: 10 ms).

2. 2. 2. 1. Particle heating

Particles absorb laser energy depending on the pulse shape of the laser. In this model, all laser energy absorbed by the particle is converted to

particle heat energy.

$$\frac{dE_{abs}}{dt} = Q_{abs}^{\lambda} \cdot \frac{\pi d^2}{4} \cdot J(t) \qquad (1)$$

Here, Q_{abs}^{λ} is the absorption efficiency based on Mie theory, $\frac{\pi d^2}{4}$ is the particle geometrical cross section, and $J(t)$ is the time-dependent laser fluence. The integral of time-dependent laser fluence corresponds to the laser fluence.

2. 2. 2. 2. Particle cooling

The heat energy of the particles diffuses to the surrounding liquid. In this model, conductive heat transfer is defined because convection around submicrometer-scale particle is neglligible.[22)]

$$\frac{dq}{dt} = h \cdot \pi d^2 \cdot \{T(t) - T_0\} \qquad (2)$$

where

$$h = \frac{Nu_d \cdot k_w}{d} \qquad (3)$$

Here, h is the heat transfer coefficient, πd^2 is the particle surface area, $T(t)$ is the particle temperature, and T_0 is the temperature of the surrounding liquid. The heat transfer coefficient is proportional to the heat conductivity of the surrounding liquid, k_w, Nusselt number, Nu_d, and inversely proportional to the particle diameter, d. In the case of submicrometer particles in water, heat transfer coefficient can be estimated

1.2 to 12 MW m^{-2} K^{-1}. This value is much larger than the value estimated in heating-melting-evaporation model. Therefore, cooling process have influence on heat dissipation of particles.

In the initial heating stage, particles contact directly with the liquid and are cooled. At the spinodal temperature of 573 K, explosive evaporation of the water is reported to occur,[23–25] and heated particles start to be cooled by vaporized liquid over 573 K with the following heat transfer coefficient value.

$$h = \frac{Nu_d \cdot k_v}{d} \qquad (4)$$

Here, k_v is the heat conductivity of the surrounding evaporating vapor. The heat conductivity of vapor is much lower than that of liquid and, therefore, the cooling rate by vapor is much slower than by liquid. Cooling process is drastically switched by evaporation of surrounding liquid.

The Nusselt number is the ratio of convective heat transfer to conductive heat transfer. In the case of natural convection on a sphere, the Nusselt number is given as below.[26]

$$\overline{Nu_d} = 2 + \frac{0.589 Ra_d^{1/4}}{\left[1 + (0.469/Pr)^{9/16}\right]^{4/9}} \qquad (5)$$

Here, Ra_d is the Rayleigh number and Pr is the Prandtl number. In submicrometer scale heating, heat transfer is governed by heat conduction but not by fluid convection. In this case, the Nusselt number is constant, $Nu_d \approx 2$, because the Rayleigh number is negligibly small on the submicrometer scale.[22]

Thermal particle-water interface resistance is considered in the case of Au nanoparticles irradiated with femtosecond, picosecond and nanosecond lasers.[27, 28] However, conductive heat transfer does not contain interfacial condition, and the step of temperature across the interface of

particle and liquid is in quasi-equilibrium for the nanosecond case.[29] Therefore, we considered the step of temperature would be negligible during several tens of nanosecond heating.

2. 2. 2. 3. Time-dependent particle temperature

The accumulated heat energy in a particle is the difference between the laser energy absorbed by a particle and the energy dissipated by conductive heat transfer.

$$\frac{dE}{dt} = \frac{dE_{abs}}{dt} - \frac{dq}{dt} \qquad (6)$$

If the laser energy is not enough to melt the agglomerate of raw particles, only particle heating in the solid state is expected.

$$T(t) = T_0 + \frac{1}{\rho_p \cdot \frac{\pi d^3}{6} \cdot c_s} \cdot E(t) \quad (7)$$

Here, ρ_p is the density of the particle, $\frac{\pi d^3}{6}$ is the particle volume, and c_s is the particle specific heat in the solid state.

If the agglomerate absorbs more energy, particle melting occurs.

$$T(t) = T_m \qquad (8)$$

Here, T_m is the melting point of the material. During particle melting, the particle temperature stays at the melting point.

With more absorbed energy, the particle completely melts and the

temperature of the droplet increases further.

$$T(t) = T_{\mathrm{m}} + \frac{1}{\rho_p \cdot \frac{\pi d^3}{6} \cdot c_l} \cdot \left[E(t) - \rho_p \cdot \frac{\pi d^3}{6} \cdot \left(H_{T_m} - H_{T_0} + \Delta H_m\right)\right] \quad (9)$$

Here, $H_{T_m} - H_{T_0}$ is the relative enthalpy required for start of melting, ΔH_m is the latent enthalpy of melting, and c_l is the particle specific heat in the liquid state.

2. 2. 3. Temporal temperature profile

By numerically solving the differential equation using a fourth-order Runge–Kutta method, the time profile of the particle temperature of ZnO spherical particles can be calculated. The pulse shape of the time-dependent laser fluence used in the calculation is plotted in Figure 2. 1. The optical data used in the calculation are listed in Table 2. 1,[30] and all thermodynamic data are listed in Tables 2. 2 and 3.[25, 31, 32] The absorption efficiency of ZnO spherical particles at a wavelength of 248 nm was calculated from refractive index and extinction coefficient using Mie theory (Figure 2. 5).

Figure 2. 6 depicts the calculated time-dependent temperature profile of ZnO spherical particles 60 nm in diameter irradiated with a KrF excimer laser (wavelength 248 nm, pulse width 50 or 70 ns) at laser fluences of 61, 81, and 101 mJ pulse^{-1} cm^{-2}. These laser fluences are sufficient for particle melting (dotted line: T_m) when the adiabatic condition is satisfied. The particle temperature calculated under the adiabatic condition (dashed line: T_{ad}) increased with increasing laser fluence. However, in this experiment, submicrometer spherical particles were formed from 81 mJ pulse^{-1} cm^{-2} for 50 ns pulse width and from 101 mJ pulse^{-1} cm^{-2} for 70 ns pulse width.

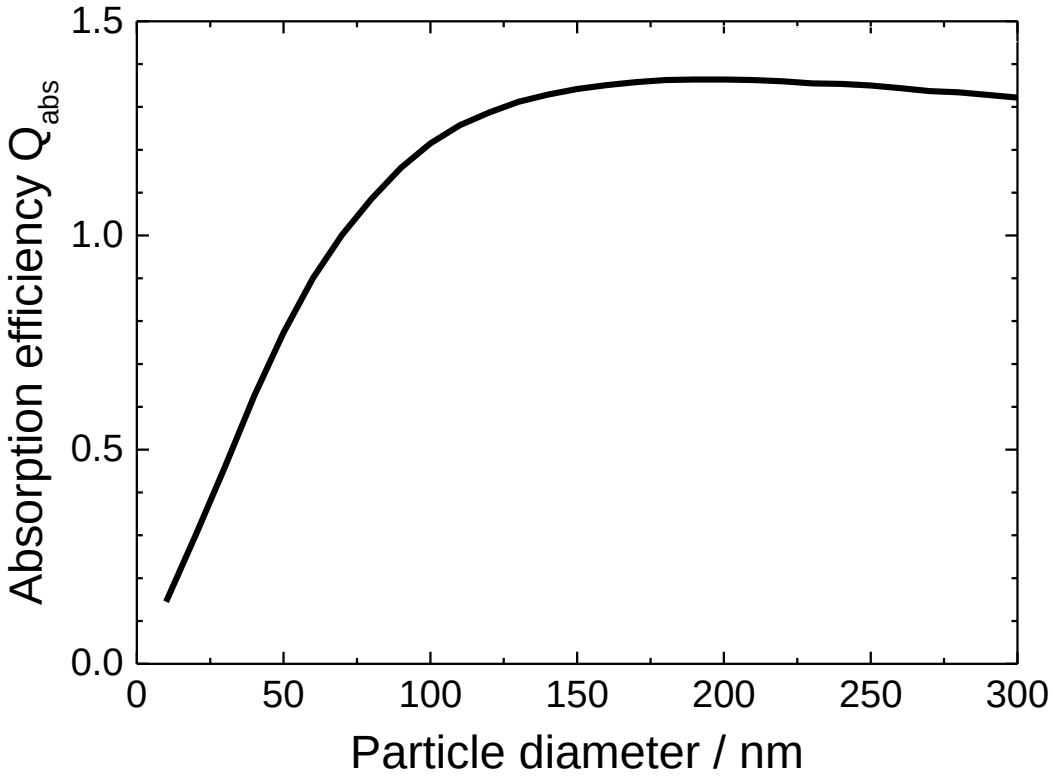

Figure 2. 5. Absorption efficiency of ZnO spherical particles at a wavelength of 248 nm calculated using Mie theory.

Table 2. 1. Refractive index and extinction coefficient of zinc oxide at a wavelength of 248 nm.

	n	k
ZnO	1.808	0.509

Table 2. 2. Thermodynamic data of water used in the calculations.

	T_0	$T_{spinodal}$	k_w (298 K)	k_v (573 K)
	K	K	$\mathrm{W/m \cdot K}$	$\mathrm{W/m \cdot K}$
Water	298	573	0.61	0.043

Table 2. 3. Thermodynamic data of zinc oxide used in the calculations.

	ρ	T_{melt}	ΔH_m	$H_{T_m} - H_{T_0}$	C_s	C_l
	$\mathrm{g/cm^3}$	K	kJ/kg	kJ/kg	$\mathrm{kJ/kg \cdot K}$	$\mathrm{kJ/kg \cdot K}$
ZnO	5.606	2243	870.65	1284.37	0.660	0.757

At a laser fluence of 61 mJ pulse^{-1} cm^{-2}, which is sufficient for particle melting under the adiabatic condition, the maximum particle temperature is below the melting point in both cases of 50 and 70 ns pulse widths (Figure 2. 6(a)). For a 70 ns pulse width, the particle temperature is below the spinodal temperature of the surrounding water (chained line: T_{sp}), and the particles are rapidly cooled by liquid water. In contrast, for the 50 ns pulse width, the particle temperature is above the spinodal temperature and, therefore, the surrounding liquid evaporates and the generated vapor disturbs heat dissipation from the particles. Therefore, the particle temperature is much higher when irradiated with 50 ns pulses than with 70 ns pulses due to the lower heat loss of 50 ns pulses.

At a laser fluence of 81 mJ pulse^{-1} cm^{-2}, the particle temperature reaches the melting point of ZnO for a 50 ns pulse width, but is below the spinodal temperature for a 70 ns pulse width because heating rate is comparatively lower than cooling rate by water (Figure 2. 6(b)). At a laser fluence of 101 mJ pulse^{-1} cm^{-2}, the particle temperature reaches the melting point of ZnO for 70 ns pulse widths (Figure 2. 6(c)). Once particle temperature exceeds the spinodal temperature, attained temperature is drastically increased. These calculation results considering the cooling effect by the surrounding liquid are in good agreement with the experimental results on spherical particle formation. When the temperature of the raw particles reaches the melting point of the material, submicrometer spherical particles are formed. During nanosecond pulsed heating of submicrometer particles, the formation of vapor films around particles is essential for them to melt in liquid.

a) 61 mJ pulse^{-1} cm^{-2}

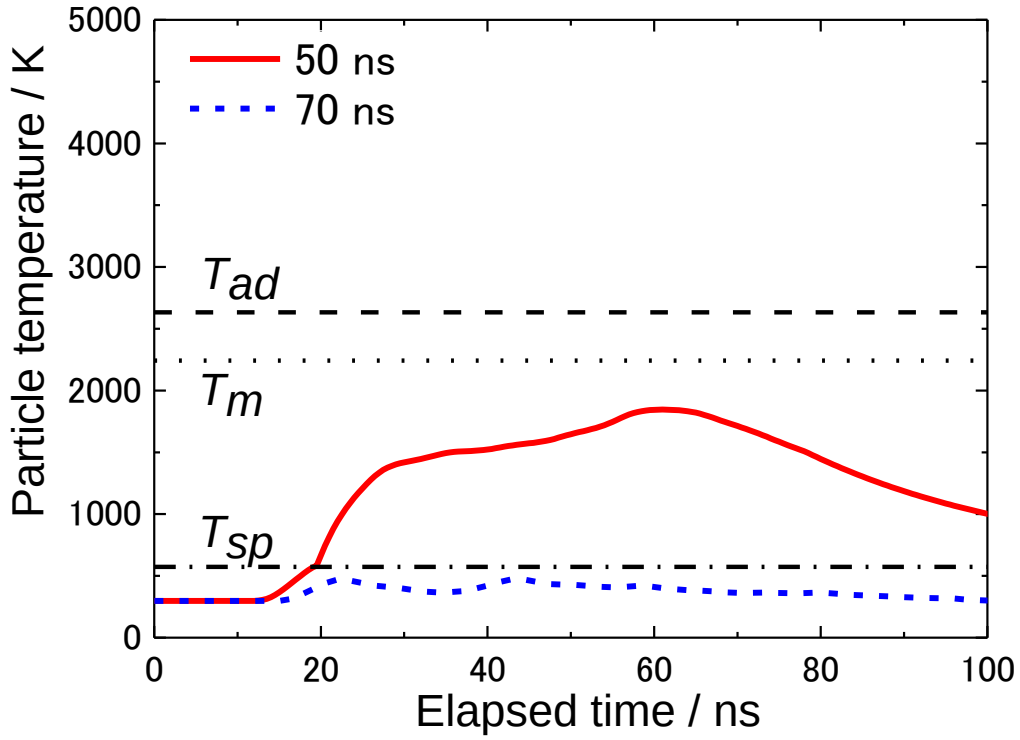

b) 81 mJ pulse^{-1} cm^{-2}

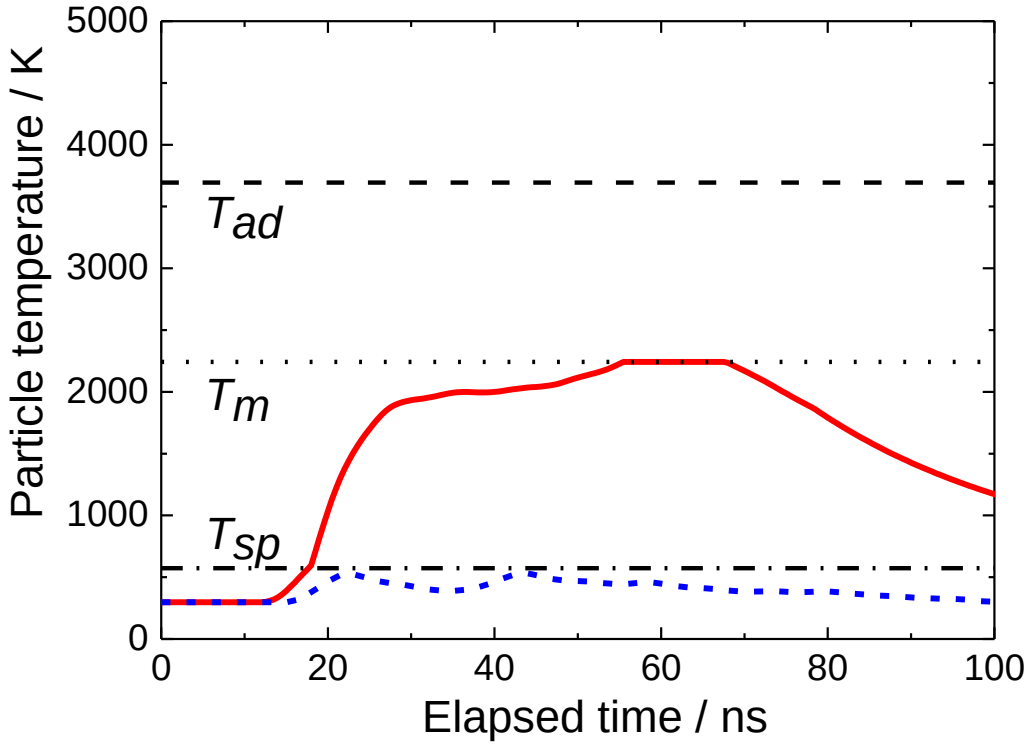

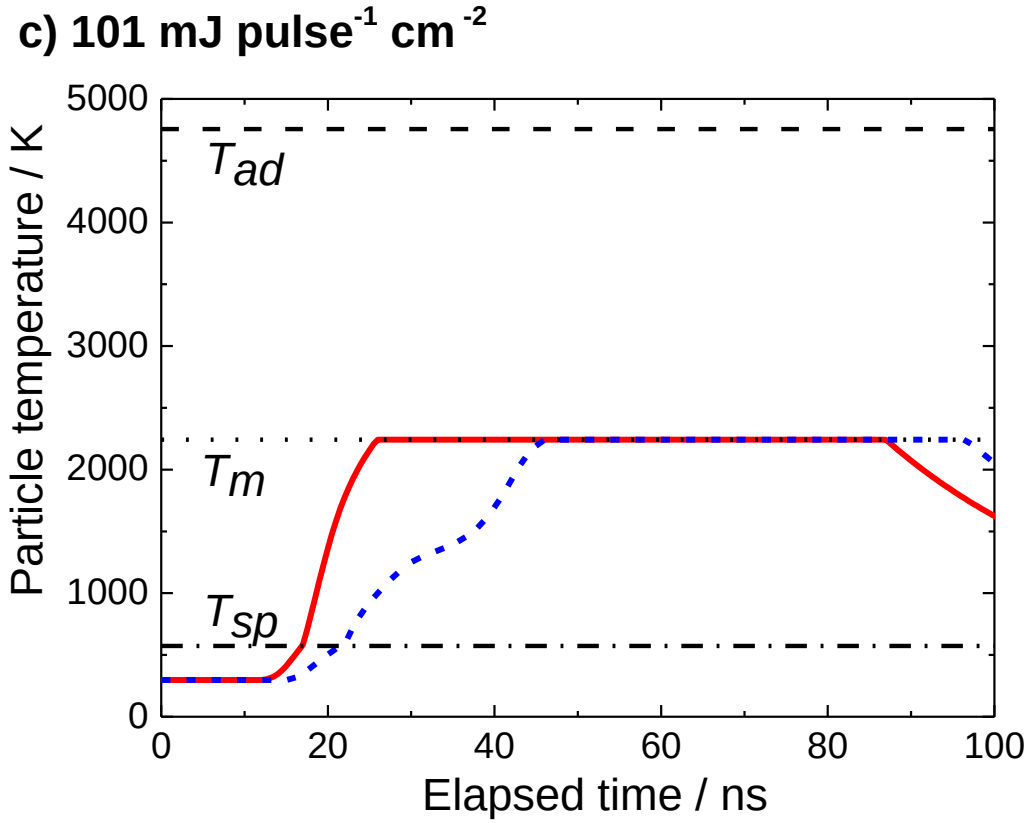

Figure 2. 6. Time-dependent temperature profile of ZnO particles 60 nm in diameter irradiated with a KrF excimer laser at laser fluences of 61 mJ pulse^{-1} cm^{-2} (a), 81 mJ pulse^{-1} cm^{-2} (b), and 101 mJ pulse^{-1} cm^{-2} (c). In each graph, temperature profiles calculated using the model considering the cooling effect are shown for pulse widths of 50 ns (red solid curve) and 70 ns (blue dashed curve). The dotted horizontal line represents the melting point of zinc oxide, T_m, the dashed horizontal line represents the particle temperature under the adiabatic condition, T_{ad}, and the chained horizontal line represents the spinodal temperature of water, T_{sp}.

2. 2. 4. Fluence- and size-dependent maximum temperature

Figure 2. 7 illustrates numerical calculation results of the maximum temperature of ZnO spherical particles irradiated with a KrF excimer laser. Under the adiabatic condition, no heat is dissipated from the particles to the surrounding liquid during pulsed heating. The laser fluence required to attain the same temperature almost linearly increases with particle diameter for diameters above 100 nm and is nearly constant below 100 nm. A higher maximum temperature is attained when a larger fluence is applied (Figure 2. 7(a)). By considering the cooling effect and the pulse width of the KrF excimer laser, the maximum temperature is decreased, especially for small particles and low laser fluence (Figures 2. 7(b) and 7(c)). Thus, we find a clear dip in the fluence–size diagram, indicating that 100 nm particles can be selectively melted with smaller laser fluence. For large particles, the maximum temperature considering the cooling effect is almost the same as that under the adiabatic condition. The plotted circles and triangles in Figure 2. 7 are the experimental results shown in Figure 2. 4. Submicrometer spherical particles are formed in the region above the melting point of ZnO (gray-colored region). In contrast, raw particles are not melted and maintain their shape and size if they stay in the region below the melting point.

The region in black in Figure 2. 7, which shows where the particle temperature is barely elevated, expands toward larger particle size with increasing pulse width. At a laser fluence of 150 mJ $pulse^{-1}$ cm^{-2}, nanoparticles smaller than 40 nm or 50 nm are insufficiently heated for pulse widths of 50 ns or 70 ns, respectively (Figures 2. 7(b) and 7(c)).

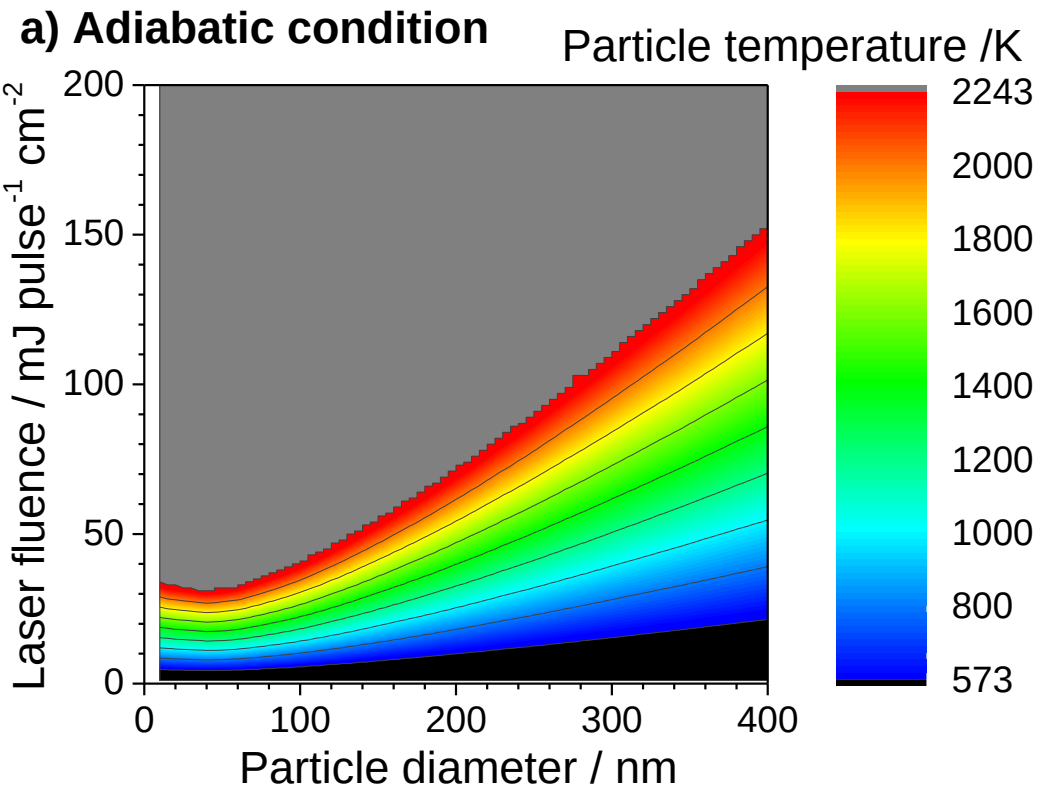
a) Adiabatic condition
Particle temperature /K
Laser fluence / mJ pulse-1 cm-2
Particle diameter / nm
0
50
100
150
200
0
100
200
300
400
2243
2000
1800
1600
1400
1200
1000
800
573

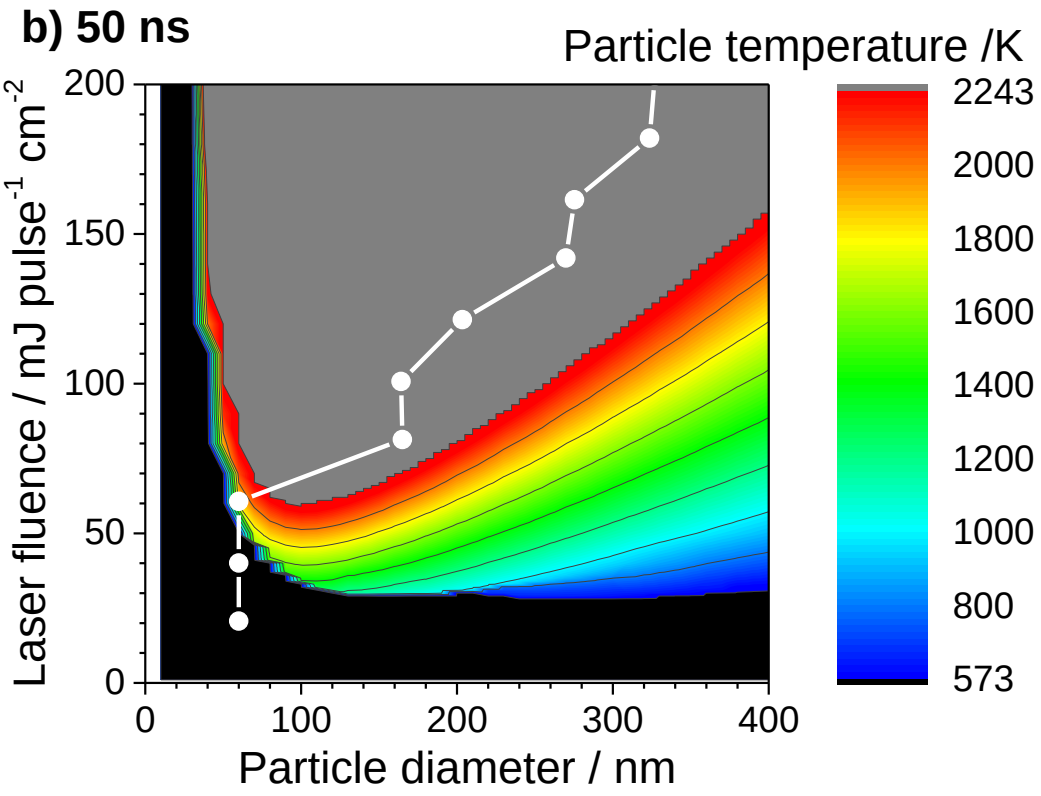
b) 50 ns
Particle temperature /K
Laser fluence / mJ pulse-1 cm-2
Particle diameter / nm
0
50
100
150
200
0
100
200
300
400
2243
2000
1800
1600
1400
1200
1000
800
573

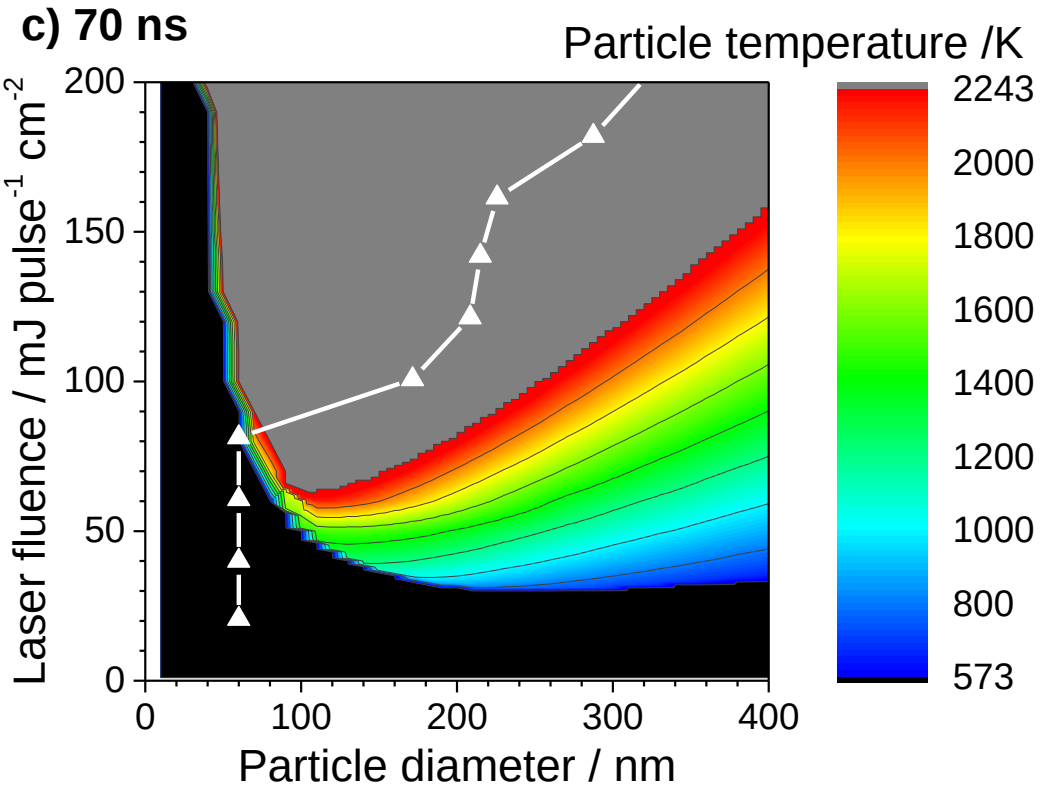

Figure 2. 7. Two-dimensional diagram of the highest temperature attained as a function of laser fluence and particle size for ZnO spherical particles irradiated with KrF excimer laser (a) under the adiabatic condition, and based on a model considering the cooling effect with laser pulse widths of 50 ns (b) and 70 ns (c).

2. 3. Conclusions

Submicrometer ZnO spherical particle formation by pulsed laser melting in liquid is examined using a nanosecond pulsed excimer laser with different pulse widths. The threshold fluence for submicrometer spherical particle formation increases with increasing pulse width from 50 to 70 ns. This result suggests that the particles dissipate heat energy even during several tens of nanoseconds pulsed heating, especially in the case of longer pulse widths with lower laser fluence. Considering the cooling effect of the surrounding liquid, a particle heating–cooling model is developed to estimate the particle temperature profile during nanosecond pulsed laser irradiation. Vapor films considered to be formed from the heated liquid surrounding the particles significantly suppress the heat dissipation from the particles to the liquid and elevate the maximum temperature attained. However, if the particle size is small or the pulse width is large, the transient temperature during heating is not high enough to form vapor films, resulting in a drastic lowering of the maximum temperature. Utilizing the heating–cooling model developed here, the threshold fluence for spherical particle formation and maximum particle temperature can be estimated, which is useful for predicting the fabrication conditions for submicrometer spherical particles.

References

[1] P. P. Patil, D. M. Phase, S. A. Kulkarni, S. V. Ghaisas, S. K. Kulkarni, S. M. Kanetkar, S. B. Ogale, and V. G. Bhide, Phys. Rev. Lett. **58**, 238 (1987).

[2] J. Neddersen, G. Chumanov, and T. M. Cotton, Appl. Spectrosc. **47**, 1959 (1993).

[3] B. G. Ershov, E. Janata, and A. Henglein, J. Phys. Chem. **97**, 339 (1993).

[4] F. Mafuné, J. Kohno, Y. Takeda, and T. Kondow, J. Phys. Chem. B **104**, 9111 (2000).

[5] C. Liang, Y. Shimizu, M. Masuda, T. Sasaki, and N. Koshizaki, Chem. Mater. **16**, 963 (2004).

[6] Y. Ishikawa, Y. Shimizu, T. Sasaki, and N. Koshizaki, Appl. Phys. Lett. **91**, 161110 (2007).

[7] H. Wang, M. Miyauchi, Y. Ishikawa, A. Pyatenko, N. Koshizaki, Y. Li, L. Li, X. Li, Y. Bando, and D. Golberg, J. Am. Chem. Soc. **133**, 19102 (2011).

[8] H. Wang, N. Koshizaki, L. Li, L. Jia, K. Kawaguchi, X. Li, A. Pyatenko, Z. Swiatkowska-Warkocka, Y. Bando, and D. Golberg, Adv. Mater. **23**, 1865 (2011).

[9] H. Wang, K. Kawaguchi, A. Pyatenko, X. Li, Z. Swiatkowska-Warkocka, Y. Katou, and N. Koshizaki, Chem. Eur. J. **18**, 163 (2012).

[10] Y. Ishikawa, Y. Katou, N. Koshizaki, and Q. Feng, Chem. Lett. **42**, 530 (2013).

[11] A. Pyatenko, H. Wang, and N. Koshizaki, J. Phys. Chem. C **118**, 4495 (2014).

[12] T. Tsuji, T. Yahata, M. Yasutomo, K. Igawa, M. Tsuji, Y. Ishikawa, and N. Koshizaki, Phys. Chem. Chem. Phys. **15**, 3099 (2013).

[13] X. Li, N. Koshizaki, A. Pyatenko, Y. Shimizu, H. Wang, J. Liu, X. Wang, M. Gao, Z. Wang, and X. Zeng, Opt. Exp. **19**, 2847 (2011).

[14] X. Li, A. Pyatenko, Y. Shimizu, H. Wang, K. Koga, and N. Koshizaki,

Langmuir **27**, 5076 (2011).
[15] A. Pyatenko, H. Wang, N. Koshizaki, and T. Tsuji, Laser Photon. Rev. **7**, 596 (2013).
[16] Y. Ishikawa, N. Koshizaki, A. Pyatenko, N. Saitoh, N. Yoshizawa, and Y. Shimizu, J. Phys. Chem. C **120**, 2439 (2016).
[17] A. Pyatenko, M. Yamaguchi, and M. Suzuki, J. Phys. Chem. C **111**, 7910 (2007).
[18] S. Link, and M. El-Sayed, J. Phys. Chem. B **103**, 4212 (1999).
[19] A. Takami, H. Kurita, and S. Koda, J. Phys. Chem. B **103**, 1226 (1999).
[20] P. V. Kamat, M. Flumiani, and G. V. Hartland, J. Phys. Chem. B **102**, 3123 (1998).
[21] A. Pyatenko, M. Yamaguchi, and M. Suzuki, J. Phys. Chem. C **113**, 9078 (2009).
[22] J. S. Donner, G. Baffou, D. McCloskey, and R. Quidant, ACS Nano **5**, 5457 (2011).
[23] F. Caupin, and E. Herbert, C. R. Phys. **7**, 1000 (2006).
[24] V. Kotaidis, C. Dahmen, G. von Plessen, F. Springer, and A. Plech, J. Chem. Phys. **124**, 184702 (2006).
[25] A. Siems, S. A. L. Weber, J. Boneberg, and A. Plech, New J. Phys. **13**, 043018 (2011).
[26] A. F. Mills, Heat Transfer 2nd edition, Prentice Hall, New York, pp. 275-282 (1998).
[27] A. Plech, and V. Kotaidis, Phys. Rev. B **70**, 195423 (2004).
[28] S. Hashimoto, D. Werner, and T. Uwada, J. Photochem. Photobiol. C **13**, 28 (2012).
[29] D. Werner, and S. Hashimoto, J. Phys. Chem. C **115**, 5063 (2011).
[30] H. Yoshikawa, and S. Adachi, Jpn. J. Appl. Phys. **36**, 6237 (1997).
[31] Thermodynamic database MALT group, Thermodynamic database MALT for Windows, Kagaku Gijutsu-Sha, 2005, (CD-ROM), available from (http://www.kagaku.com/malt/index.html), (accessed 2016-10-20).

[32] http://www.chem.msu.su/Zn/Zn/ivtan0003.html, (in Russian, accessed 2016-10-20).

Chapter 3

Comparison of picosecond and nanosecond lasers for the synthesis of TiN submicrometer spherical particles by pulsed laser melting in liquid

(Applied Physics Express; Volume 11; Number 3; 035001, https://doi.org/10.7567/APEX.11.035001, Copyright 2018 The Japan Society of Applied Physics)

Nanoparticle synthesis via irradiation with a high-power laser in a liquid medium, which is known as pulsed laser ablation in liquid (PLAL), has been studied for a few decades because of the distinctive particle formation mechanism associated with this technique.[1–5] This method can be applied to various materials such as metals,[6] oxides,[7] carbides,[8] and alloys[9]. In PLAL, high-power pulsed lasers (nanosecond,[8] picosecond,[10] and femtosecond lasers[10]) have been widely used because they can provide the high instantaneous energy density needed to elicit an explosive interaction between a target and laser light. For excitation of a target with ultrashort pulses such as femtosecond laser, intensive heating of an electron gas occurs during the pulse duration because pulse duration is shorter than electron-phonon coupling period.[11] In contrast, for excitation of a target with nanosecond pulses, the electrons and lattice are in thermal equilibrium because pulse duration is longer than electron-phonon coupling period.[11]

Recently, submicrometer spherical particle formation by pulsed laser melting in liquid (PLML) has been reported.[5,12] In PLML, nanosecond laser is usually used for synthesis of submicrometer spherical particles, since PLML is thermal process under equilibrium conditions between electrons and lattice.[13–15] Heat loss during nanosecond heating has been considered to be negligible because a typical time needed for particle cooling is much

larger than duration of nanosecond laser heating.[16] However, recent study indicated that the particles dissipate heat energy by cooling effect of surrounding liquid even during several tens of nanoseconds heating.[17] Therefore, laser irradiation with shorter pulse width than nanoseconds would be effective in reducing heat loss of pulsed heating.

Barcikowski et al. reported that submicrometer spherical particles could be synthesized by picosecond laser irradiation to colloidal particles.[18,19] This method was effective when the pulse width was longer than the electron–phonon coupling period of the material.[18] However, the difference between picosecond and nanosecond laser melting in liquid has not been investigated. Thus, in this study, submicrometer spherical particles were fabricated via both picosecond and nanosecond laser irradiation under similar conditions to study the effect of picosecond laser irradiation on the energy efficiency of particle synthesis and the properties of the obtained particles. TiN was used as the materials for the particles in this study because it has potential applications as submicrometer hard plasmonic particles.[20,21] TiN raw particles (Wako Pure Chemical Industries, Ltd., < 50 nm) were dispersed in deionized water at a concentration of 0.2 g/L. A nanosecond laser (Continuum Powerlite Precision 8000, 532 nm wavelength, 10 Hz pulse frequency, 7 ns pulse width, and 8 mm beam diameter) and a picosecond laser (Continuum PY61C−10, 532 nm wavelength, 10 Hz pulse frequency, 40 ps pulse width, and 6 mm beam diameter) were used for laser irradiation. A colloidal solution of TiN raw particles was agitated using a magnetic stirrer during laser irradiation. To obtain sufficient laser fluence for PLML, the laser beam of the picosecond laser was condensed to a 4 mm diameter through a convex lens with a focal length of 500 mm. To compensate for the difference in the sizes of the laser beams (the beam of the nanosecond laser was four times larger than that of the picosecond laser), 3 ml of suspension were irradiated for 20 min with the picosecond laser and 6 ml of the suspension were irradiated for 10 min with the nanosecond laser (total input energy per suspension volume irradiated with the picosecond laser was equal to that

with the nanosecond laser). The sizes and morphologies of the particles were measured via field−emission scanning electron microscopy (FE−SEM JEOL JSM-6500F). The crystal structures of particles were evaluated by X−ray diffraction analysis (XRD, Rigaku RINT-2000).

SEM images of particles irradiated with a nanosecond laser for 10 min are shown in Figs. 3. 1(a) and 1(b). Nanosecond laser irradiation at a laser fluence of 67 mJ pulse^{-1} cm^{-2} resulted in submicrometer spherical particles; in contrast, irradiation at a laser fluence of 50 mJ pulse^{-1} cm^{-2}, the obtained particles were almost identical to the raw particles. Figures 3. 1(c) and 1(d) show the particles irradiated with a picosecond laser for 20 min. Picosecond laser irradiation at a laser fluence of 50 and 67 mJ pulse^{-1} cm^{-2} resulted in submicrometer spherical particle formation. Thus, a low laser fluence is sufficient to synthesize submicrometer spherical particles with a small pulse width. This result indicates that the heat loss from particles irradiated with a picosecond laser is lower than that from particles irradiated with a nanosecond laser during pulsed laser heating.

Figures 3. 2(a) and 2(c) shows SEM images of particles irradiated with a pulsed laser with different pulse widths at a laser fluence of 67 mJ pulse^{-1} cm^{-2}. The final diameter of particle irradiated with a pulsed laser for sufficient time is determined by the laser fluence, because the laser fluence determines the maximum diameter of the particle which can be melted.[22)] To irradiate with a pulsed laser for sufficient time, the irradiation times were three times longer than those used on the particles shown in Fig. 3. 1; the irradiation time with the nanosecond laser was 30 min and that with the picosecond laser was 60 min. Based on these SEM images, the size distributions of the submicrometer spherical particles irradiated with a pulsed laser with different pulse widths were graphed by measuring the sizes of more than 300 particles [Figs. 3. 2(b) and 2(d)]. The average diameter of the particles irradiated with the nanosecond laser was 111 nm and that of the particles irradiated with the picosecond laser was 74 nm. This finding indicates that the average diameter of submicrometer spherical particles also

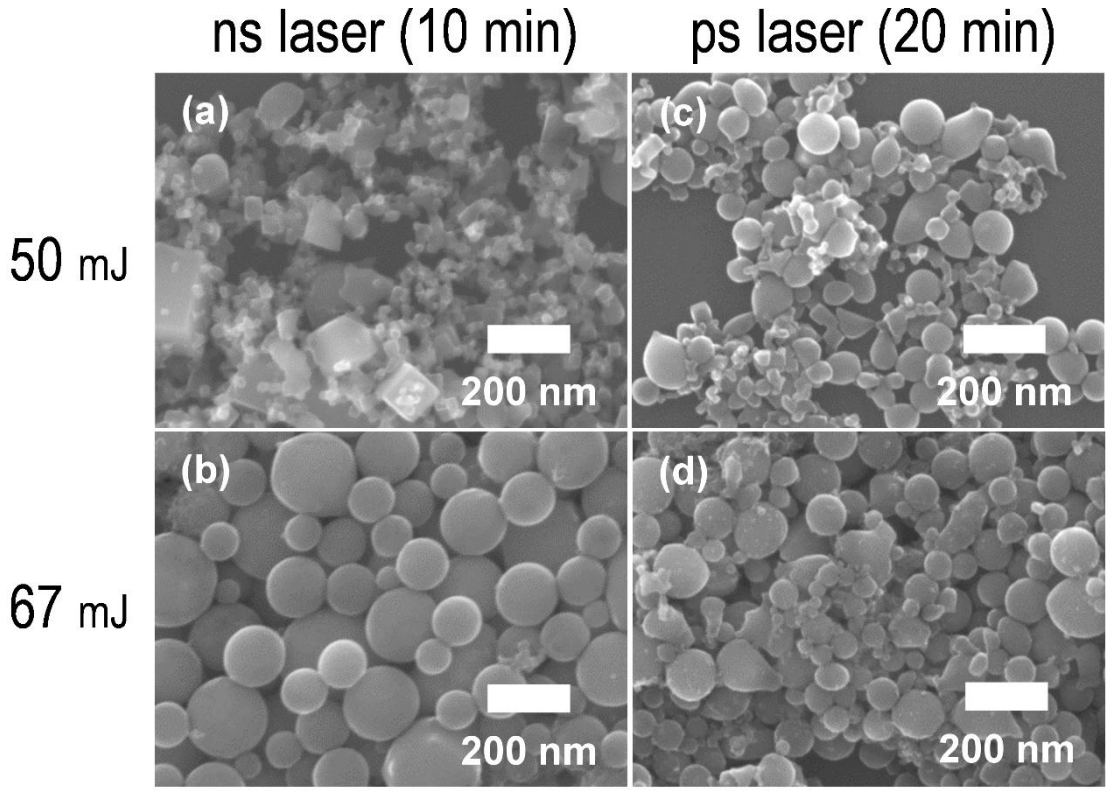

Figure 3. 1. SEM images of TiN particles irradiated (a, b) with a nanosecond laser for 10 min and (c, d) with a picosecond laser for 20 min with laser fluence values of (a, c) 50 mJ pulse^{-1} cm^{-2} and (b, d) 67 mJ pulse^{-1} cm^{-2}.

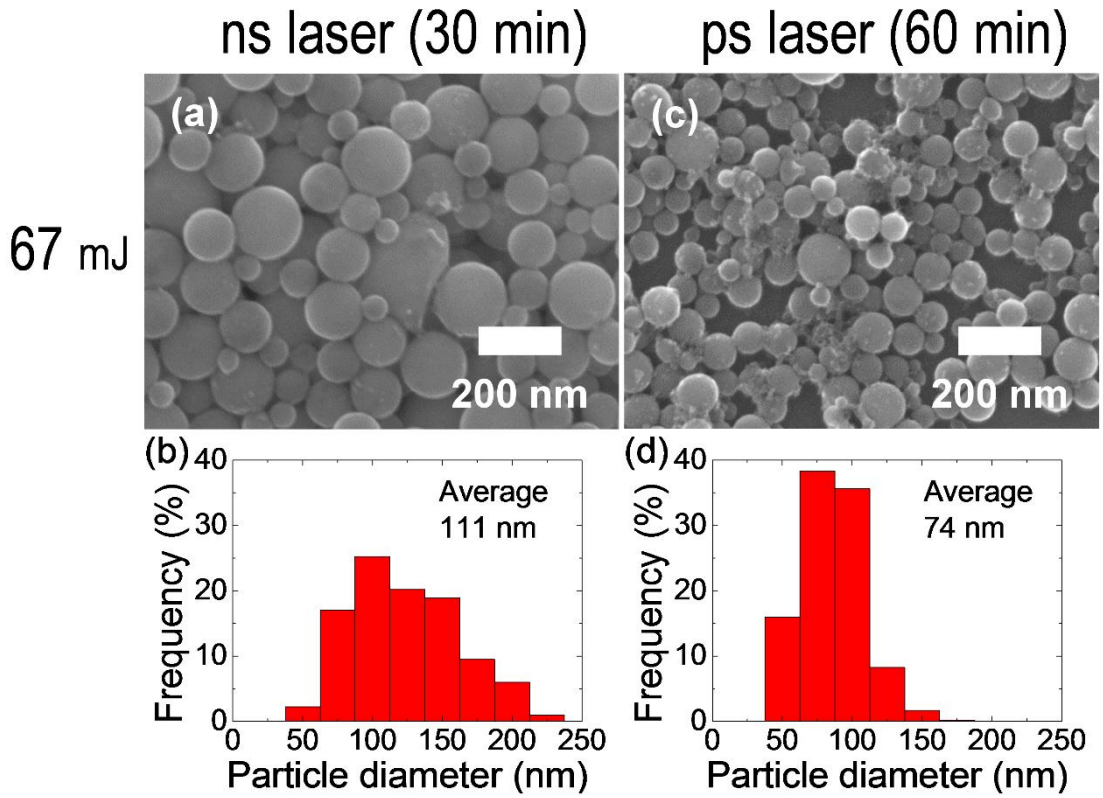

Figure 3. 2. SEM images of TiN particles irradiated (a) with a nanosecond laser for 30 min and (c) with a picosecond laser for 60 min at the laser fluence of 67 mJ pulse^{-1} cm^{-2} and the corresponding size distributions of TiN particles irradiated (b) with a nanosecond laser for 30 min and (d) with a picosecond laser for 60 min.

decreases with decreasing pulse width.

Figure 3. 3 shows XRD patterns of the particles depicted in Fig. 3. 2, which were irradiated with picosecond and nanosecond lasers at a laser fluence of 67 mJ pulse^{-1} cm^{-2}; a logarithmic ordinate scale was used to emphasize peaks from minor components of particles. Both samples exhibited strong XRD peaks corresponding to TiN. For nanosecond laser irradiation, peaks corresponding to rutile TiO_2 appeared, indicating a slight oxidation of TiN. This result is consistent with a previous report of the formation of TiO_2 and TiO_xN_y by PLML.[23] In contrast, for picosecond laser irradiation, there was no peak indicating the presence of rutile TiO_2, but the broad and weak peaks in the XRD diffraction pattern corresponding to TiO_xN_y were observed in higher 2θ angles relative to the peaks corresponding to TiN.[24] The particle heating time with a picosecond laser is shorter than that with a nanosecond laser, and the cooling time of the small particles obtained by picosecond laser irradiation is shorter than that of the large particles obtained by nanosecond laser irradiation.[16,17] Therefore, the oxidation reaction between particles and liquid may be suppressed due to the reduction in reaction time at high temperature.

The thermal diffusion length during pulsed laser heating is given by the following well-known diffusion equation:

$$l(t) = \sqrt{\frac{2 \cdot k \cdot \tau}{\rho \cdot C}}, \qquad (1)$$

where k is the heat conductivity of the particles, τ is the pulse width, ρ is the density of the particles, and C is the specific heat of the particles. Thermal diffusion length in TiN particles during pulsed laser heating calculated by Eq. (1) based on the physical properties of TiN[25] in Table 3. 1 is 17.6 nm for picosecond laser and 233 nm for nanosecond laser. The thermal diffusion length increases with the heating duration.

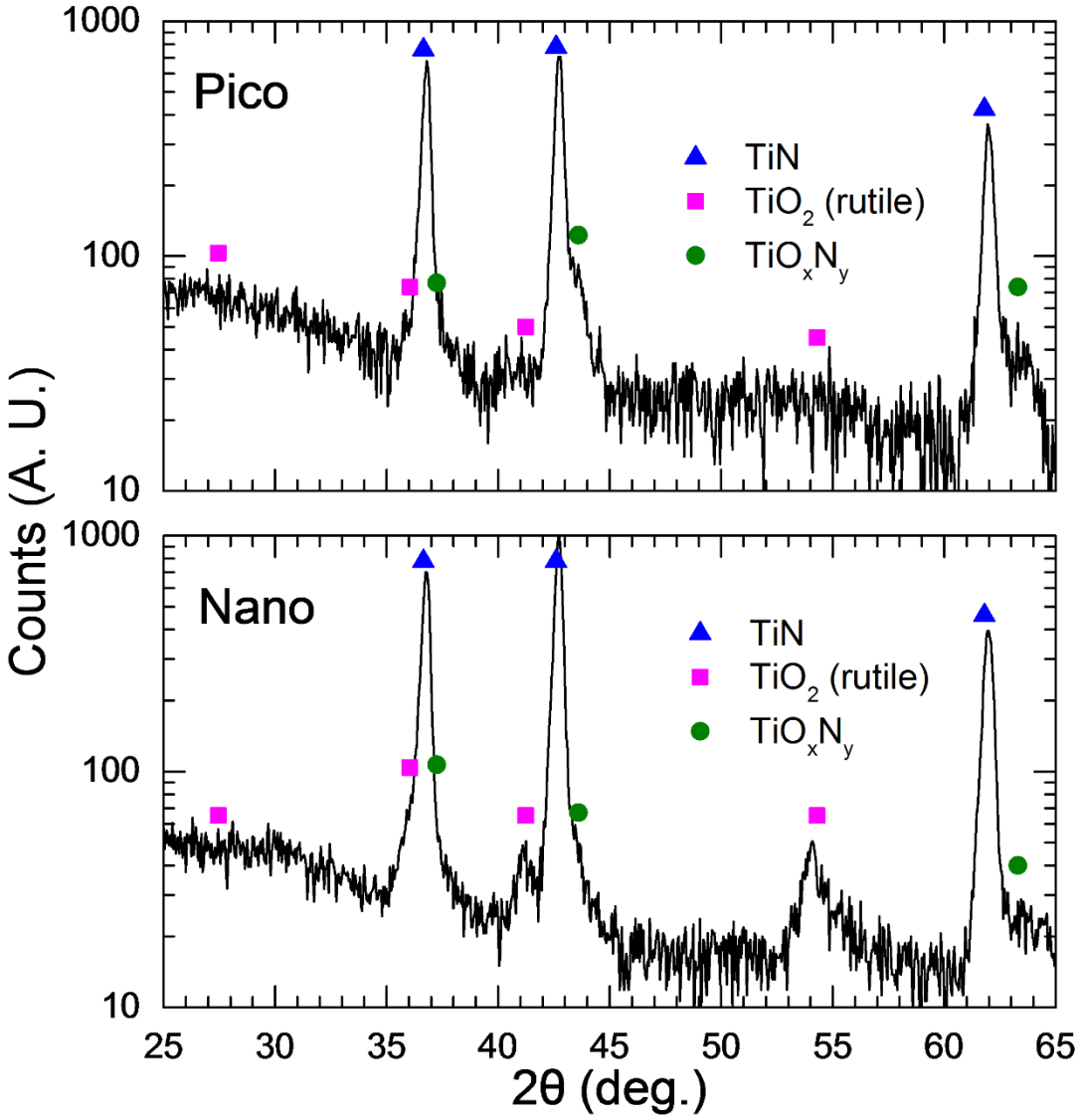

Figure 3. 3. XRD patterns of the particles irradiated with a picosecond and nanosecond lasers at a laser fluence of 67 mJ pulse^{-1} cm^{-2} depicted in Fig. 3. 3. 2.

Figure 3. 4 shows the spatial distribution of the resistive heat loss density from TiN spherical particles of 50 nm and 100 nm in diameter owing to electromagnetic wave irradiation by a plane-polarized light with a wavelength of 532 nm using the constants in Table 3. 2. The distributions were calculated using COMSOL Multiphysics®, a commercial software based on the finite element method. In this size range, TiN particles are heated mainly at their surfaces by the laser light irradiation. The thermal diffusion length during nanosecond laser heating (233 nm) is larger than the diameter of the particles obtained by nanosecond laser irradiation. Therefore, thermal energy diffuses from the particle surface which absorbs laser energy to the entire particle during pulsed laser heating, resulting in homogeneous heating and melting the particles. In contrast, the thermal diffusion length during picosecond laser heating (17.6 nm) is smaller than the diameter of the particles obtained by picosecond laser irradiation. Therefore, particles are partially heated at the incident light side of the particle surface during pulsed laser heating. The size of the obtained particles decreases with decreasing thermal diffusion length, which depends on the pulse width.

As shown experimentally and theoretically, the particle heating−cooling model developed by our group can be applied to calculate the particle temperature during pulsed laser irradiation.[17)] Particles are heated via laser absorption depending on the time profile of laser pulse. The absorption efficiency can be calculated from the refractive index and extinction coefficient of TiN[26)] shown in Table 3. 2 based on the Mie theory. In this model, the heat loss due to particle cooling is considered, and it is assumed that all laser energy absorbed by the particles is converted into heat energy. Hence, the laser fluence required for the melting start are calculated based on this particle heating–cooling model considering the cooling effect of the surrounding liquid.

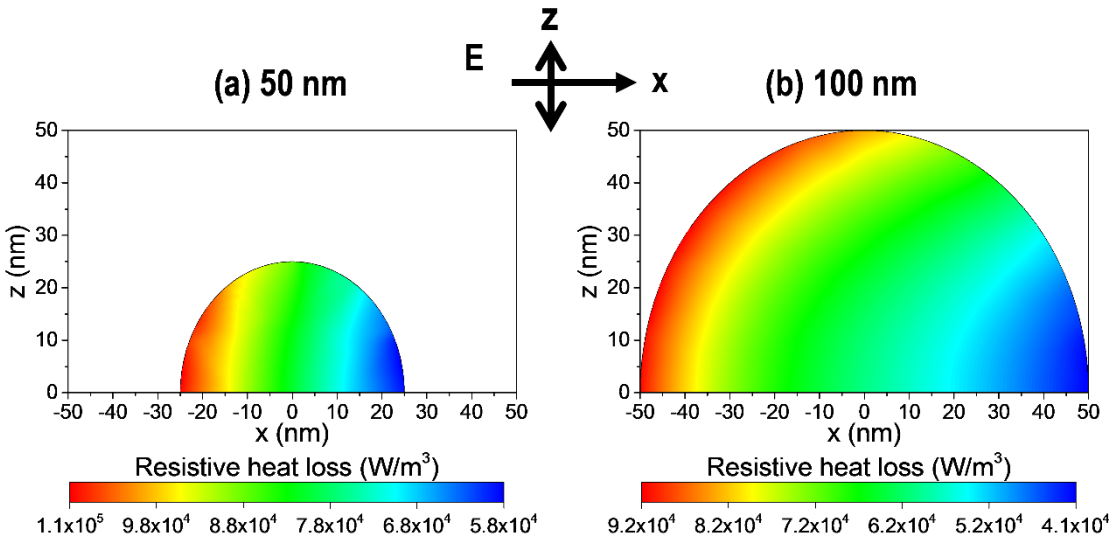

Figure 3. 4. Spatial distribution of density of the electromagnetic heat loss from TiN spherical particles with diameters of (a) 50 nm and (b) 100 nm when excited by plane-polarized light with a wavelength of 532 nm, resulting in local thermal heating by the electromagnetic wave (light) irradiation. Here, the light propagates in the X-direction, the electric field oscillates in the X–Z plane, and the magnetic field oscillates in the X–Y plane. The distributions were calculated using COMSOL Multiphysics®.

Table 3. 1. Physical properties of TiN

ρ (g/cm^3)	k (W/m · K)	C (kJ/kg · K)
5.22	19.2	0.951

Table 3. 2. Optical properties of TiN (532 nm)

refractive index	extinction coefficient
1.42	1.48

The fluence–size phase diagram for TiN spherical particles determined by the previously reported procedure is shown in Fig. 3. 5.[16,17] The phase diagram shows the phase boundary curves for the melting start when particles are irradiated with a nanosecond laser (red dotted line), a picosecond laser (blue solid line), and a pulsed laser without heat loss (black dashed line). With nanosecond laser heating, a higher amount of laser energy is needed to start the melting than under conditions without heat loss, especially with small particles (< 50 nm). Small particles are drastically cooled by the surrounding liquid because the cooling effect depends on the heat transfer coefficient, which is inversely proportional to the particle diameter.[17] With picosecond laser heating, however, the laser energy required to start the melting is almost the same as that without heat loss; almost all of the laser energy is transferred for particle heating because the heating rate is much faster than the cooling rate. Therefore, picosecond laser heating is an energy-efficient process for synthesizing submicrometer spherical particles.

This phase diagram illustrates that nanosecond laser irradiation at a laser fluence of 50 mJ pulse^{-1} cm^{-2} is insufficient to melt the particles owing to the particle cooling effect. Therefore, submicrometer spherical particles could not be synthesized via nanosecond laser irradiation with a laser fluence of 50 mJ pulse^{-1} cm^{-2}. By increasing the laser fluence, the size of the particles produced via nanosecond PLML is reported to be increased.[14–17] This is probably due to the repetitive melting and fusing process of the particles.[22] In PLML, the agglomerates of the particles melt and fuse, resulting in relatively large particles formation. Then, the growth process continues as long as the particles can be melted. The phase diagram shown in Fig. 3. 5 suggests that at a laser fluence of 67 mJ pulse^{-1} cm^{-2}, particles smaller than 120 nm melt to form submicrometer spherical particles; the particles experimentally obtained by nanosecond laser irradiation are approximately 111 nm in size, as measured from the SEM images. However, the particles obtained by picosecond laser irradiation were much smaller than

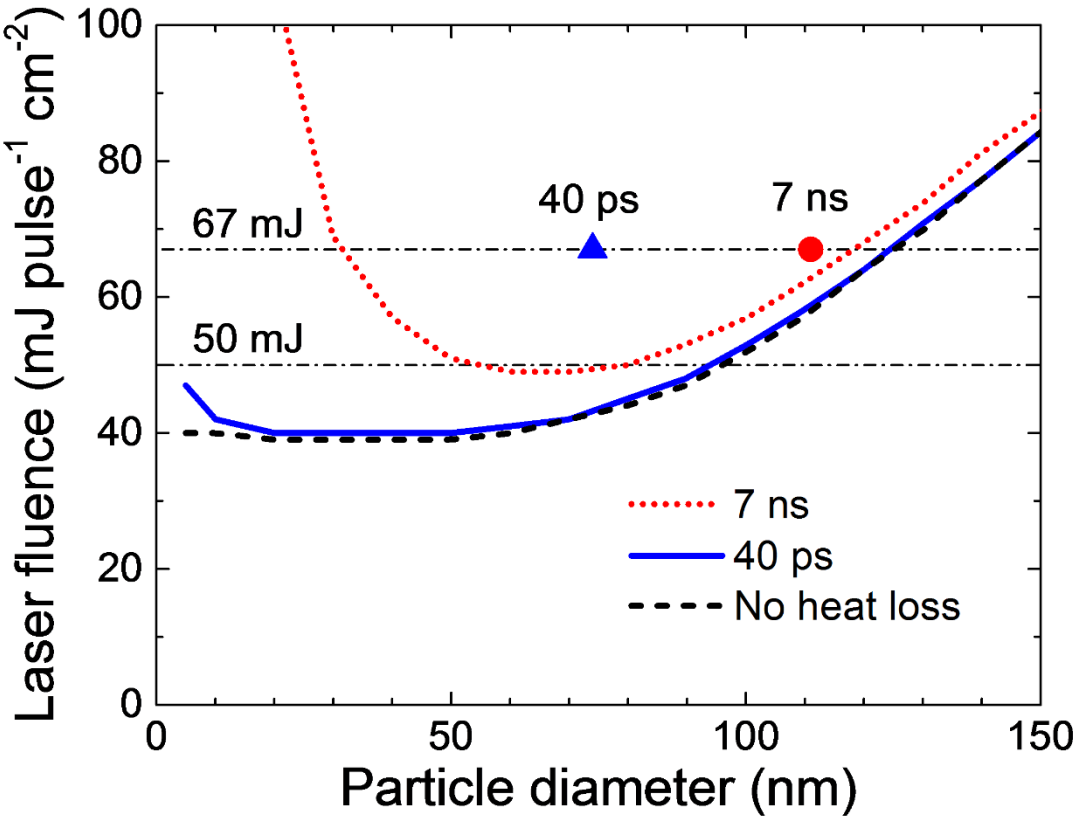

Figure 3. 5. Phase diagram of TiN spherical particles at the melting start calculated according to the particle heating–cooling model and accounting for the cooling effect of the surrounding liquid. Irradiation with a nanosecond laser (red dotted line), a picosecond laser (blue line), and a laser without heat loss (black dashed line) are shown. The average diameters of the obtained particles after nanosecond laser irradiation (red circle) and picosecond laser irradiation (blue triangle) are also plotted.

the size estimated from the fluence-size phase diagram and were close to the raw particle size. This is probably due to insufficient fusing induced by the inhomogeneous heating of raw particles by picosecond laser heating.

Figure 3. 6 shows an SEM image of particles irradiated with a picosecond laser for 20 min at a laser fluence of 167 mJ pulse^{-1} cm^{-2}. Nanoparticles were mainly observed, but a few submicrometer spherical particles were seen. In case of nanosecond laser heating, nanoparticles were main product at a laser fluence of 350 mJ pulse^{-1} cm^{-2}.[23] The laser fluence at which nanoparticles were mainly formed decreased with decreasing pulse width. The laser intensity ($I = J/\tau$ where J is the laser fluence and τ is pulse width) of the picosecond (40 ps) laser exceeds 10^{13} W/m^2, which is two orders of magnitude larger than that of nanosecond (7 ns) laser. The thermal diffusion length during picosecond laser heating is smaller than the size of the agglomerates. Therefore, the agglomerates of raw particles partially evaporate under high-intensity picosecond laser irradiation, resulting in nanoparticle formation. The Coulomb explosion of the particles would not occur because the electron–phonon coupling period (10 fs for TiN at 298 K) is shorter than the picosecond time scale.[27]

Because the laser fluence threshold for submicrometer spherical particle formation decreased as the pulse width decreased (from nanoseconds to picoseconds), it can be concluded that the heat loss during pulsed laser melting in liquid is reduced in the case of ultrafast heating. The calculations also show that particles are heated with negligible heat loss during the pulsed laser heating with a picosecond laser. Therefore, the picosecond laser irradiation of colloidal particles is an energy-efficient method for pulsed laser melting in liquid. The oxidation reaction is suppressed by picosecond laser irradiation because the reaction time at the high temperature induced by picosecond laser irradiation is shorter than that with nanosecond laser irradiation. The size of the obtained particles also decreased with decreasing pulse width from nanoseconds to picoseconds, which can be attributed to the decrease in the thermal diffusion length in the particles. The thermal

diffusion length during picosecond laser heating is smaller than the size of the particles, implying that the particles irradiated with a picosecond laser are only partially heated. This result suggests that tuning the thermal diffusion length by varying the pulse width may lead to size control of submicrometer spherical particles.

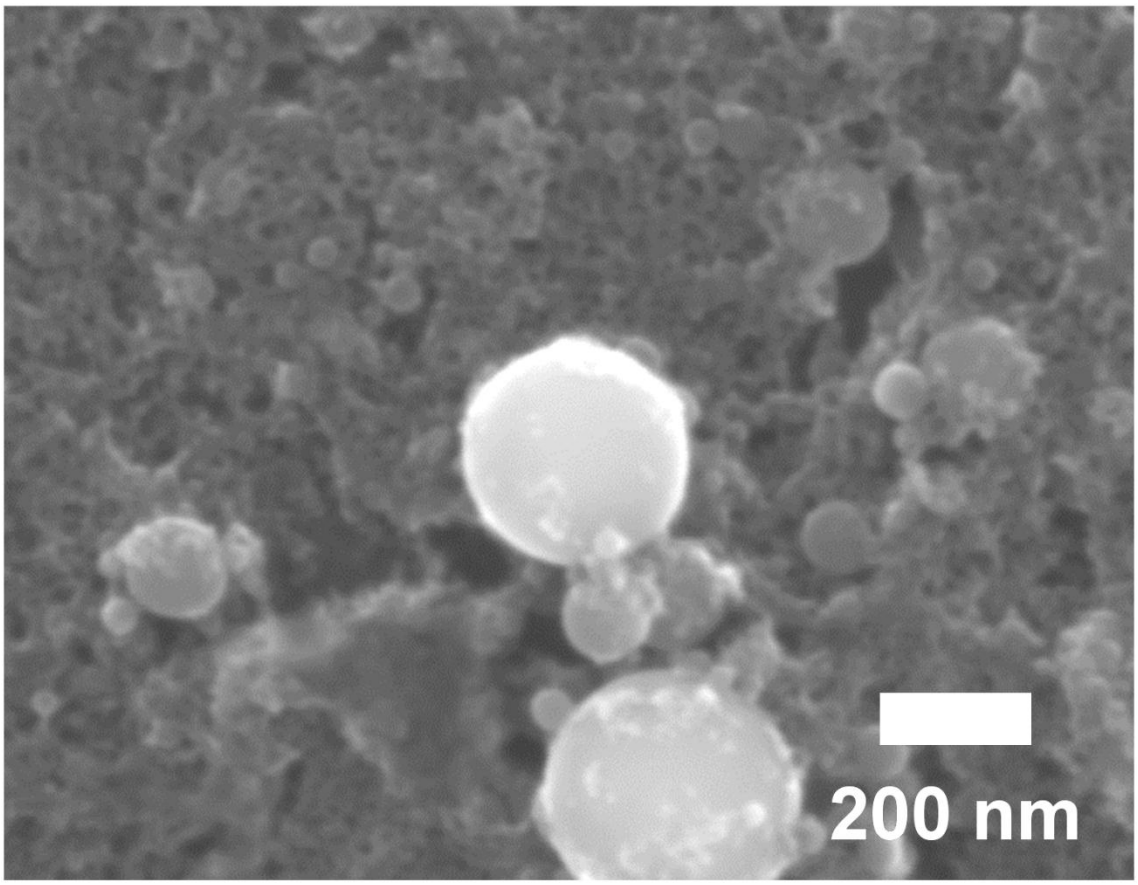

Figure 3. 6. SEM image of TiN particles irradiated with a picosecond laser for 20 min with a laser fluence of 167 mJ pulse^{-1} cm^{-2}.

References

[1] C.-Y. Shih, C. Wu, M. V. Shugaev, and L. V. Zhigilei, J. Colloid Interface Sci. **489**, 3 (2017).

[2] S. Ibrahimkutty, P. Wagener, T. d. S. Rolo, D. Karpov, A. Menzel, T. Baumbach, S. Barcikowski, and A. Plech, Sci. Rep. **5**, 16313 (2015).

[3] K. Sasaki, T. Nakano, W. Soliman, and N. Takada, Appl. Phys. Exp. **2**, 046501 (2009).

[4] S. Ibrahimkutty, P. Wagener, A. Menzel, A. Plech, and S. Barcikowski, Appl. Phys. Lett. **101**, 103104 (2012).

[5] D. Zhang, B. Gökce, and S. Barcikowski, Chem. Rev. **117**, 3990 (2017).

[6] F. Mafuné, J.-y. Kohno, Y. Takeda, T. Kondow, and H. Sawabe, J. Phys. Chem. C **104**, 9111 (2000).

[7] N. N. Luo, X. Tian, C. Yang, J. Xiao, W. Hu, D. Chen, and L. Li, Phys. Chem. Chem. Phys. **15**, 12235 (2013).

[8] V. Amendola, P. Riello, and M. Meneghetti, J. Phys. Chem. C **115**, 5140 (2011).

[9] Y. Ishikawa, K. Kawaguchi, Y. Shimizu, T. Sasaki, and N. Koshizaki, Chem. Phys. Lett. **428**, 426 (2006).

[10] S. Barcikowski, A. Menéndez-Manjón, B. Chichkov, M. Brikas, and G. Račiukaitis, Appl. Phys. Lett. **91**, 083113 (2007).

[11] S.-S. Wellershoff, J. Hohlfeld, J. Güdde, and E. Matthias, Appl. Phys. A **69**, 99 (1999).

[12] Y. Ishikawa, Y. Shimizu, T. Sasaki, and N. Koshizaki, Appl. Phys. Lett. **91**, 161110 (2007).

[13] H. Wang, M. Miyauchi, Y. Ishikawa, A. Pyatenko, N. Koshizaki, Y. Li, L. Li, X. Li, Y. Bando, and D. Golberg, J. Am. Chem. Soc. **133**, 19102 (2011).

[14] H. Wang, N. Koshizaki, L. Li, L. Jia, K. Kawaguchi, X. Li, A. Pyatenko, Z. Swiatkowska-Warkocka, Y. Bando, and D. Golberg, Adv. Mater. **23**, 1865 (2011).

[15] H. Wang, A. Pyatenko, K. Kawaguchi, X. Li, Z. Swiatkowska-Warkocka, and N. Koshizaki, Angew. Chem. Int. Ed. **49**, 6361 (2010).
[16] A. Pyatenko, H. Wang, N. Koshizaki, and T. Tsuji, Laser Photonics Rev. **7**, 596 (2013).
[17] S. Sakaki, H. Ikenoue, T. Tsuji, Y. Ishikawa, and N. Koshizaki, ChemPhysChem **18**, 1101 (2017).
[18] D. Zhang, M. Lau, S. Lu, S. Barcikowski, and B. Gökce, Sci. Rep. **7**, 40355 (2017).
[19] M. Lau, and S. Barcikowski, Appl. Surf. Sci. **348**, 22 (2015).
[20] S. Ishii, R. P. Sugavaneshwar, and T. Nagao, J. Phys. Chem. C **120**, 2343 (2016).
[21] G. V. Naik, J. L. Schroeder, X. Ni, A. V. Kildishev, T. D. Sands, and A. Boltasseva, Opt. Mater. Express **2**, 478 (2012).
[22] A. Pyatenko, H. Wang, and Naoto Koshizaki, J. Phys. Chem. C **118**, 4495 (2014).
[23] K. Kawasoe, Y. Ishikawa, N. Koshizaki, T. Yano, O. Odawara, and H. Wada, Appl. Phys. B **119**, 475 (2015).
[24] N. Martin, O. Banakh, A.M.E. Santo, S. Springer, R. Sanjinés, J. Takadoum, and F. Lévy, Appl. Surf. Sci. **185**, 123 (2001).
[25] S. Jeon, C. J. V. Tyne, and H. Lee, Ceram. Int. **40**, 8677 (2014).
[26] P. Patsalas, N. Kalfagiannis, and S. Kassavetis, Materials **8**, 3128 (2015).
[27] A. B. Mei, A. Rockett, L. Hultman, I. Petrov, and J. E. Greene, J. Appl. Phys. **114**, 193708 (2013).

Chapter 4

Influence of Pulse Frequency on Synthesis of Nano and Submicrometer Spherical Particles by Pulsed Laser Melting in Liquid

(This is the following article: https://doi.org/10.1016/j.apsusc.2017.10.235)

4. 1. Introduction

In recent years, much attention has been focused on nanoparticle fabrication by pulsed laser ablation in liquid (PLAL).[1–6] In PLAL, a bulk target immersed in liquid is irradiated with a high power pulsed laser, and nanoparticles are formed through explosive interaction between the bulk target and the laser pulses.[5] Size reduction of nanoparticles caused by pulsed laser fragmentation in liquid (PLFL) has also been investigated.[6–12] In PLFL, dispersed particles interact explosively with a high power pulsed laser, and nanoparticles are formed.[12] These techniques require fewer chemical reagents and no vacuum equipment.

SMSPs of various materials are fabricated by pulsed laser irradiation with relatively low laser fluence onto colloidal nanoparticles dispersed in liquid.[6, 13–20] In this method, a suspension in a glass vessel is generally irradiated for an appropriate time with magnetic stirring. Parts of the raw nanoparticles dispersed in the suspension are irradiated and absorb laser energy; SMSPs are then formed by particle melting, fusing, and quenching.[20] By repeating this process, almost all the agglomerates consisting of raw nanoparticles in the suspension are modified to form SMSPs. NSPs are also fabricated by this method at higher laser fluence than that used to form submicrometer particles.[21] Raw particles that absorb the laser energy are heated above the boiling point of the material and evaporated,

resulting in NSP formation at relatively high laser fluence.

In this method, an Nd:YAG laser with a pulse frequency of several tens of hertz is usually used.[15] Therefore, laser irradiation at higher pulse frequencies is probably effective in reducing the total irradiation time required to treat almost all the raw particles in the vessel. In PLAL, ablated mass linearly increases with pulse frequency in the kHz and MHz regime until the temporal bubble-shielding effect arises.[22, 23] In PLML, kHz laser is also used to fabricate SMSPs.[24] However, the pulse frequency might affect particle cooling, because the interval between two consecutive laser pulses, that is, the maximum available time to cool particles heated over the melting point, would be comparable to the cooling time reported as 10^{-4} to 10^{-3} s when a high-frequency pulsed laser is used.[25] If the pulse interval is shorter than the cooling time, heat energy acquired from a single laser pulse cannot be completely dissipated within the pulse interval and will persist until a subsequent pulse arrives, resulting in a gradual temperature increase by heat accumulation in a particle even during the pulse interval. In this study, SMSPs are fabricated by KrF excimer laser irradiation at higher pulse frequencies than before to study the pulse frequency effect on the obtained particles.

4. 2. Experimental section

Commercial ZnO particles (Sigma-Aldrich Co., LLC, < 100 nm) were dispersed in deionized water at a concentration of 200 ppm. Then, 6 ml of the suspension in a glass vessel was irradiated with a KrF excimer laser (Gigaphoton Inc., wavelength 248 nm, pulse width 50 ns) at various pulse frequencies (25–800 Hz). The beam size was 0.13 cm^2 (1.5 mm × 8.7 mm rectangle). The total number of pulses was fixed at 48,000 irrespective of the pulse frequency. Therefore, laser irradiation with a higher pulse frequency requires a shorter time to produce 48,000 pulses. The suspension temperature

was measured with a thermocouple immersed in the liquid. After laser irradiation, the suspension was dropped onto a Si substrate to observe the particle morphology using a field-emission scanning electron microscope (FE-SEM, JSM-7001FA, JEOL Ltd.). To measure the size of the obtained SMSPs, the suspension was settled for a day to separate the NSPs from the produced SMSPs. A precipitate of the suspension was also dropped onto a Si substrate for FE-SEM observation.

4. 3. Results and discussion

4. 3. 1. Particle morphology

SEM images of raw ZnO particles and particles obtained by KrF excimer laser irradiation at 100 Hz are presented in Fig. 4. 1. Raw particles have angular morphology, and the average diameter of the raw particles is about 60 nm (Figure 4. 1(a)). At a laser fluence of 182 mJ pulse^{-1} cm^{-2}, agglomerates of raw particles melted, and SMSPs with an average diameter of 324 nm were formed (Fig. 4. 1(b)). In contrast, at a laser fluence of 203 mJ pulse^{-1} cm^{-2}, NSPs with an average diameter of 44 nm were formed in addition to SMSPs with an average diameter of 327 nm (Fig. 4. 1(c)). In this case, agglomerates of raw ZnO particles would be vaporized by high-fluence laser irradiation. The vapor condenses and then solidifies to form spherical nanoparticles.

Fig. 4. 2 shows SEM images of particles obtained after KrF excimer laser irradiation (182 mJ pulse^{-1} cm^{-2}) at various pulse frequencies. The time taken to produce 48,000 pulses is 1,920 seconds at 25 Hz, 240 seconds at 200 Hz, 120 seconds at 400 Hz, and 60 seconds at 800 Hz. At pulse frequencies of 25 Hz to 200 Hz, almost all the obtained particles were SMSPs (Figs 4. 2(a) and 2(b)). In contrast, at a pulse frequency of 400 Hz and above (Figs 4. 2(c) and 2(d)), NSPs were formed in addition to SMSPs, although a

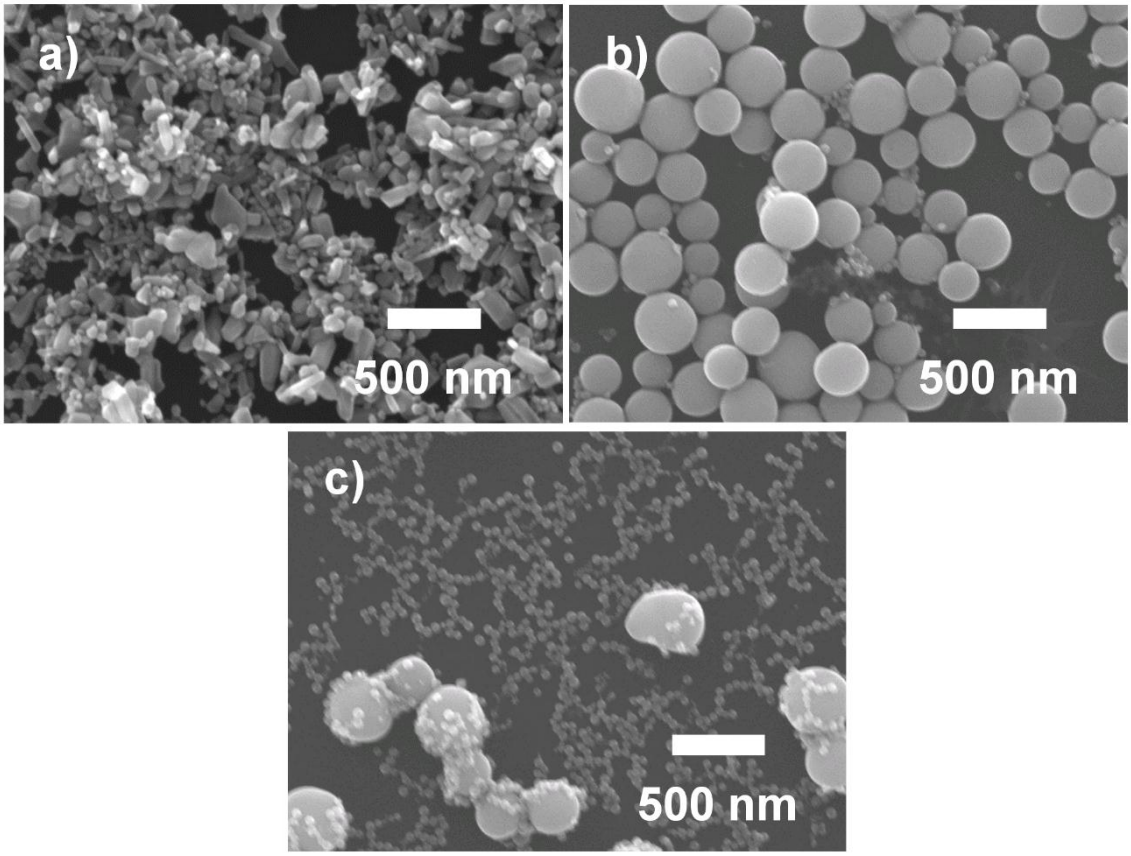

Figure 4. 1. SEM images of (a) raw ZnO particles and particles irradiated with a KrF excimer laser (100 Hz) at a laser fluence of (b) 182 mJ pulse^{-1} cm^{-2} and (c) 203 mJ pulse^{-1} cm^{-2}.

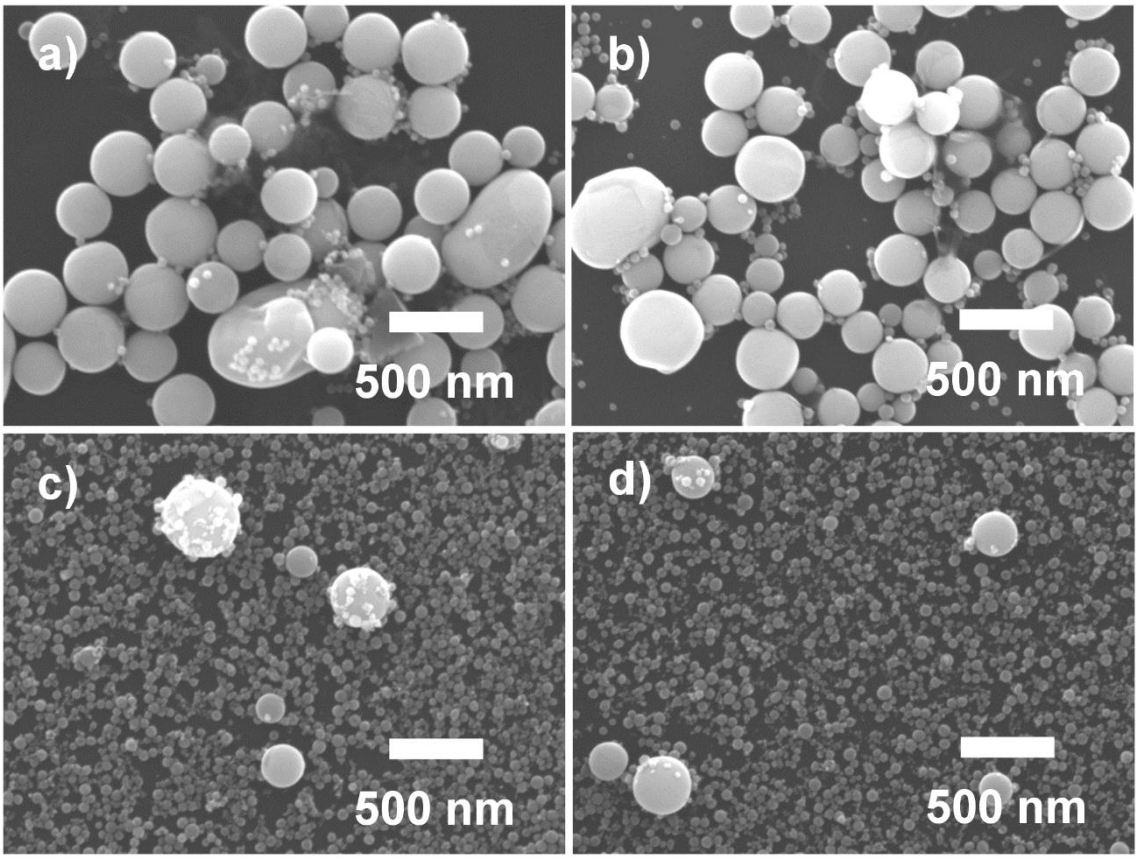

Figure 4. 2. SEM images of ZnO particles irradiated with a KrF excimer laser at a laser fluence of 182 mJ pulse^{-1} cm^{-2}. Pulse frequency of (a) 25 Hz, (b) 200 Hz, (c) 400 Hz, and (d) 800 Hz.

laser fluence of 182 mJ pulse^{-1} cm^{-2} was insufficient to obtain NSPs by vaporization at a pulse frequency of 100 Hz, as indicated in Fig. 4. 1. This result suggests that heat energy absorbed by a particle is not completely dissipated during the pulse interval and subsequently accumulates with consecutive laser pulses. Figs 4. 3(a-d) shows SEM images of ZnO particle precipitates by natural sedimentation of the suspension irradiated with a KrF excimer laser at various pulse frequencies as depicted in Fig. 4. 2. NSPs were easily separated from the suspension by natural sedimentation over one day. By counting the SMSPs in the SEM images of Figs 4. 3(a-d), histograms of particle diameter distribution are graphed, respectively (Figs 4. 3(e-f)).

Fig. 4. 4(a) shows the pulse frequency dependence of the mass fraction of SMSPs in the products estimated from SEM images shown in Fig. 4. 2. The mass fraction of the SMSPs to the all particles (SMSPs and NSPs) in the products was estimated by converting the size distribution data of all the SMSPs and NSPs in the SEM images into mass ratio of SMSPs to NSPs assuming that all particles are spherical and ZnO. Since the particle mass is proportional to the cube of the particle diameter, SMSPs are much heavier than NSPs. Before natural sedimentation, most particles obtained were SMSPs at a pulse frequency of 25 to 200 Hz. In contrast, at 400 Hz or higher, the mass fraction of SMSPs was drastically decreased through vaporization. Therefore, laser irradiation at a pulse frequency of 200 Hz and below is appropriate for effectively obtaining SMSPs. By natural sedimentation over one day, we could remove NSPs from the suspension and prepare an SMSP suspension with a mass fraction of over 90%.

The pulse frequency dependence on the average diameter of SMSPs measured from the histograms of particle diameter distribution (Figs 4. 3(e-h)) at a laser fluence of 182 mJ pulse^{-1} cm^{-2} is depicted in Fig. 4. 4(b). For a pulse frequency range where mainly SMSPs are obtained, as shown in Fig. 4. 2 ($\leq$ 200 Hz), obtained particles have similar sizes of about 300 nm. Thus, a larger pulse frequency up to 200 Hz is effective in reducing the irradiation time for SMSP synthesis. Above the threshold for NSP formation in Fig. 4. 2

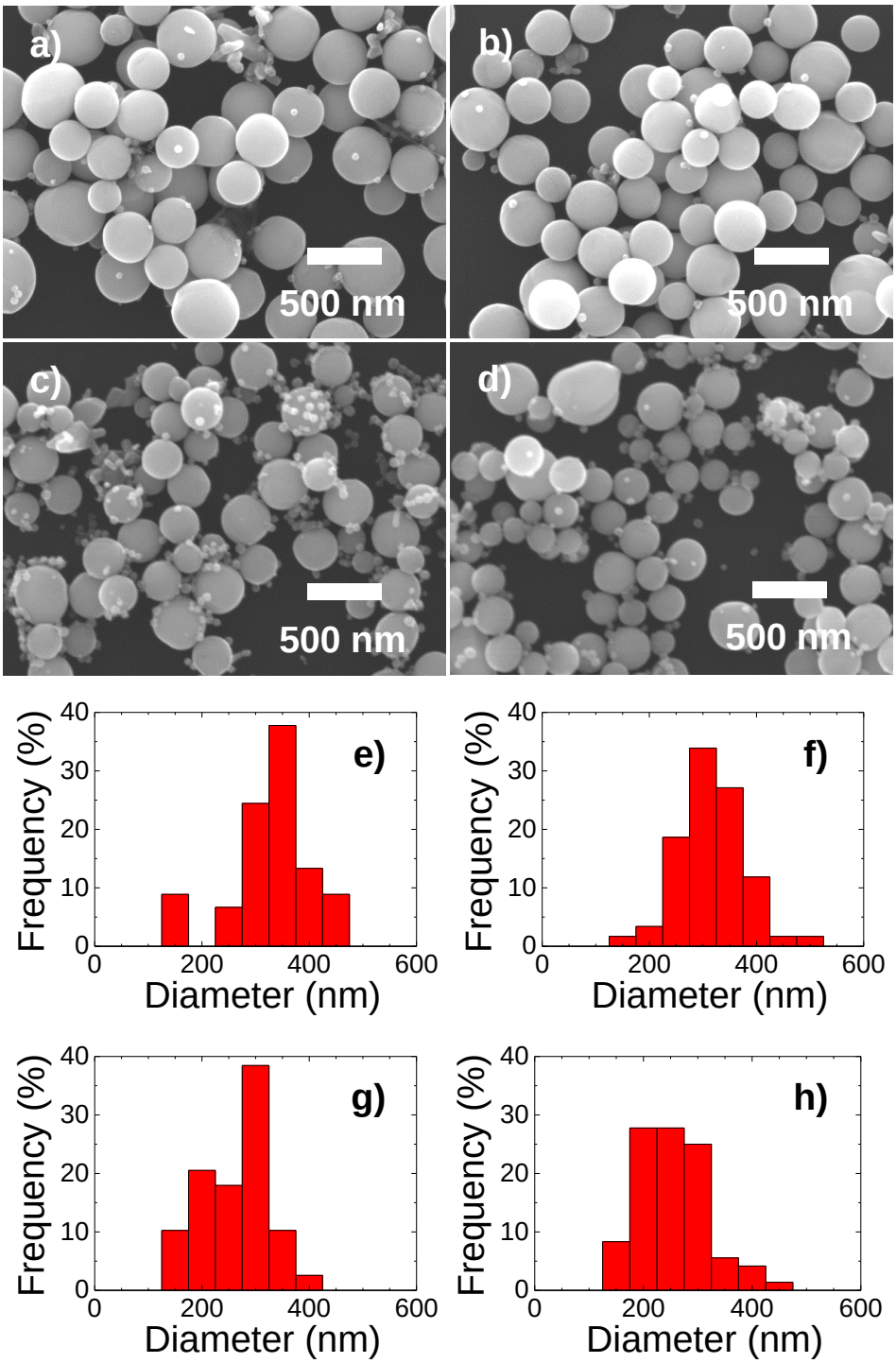

Figure 4. 3. SEM images of ZnO particle precipitates by natural sedimentation of the suspension irradiated with a KrF excimer laser irradiation at a laser fluence of 182 mJ pulse^{-1} cm^{-2}. Pulse frequency of (a) 25 Hz, (b) 200 Hz, (c) 400 Hz, and (d) 800 Hz. The corresponding particle diameter distributions of (a-d) are shown in (e-f), respectively.

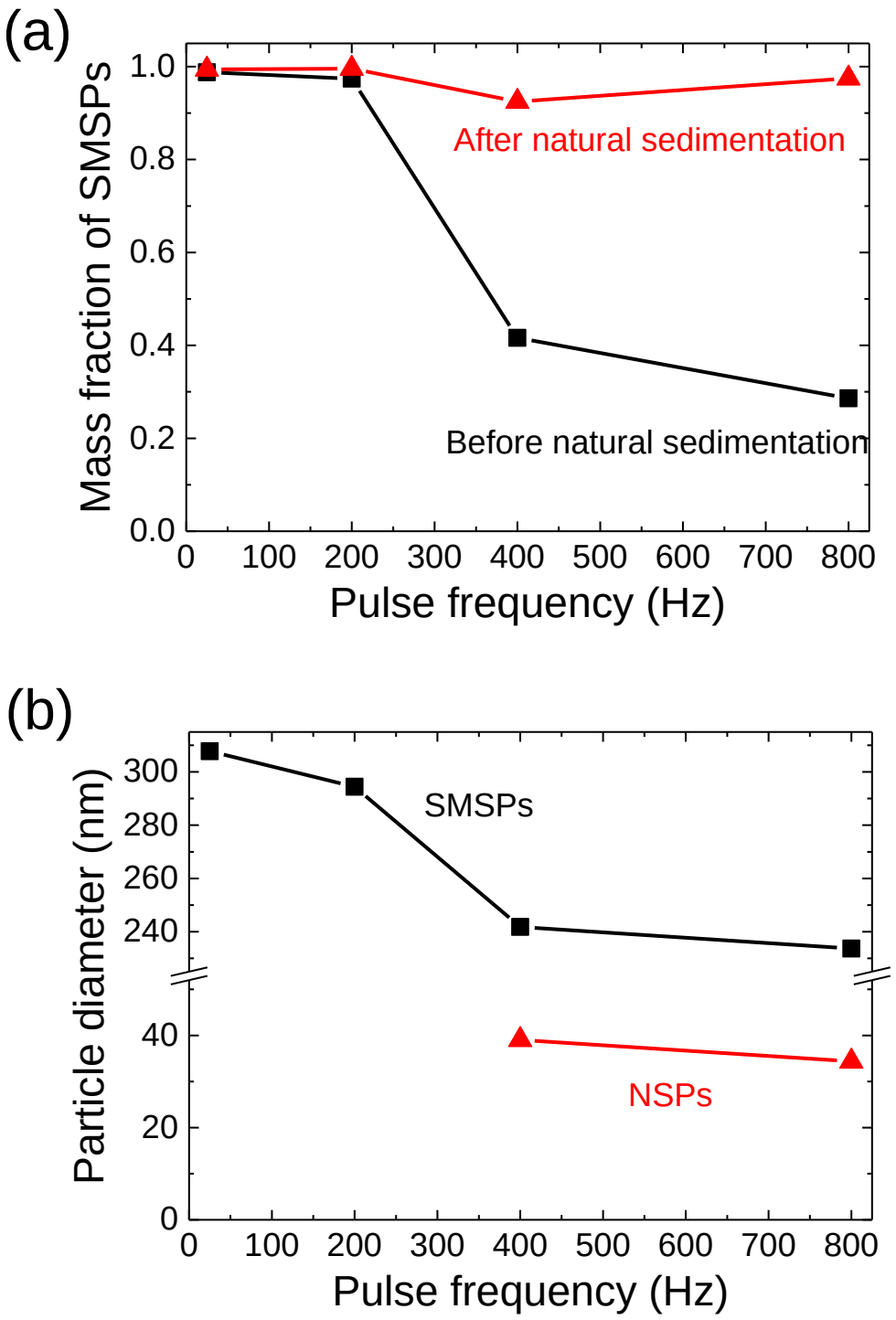

Figure 4. 4. Pulse frequency dependence on (a) mass fraction of SMSPs in the products and (b) average particle diameter measured by counting only ZnO SMSPs in Fig. 4. 3 and only NSPs in Fig. 4. 2 obtained by nanosecond pulsed KrF excimer laser irradiation at a laser fluence of 182 mJ $pulse^{-1}$ cm^{-2}.

(≥400 Hz), however, the obtained large particles have a submicrometer size of about 240 nm, which is smaller than those obtained at a lower pulse frequency (≤ 200 Hz). This result suggests that particles irradiated with a pulsed laser at high frequency might be heated, resulting in size reduction of the SMSPs due to partial evaporation.

Fig. 4. 4(b) also shows the pulse frequency dependence on the average diameter of NSPs measured from SEM images in Fig. 4. 2. The average particle diameter decreases with the pulse frequency above the threshold for NSP formation determined from Fig. 4. 2 (≥400 Hz). The average diameter of nanoparticles obtained by pulsed laser irradiation is reported to gradually decrease as the laser fluence increases.[9, 10)] Therefore, above the threshold for NSP formation, the effect of the pulse frequency on the change in nanoparticle size would correspond to the effect of laser fluence reported earlier. Heat accumulation resulting from consecutive high-frequency laser pulses would cause further heating of the particles.

4. 3. 2. Liquid temperature

The average suspension temperature during laser irradiation is gradually elevated by heat dissipation from the particles that absorb laser energy to the surrounding liquid. Fig. 4. 5 shows the suspension temperature increase in a glass vessel during laser irradiation at various pulse frequencies. The highest attained suspension temperature increases with pulse frequency because the input energy per unit time increases in proportion to the pulse frequency. However, the temperature of the liquid adjacent to the particles in the laser-irradiated region is higher than that of the laser-irradiated region remote from the particles, because the particles irradiated with laser pulses are the heat source for the suspension. Therefore, the temperature of the liquid adjacent to the particles is much higher than the average suspension temperature, and adjacent liquid would probably evaporate depending on the

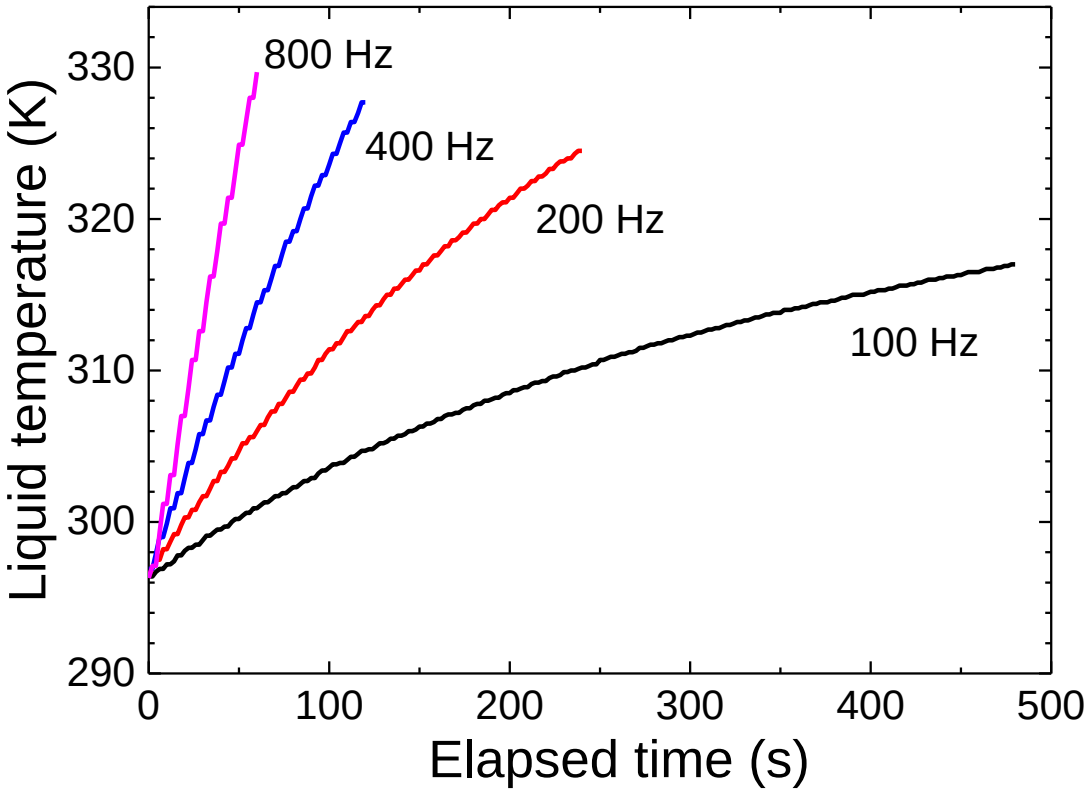

Figure 4. 5. Increase in the suspension temperature during laser irradiation at various pulse frequencies measured by thermocouple immersed in the liquid.

laser irradiation conditions, especially at the high input energy per unit time accompanying a high pulse frequency. Such a high liquid temperature would induce vaporization of the liquid at the interface and affect the highest attained temperature discussed in the following section.

4. 3. 3. Calculation of particle temperature

These experimental results suggest that the heat energy absorbed from a single laser pulse is not completely dissipated before the arrival of the subsequent laser pulse, and it accumulates in a particle as a result of consecutive laser pulses at high frequencies. Thus, the time required to completely dissipate the energy supplied by a laser pulse is estimated to be longer than 2.5 ms, which is the corresponding laser pulse interval for a pulse frequency of 400 Hz. However, this cooling time is much longer than the value estimated by conductive heat transfer calculation using the particle heating-cooling model.[26] The heat energy dissipated from the particles q_p is described by the following equation:

$$\frac{dq_p}{dt} = h \cdot \pi d^2 \cdot \{T_p - T_0\} \quad (1)$$

where

$$h = \frac{Nu_d \cdot k}{d} \quad (2)$$

Here, h is the heat transfer coefficient, d is the particle diameter, T_p is the particle temperature, T_0 is the temperature of the surrounding liquid, Nu_d is the Nusselt number, and k is the heat conductivity of the

surrounding liquid or vapor generated by liquid evaporation. On the submicrometer scale, the Nusselt number is constant at $Nu_d \approx 2$, because the convection around a submicrometer particle is negligible.[27, 28] When the particles are cooled by evaporated liquid, the heat transfer coefficient of particles 300 nm in diameter can be estimated as 0.29 MW m^{-2} K^{-1} from Eq. (2). In this case, particles heated to the melting point are cooled to the temperature of the surrounding liquid on a microsecond time scale. Therefore, a pulse interval of 2.5 ms is sufficient for particle cooling.

The heat energy accumulated in the particles E_p is the difference between particle heating by laser absorption and particle cooling by conductive heat transfer.

$$\frac{dE_p}{dt} = Q_{abs}^{\lambda} \cdot \frac{\pi d^2}{4} \cdot J(t) - \frac{dq}{dt} \quad (3)$$

Here, Q_{abs}^{λ} is the absorption efficiency, $\frac{\pi d^2}{4}$ is the particle geometric cross section, and $J(t)$ is the time-dependent laser fluence. The absorption efficiency of SMSPs is calculated from refractive index and extinction coefficient using Mie theory.[25, 29]

The particle temperature T_p below the melting point, at the melting point, and above the melting point is defined by the following equations.

$$T_p(t) = T_0 + \frac{1}{\rho_p \cdot \frac{\pi d^3}{6} \cdot c_s} \cdot E(t) \quad (4)$$

$$T_p(t) = T_m \quad (5)$$

$$T_p(t) = T_{\mathrm{m}} + \frac{1}{\rho_p \cdot \frac{\pi d^3}{6} \cdot c_l} \cdot \left[E(t) - \rho_p \cdot \frac{\pi d^3}{6} \cdot \left(H_{T_m} - H_{T_0} + \Delta H_m\right)\right] \quad (6)$$

Here, ρ_p is the density of the particle, $\frac{\pi d^3}{6}$ is the particle volume, c_s is the particle specific heat in the solid state, T_m is the melting point of the material, $H_{T_m} - H_{T_0}$ is the relative enthalpy required for the start of melting, ΔH_m is the latent enthalpy of melting, and c_l is the particle specific heat in the liquid state.

Fig. 4. 6 shows the calculated highest attained temperature of a ZnO spherical particle 250 nm in diameter irradiated with a nanosecond laser (pulse width 50 ns, laser fluence 182 mJ pulse^{-1} cm^{-2}). The highest attained temperature is elevated by an increase in the temperature of the surrounding liquid because this increases the initial particle temperature. Moreover, the highest attained temperature of the particles constantly cooled by a liquid vapor film (red line) was higher than that of the particles cooled by a liquid undergoing a phase transition from liquid to vapor (black line). When using a laser with a pulse width of several tens of nanoseconds, the particles dissipate heat energy to the surrounding liquid because heated particles are cooled by a liquid with high heat conductivity during the initial stage of heating.[26)] Therefore, a low-heat-conductive vapor film around the particles generated by heat accumulation reduces heat dissipation.

Calculations suggest that the highest attained temperature of a particle increases by a few hundred K through heat accumulation in the adjacent liquid. The actual attained temperature of particles irradiated with a pulsed laser at a laser fluence of 182 mJ pulse^{-1} cm^{-2} would be near the boiling point because NSPs were formed at a laser fluence of 203 mJ pulse^{-1} cm^{-2} (Fig. 4. 1). Therefore, heat accumulation in the liquid adjacent to particles may cause heating of the particles to the boiling point, resulting in nanoparticle formation at a pulse frequency of above 400 Hz.

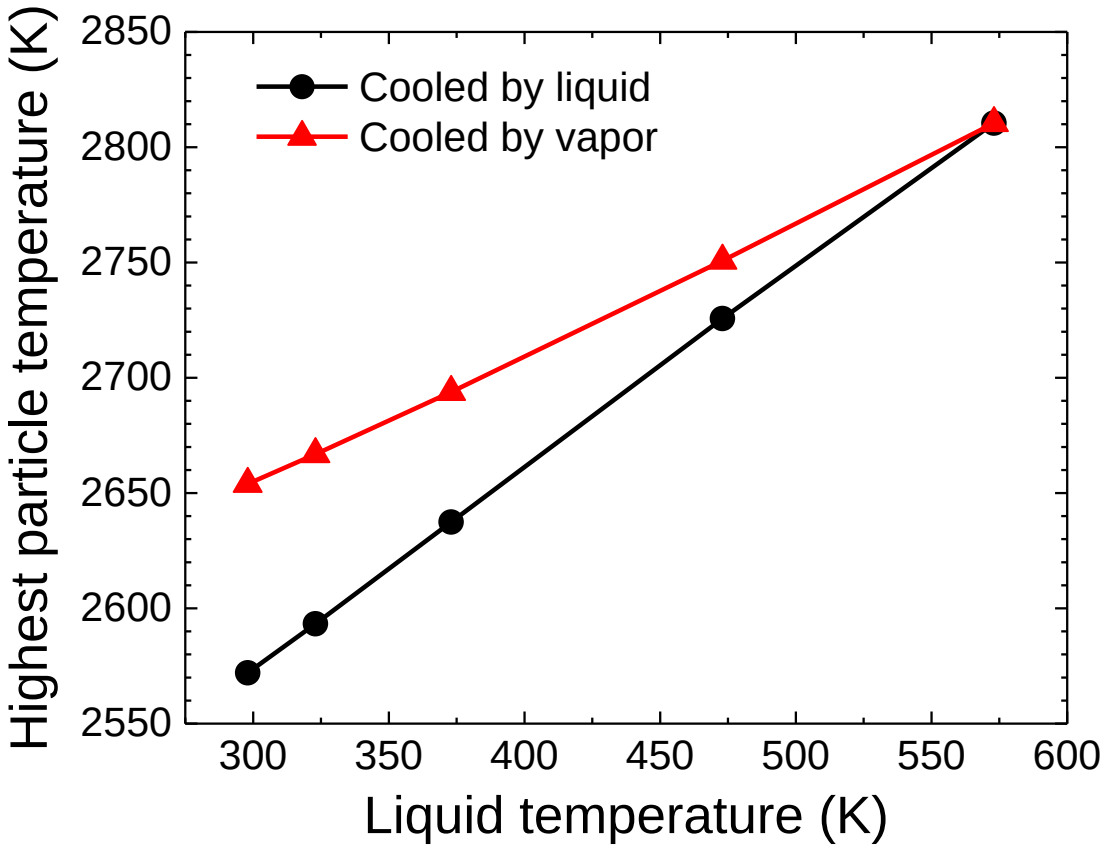

Figure 4. 6. Highest attained temperature of SMSPs 250 nm in diameter irradiated with a nanosecond laser with pulse width of 50 ns at a laser fluence of 182 mJ pulse^{-1} cm^{-2}. Cooling by surrounding liquid undergoing phase transition from liquid to vapor (Black line), and cooling by surrounding vapor generated by liquid evaporation (Red line).

4. 4. Conclusions

SMSPs were fabricated by irradiation with a KrF excimer laser (wavelength 248 nm, pulse width 50 ns) onto 6 ml of the suspension with a particle concentration of 200 ppm in a glass vessel. The total time of laser irradiation for the synthesis of SMSPs can be reduced using a high-frequency pulsed laser at a laser fluence of 182 mJ $pulse^{-1}$ cm^{-2} (≤ 200 Hz). The size of the obtained SMSPs is similar in this frequency range. In contrast, NSPs and SMSPs are simultaneously formed using a pulsed laser with a frequency of 400 Hz or higher. This result suggests that the laser energy is accumulated in particles and liquid by consecutive laser pulses, resulting in partial evaporation of the particles above the pulse frequency threshold (≥400 Hz). Through this vaporization process, the average diameter of the obtained SMSPs decreased. However, the time required to cool particles from the melting point to ambient temperature is much shorter than 2.5 ms (pulse interval for a pulse frequency of 400 Hz). Therefore, nanoparticle formation was attributed to an increase in the suspension temperature. The average suspension temperature was elevated during laser irradiation, especially at a high pulse frequency. The liquid temperature adjacent to the particles is higher than the average suspension temperature because the particles irradiated with laser pulses are the heat source for the suspension. Calculations suggest that the highest attained temperature of the particles increases by a few hundred K through heat accumulation in the adjacent liquid, resulting in nanoparticle formation at a high pulse frequency.

References

[1] P.P. Patil, D.M. Phase, S.A. Kulkarni, S.V. Ghaisas, S.K. Kulkarni, S.M. Kanetkar, S.B. Ogale, and V.G. Bhide, Phys. Rev. Lett. **58**, 238 (1987).

[2] J. Neddersen, G. Chumanov, and T.M. Cotton, Appl. Spectrosc. **47**, 1959 (1993).

[3] B.G. Ershov, E. Janata, and A. Henglein, J. Phys. Chem. **97**, 339 (1993).

[4] F. Mafuné, J. Kohno, Y. Takeda, and T. Kondow, J. Phys. Chem. B **104**, 9111 (2000).

[5] C. Liang, Y. Shimizu, M. Masuda, T. Sasaki, and N. Koshizaki, Chem. Mater. **16**, 963 (2004).

[6] D. Zhang, B. Gökce, and S. Barcikowski, Chem. Rev. **117**, 3990 (2017).

[7] P.V. Kamat, J. Phys. Chem. B **106**, 7729 (2002).

[8] D. Werner, A. Furube, T. Okamoto, and S. Hashimoto, J. Phys. Chem. C **115**, 8503 (2011).

[9] D. Werner, T. Ueki, and S. Hashimoto, J. Phys. Chem. C **116**, 5482 (2012).

[10] D. Werner, and S. Hashimoto, Langmuir **29**, 1295 (2013).

[11] P. Boyer, D. Ménard, and M. Meunier, J. Phys. Chem. C **114**, 13497 (2010).

[12] H. Usui, T. Sasaki, and N. Koshizaki, J. Phys. Chem. B **110**, 12890 (2006).

[13] Y. Ishikawa, Y. Shimizu, T. Sasaki, and N. Koshizaki, Appl. Phys. Lett. **91**, 161110 (2007).

[14] H. Wang, M. Miyauchi, Y. Ishikawa, A. Pyatenko, N. Koshizaki, Y. Li, L. Li, X. Li, Y. Bando, and D. Golberg, J. Am. Chem. Soc. **133**, 19102 (2011).

[15] H. Wang, N. Koshizaki, L. Li, L. Jia, K. Kawaguchi, X. Li, A. Pyatenko, Z. Swiatkowska-Warkocka, Y. Bando, and D. Golberg, Adv. Mater. **23**, 1865 (2011).

[16] T. Tsuji, T. Yahata, M. Yasutomo, K. Igawa, M. Tsuji, Y. Ishikawa, and

N. Koshizaki, Phys. Chem. Chem. Phys. **15**, 3099 (2013).
[17] X. Li, N. Koshizaki, A. Pyatenko, Y. Shimizu, H. Wang, J. Liu, X. Wang, M. Gao, Z. Wang, and X. Zeng, Opt. Express **19**, 2846 (2011).
[18] X. Li, A. Pyatenko, Y. Shimizu, H. Wang, K. Koga, and N. Koshizaki, Langmuir **27**, 5076 (2011).
[19] K. Kawasoe, Y. Ishikawa, N. Koshizaki, T. Yano, O. Odawara, and H. wada, Appl. Phys. B **119**, 475 (2015).
[20] H. Wang, A. Pyatenko, K. Kawaguchi, X. Li, Z. Swiatkowska-Warkocka, and N. Koshizaki, Angew. Chem. Int. Ed. **49**, 6361 (2010).
[21] Y. Ishikawa, N. Koshizaki, A. Pyatenko, N. Saitoh, N. Yoshizawa, and Y. Shimizu, J. Phys. Chem. C **120**, 2439 (2016).
[22] C. L. Sajti, R. Sattari, B. N. Chichkov, and S. Barcikowski, J. Phys. Chem. C **114**, 2421 (2010).
[23] R. Streubel, S. Barcikowski, and B. Gökce, Opt. Lett. **41**, 1486 (2016).
[24] D. Zhang, M. Lau, S. Lu, S. Barcikowski, and B. Gökce, Sci. Rep. **7**, 40355 (2017).
[25] A. Pyatenko, H. Wang, N. Koshizaki, and T. Tsuji, Laser Photonics Rev. **7**, 596 (2013).
[26] S. Sakaki, H. Ikenoue, T. Tsuji, Y. Ishikawa, and N. Koshizaki, ChemPhysChem **18**, 1101 (2017).
[27] A.F. Mills, Heat Transfer, 2nd ed., Prentice Hall, New York, pp. 275–282 (1998).
[28] J.S. Donner, G. Baffou, D. McCloskey, and R. Quidant, ACS Nano **5** 5457 (2011).
[29] G. Mie, Ann. Phys. **330**, 377 (1908).

Chapter 5

Heating process control of pulsed-laser melting in liquid via a burst-mode laser

(Applied Physics Express; Volume 12; Number 1; 015002, https://doi.org/10.7567/1882-0786/aaf284, Copyright 2019 The Japan Society of Applied Physics)

Laser synthesis methods of particles, such as pulsed-laser ablation in liquid (PLAL) and pulsed-laser melting in liquid (PLML), have attracted much attention because of their unique particle formation mechanism.[1–11] In PLAL, nanoparticles are formed through an explosive interaction caused by high-energy-density laser irradiation of a bulk target in liquid.[2–5] In PLML, submicrometer spherical particles (> 100 nm) are formed through an instantaneous melting caused by relatively low-energy-density pulsed-laser irradiation of nanoparticles dispersed in a liquid, followed by rapid cooling of the nanoparticles by the surrounding liquid.[6–11]

Particle synthesis by laser processing has advanced concurrently with laser technology. Recently, ultrafast laser systems have become commercially available as high-power laser sources. Barcikowski et al. synthesized nanoparticles by PLAL with a productivity of 4 g h^{-1} using a novel laser system consisting of a 500-W, 3-ps laser source.[12] In PLML, however, submicrometer spherical particles were synthesized by batch type irradiation with a low productivity of 7 mg h^{-1} using a typical laboratory-scale flash lamp pumping laser system consisting of a 3-W, 10-ns laser source.[13] By adopting the slit nozzle system, Ishikawa et al. improved a production rate of submicrometer spherical particle up to 195 mg h^{-1} using the same typical laser system.[14] High-power laser irradiation would also effectively increase the productivity of a method to synthesize

submicrometer spherical particles by PLML because the possible mass of particles melted by pulsed-laser irradiation is, in theory, proportional to the total energy input by the laser irradiation.

Compared with nanosecond laser irradiation, picosecond laser irradiation at a relatively low laser fluence is an energy-efficient method of synthesizing submicrometer spherical particles by PLML.[15, 16] In the case of picosecond laser irradiation, however, byproducts of nanoparticles (< 100 nm) are formed through the partial evaporation of particles, in addition to the formation of submicrometer spherical particles, even if the laser fluence is below the threshold for particle evaporation.[16] Submicrometer particles irradiated with a picosecond laser are inhomogeneously heated because of the complex electromagnetic interaction between the laser and the submicrometer particles.[16] If the thermal diffusion length in the particles during ultrafast laser heating is smaller than the size of the particles, as in the case of nonmetallic particles, the inhomogeneous heating effect will be evident from the formation of nanoparticles as a byproduct. Therefore, a method for controlling the particle heating process to suppress byproduct formation through partial evaporation is needed to enable the utilization of a high-power ultrafast laser system for synthesizing submicrometer spherical particles.

In this study, Fe_3O_4 particles (Hitachi Maxell, 220 nm) were dispersed in deionized water at a concentration of 0.1 g L^{-1}. Next, 6 mL of this colloidal suspension in a glass vessel was irradiated with a high-repetition-rate picosecond pulsed laser (Photonics Industries, RGH-532-20, wavelength 532 nm, pulse width 7 ps, repetition rate 0.1 MHz) for 30 min at a laser fluence of 100 mJ cm^{-2}. This laser can operate in either burst or single-pulse mode. In burst mode, the laser produces a series of pulse trains, each consisting of an adjustable number of burst pulses with a nanosecond-scale pulse interval.[17, 18] The laser fluence in either a burst pulse train or a single pulse is 100 mJ cm^{-2}, as shown in Fig. 5. 1. Therefore, the laser fluence per burst pulse decreases with increasing number of burst pulses. Utilizing this burst

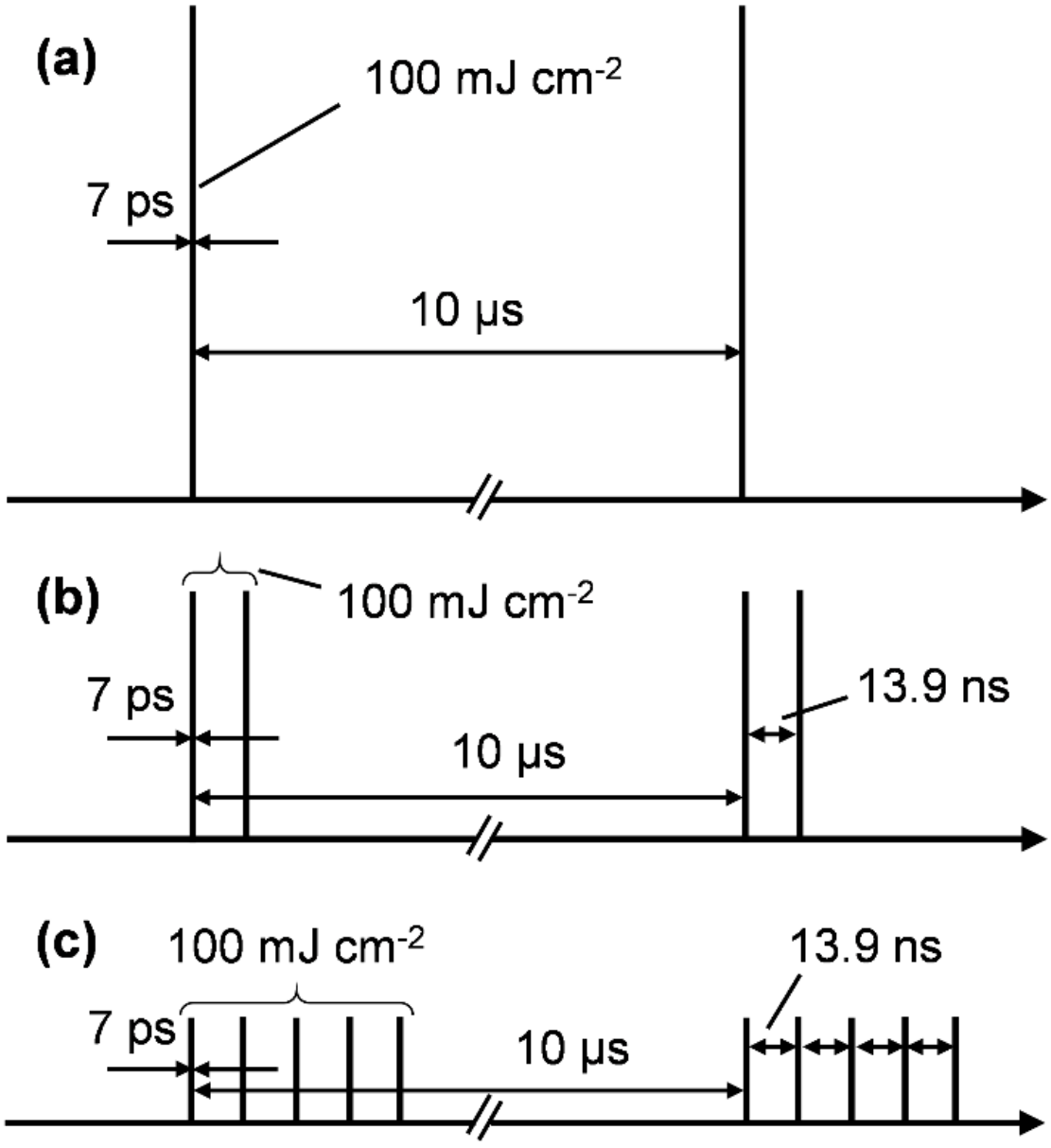

Figure 5. 1. Schematics of pulse temporal profiles with a pulse width of 7 ps and a repetition rate of 100 kHz: (a) single-pulse mode with a pulse interval time of 10 µs; (b) 2-burst mode; and (c) 5-burst mode, where the pulse interval time is 13.9 ns within a burst.

mode, we controlled the temperature increase of the Fe_3O_4 particles via burst pulse irradiation. The morphology of the particles was characterized by field-emission scanning electron microscopy (FE-SEM; JEOL JSM-6500F). The colloidal suspension was allowed to settle for 1 day to precipitate submicrometer spherical particles, and then the supernatant containing byproducts of nanoparticles were separated. The concentration of Fe_3O_4 particles in the suspension before and after separation was measured by inductively coupled plasma atomic emission spectrometry (Shimadzu ICPE-9000).

SEM images of the raw Fe_3O_4 particles and the particles obtained by pulsed-laser irradiation at a laser fluence of 100 mJ cm^{-2} are presented in Fig. 2. The raw particles have an average diameter of 220 nm and a cubic shape [Fig. 5. 2(a)]. After single-pulse-mode picosecond laser irradiation, byproducts of nanoparticles were formed in addition to the submicrometer spherical particles [Fig. 5. 2(b)], although only submicrometer spherical particles were formed at a laser fluence of 100 mJ cm^{-2} in the case of nanosecond laser irradiation.[19, 20] The particles irradiated with a picosecond laser are inhomogeneously heated by laser absorption, and the period of thermal diffusion in the particles is insufficient. Therefore, particles irradiated with a picosecond laser are partially evaporated, resulting in byproduct formation at a laser fluence lower than that of a nanosecond laser. In burst mode, Fe_3O_4 particles are irradiated with 2-burst pulse (average laser fluence per burst pulse 50 mJ $pulse^{-1}$ cm^{-2}), 5-burst pulse (20 mJ $pulse^{-1}$ cm^{-2}), 20-burst pulse (5 mJ $pulse^{-1}$ cm^{-2}) and 50-burst pulse (2 mJ $pulse^{-1}$ cm^{-2}). The formation of byproducts consisting of nanoparticles was reduced with increasing number of burst pulses [Fig. 5. 2(b–f)]. This result indicates that partial evaporation is suppressed by burst-pulse irradiation. In 50-burst mode, however, some of the particles have a similar shape to the raw particles [Fig. 5. 2(f)]. These particles did not melt and their shape remained unchanged because long heating duration of 50-burst pulse train (681.1 ns) caused much heat dissipation to the surrounding liquid.[11)] UV–vis extinction spectra of same

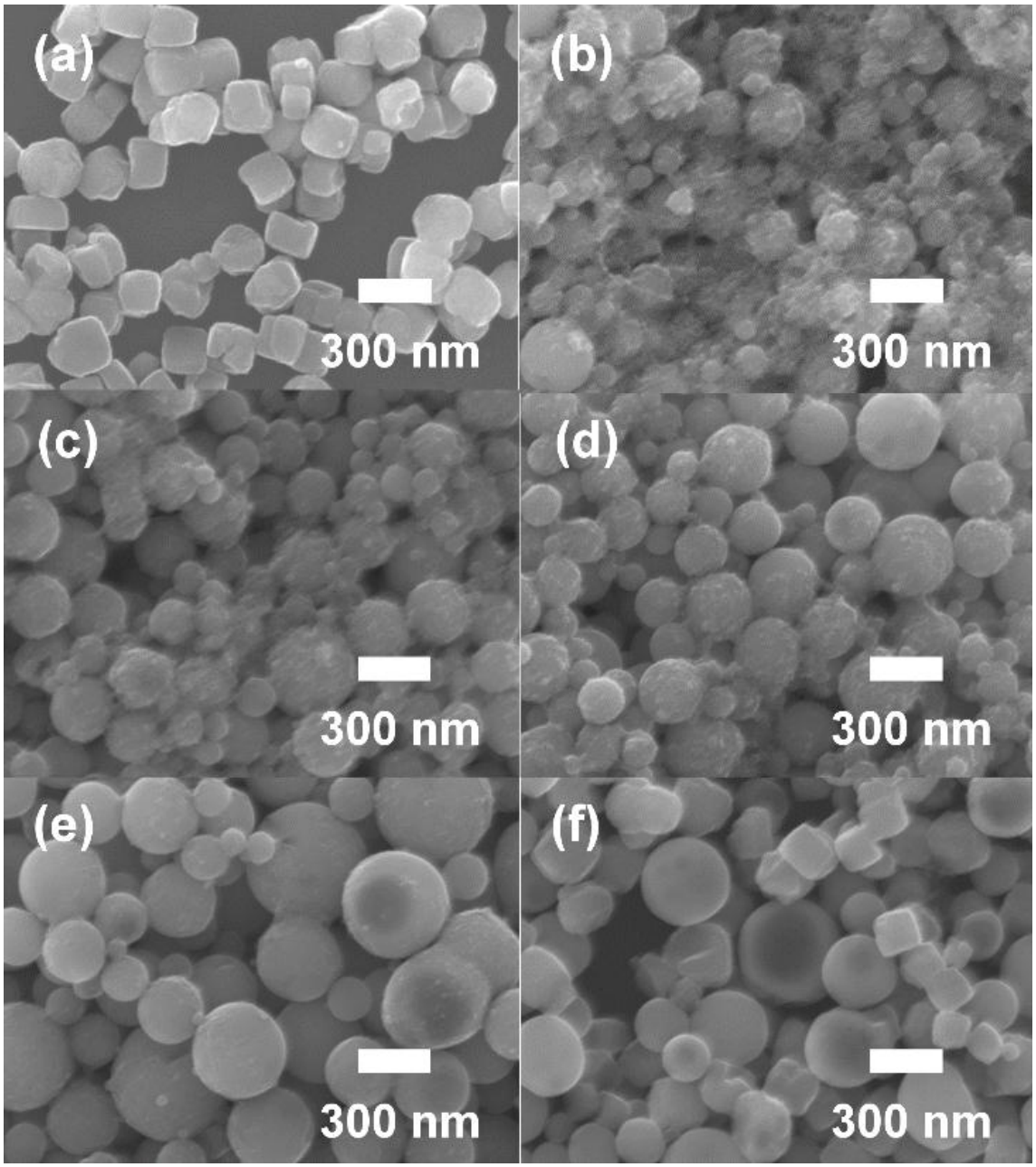

Figure 5. 2. SEM images of Fe_3O_4 particles. (a) Raw particles. Particles after laser irradiation at a laser fluence of 100 mJ cm^{-2}: (b) single-pulse mode, (c) 2-burst mode, (d) 5-burst mode, (e) 20-burst mode, and (f) 50-burst mode.

samples supports these results (see Fig. 5. S1 in supplementary data). In 5-burst and 20-burst pulse mode, particles irradiated with burst pulse train were melted, although average laser fluence per burst pulse was smaller than the value for particle melting (see Fig. 5. S2 in Supplementary data). This result suggests that heat energy of a particle is not completely dissipated during the pulse interval between two consecutive burst pulses and subsequently accumulates with consecutive burst pulses, resulting in particle melting.

Figure 5. 3 shows the collection rate of the submicrometer particles, which consist of raw particles and submicrometer spherical particles, relative to all the particles in the suspension irradiated with different numbers of pulses per pulse train. The collection rate was calculated by measuring the concentration of submicrometer particles after separation of the byproducts and concentration of all of the particles before the separation using inductively coupled plasma atomic emission spectrometry. The collection rate of the submicrometer particles increased with increasing number of pulses per pulse train, although some of the particles irradiated with 50-burst pulses were not melted and their shape remained unchanged. Thus, burst-pulse irradiation suppresses both the partial evaporation of the particles and the formation of byproduct nanoparticles.

When the thermal diffusion length during pulsed-laser heating is smaller than the particle size, the particles are partially heated around the space where the laser energy is inhomogeneously absorbed in the particle. Figure 5. 4 shows the spatial distribution of the resistive heat loss density from Fe_3O_4 spherical particles of 220 nm diameters due to electromagnetic wave irradiation by plane polarized light with a wavelength of 532 nm. The distributions were calculated using COMSOL Multiphysics®, a commercial software based on the finite element method from the refractive index and extinction coefficient. Fe_3O_4 submicrometer particles are imhomogeneously heated because the particles strongly absorb laser energy in the space where the laser energy converts to the resistive heat. The thermal diffusion length during pulsed-laser heating is given by the well-known diffusion equation.[16, 21)]

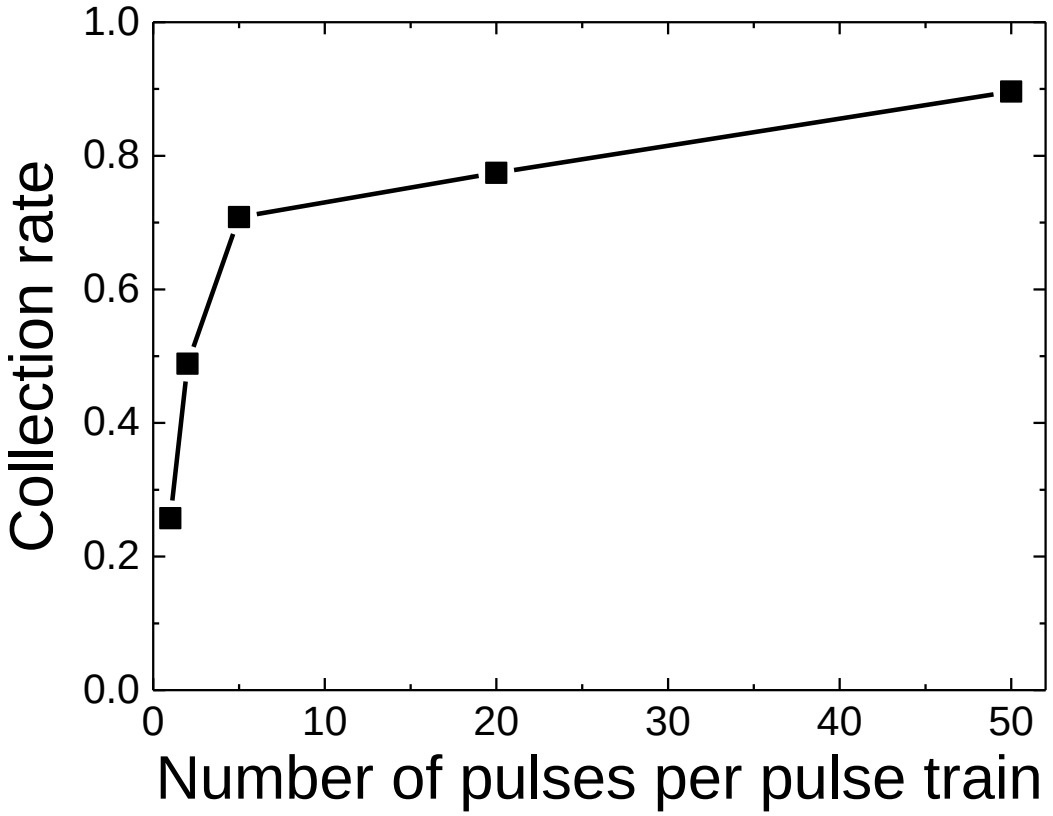

Figure 5. 3. Collection rate of the submicrometer particles relative to all of the particles in the suspension irradiated with different numbers of pulses per pulse train calculated by measuring the concentration of suspension using inductively coupled plasma atomic emission spectrometry.

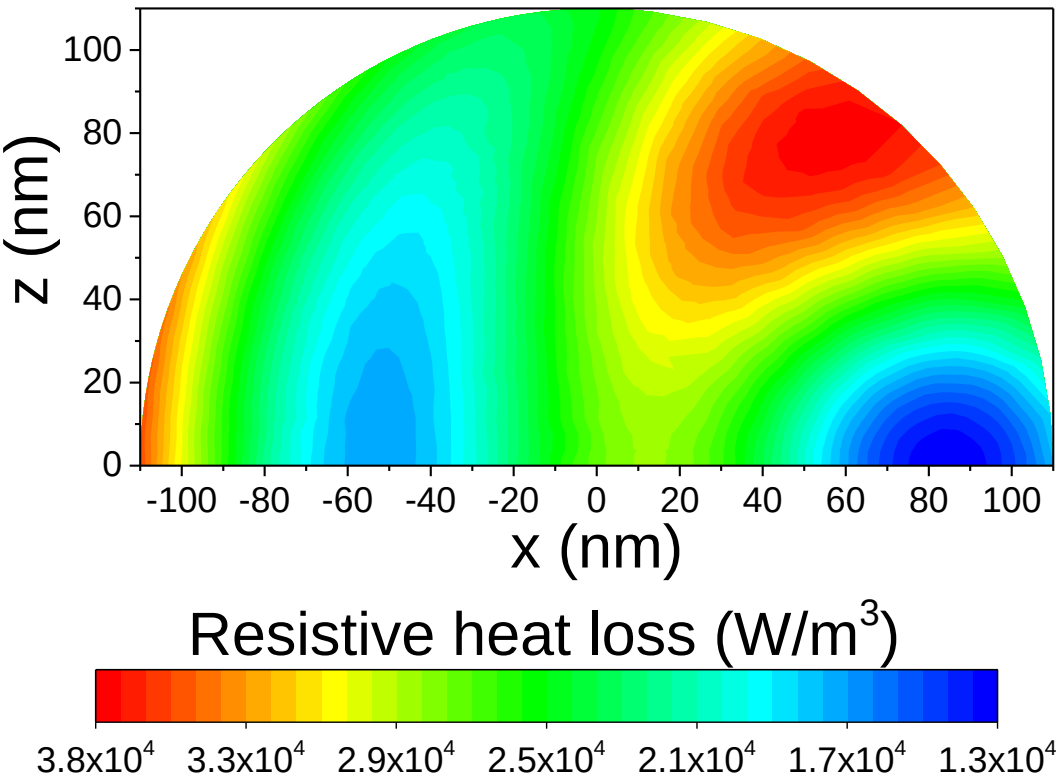

Figure 5. 4. Spatial distribution of density of the resistive heat loss from Fe_3O_4 spherical particles with diameters of 220nm when excited by plane-polarized light with a wavelength of 532 nm. Here, the light propagates in the positive X-direction, the electric field oscillates in the X–Z plane, and the magnetic field oscillates in the X–Y plane. Y-axis is perpendicular to the X–Z plane.

The thermal diffusion length during picosecond laser (7 ps) heating in this experiment, as calculated using the diffusion equation on the basis of the physical properties of Fe_3O_4,[22, 23] is 14.6 nm, which is smaller than the size of the raw Fe_3O_4 particles. Therefore, particles irradiated with the picosecond laser are partially heated and the heat distribution in the particles is inhomogeneous. During the interval between the burst pulses (13.9 ns), the heat distribution in the particles is homogenized because the thermal diffusion length during the pulse interval is 653 nm, which is larger than the particle size. This heat homogenization during the pulse interval suppresses byproduct formation through partial evaporation.

Particles are heated by pulsed-laser irradiation and cooled by the surrounding liquid. The change in particle temperature during the process of PLML was calculated using the particle heating–cooling model (see supplementary data).[11] In this model, all of the laser energy is assumed to be converted into particle heat and the temperature distribution in the particle is assumed to be homogeneous. In the initial heating stage, particles are rapidly cooled by liquid water with a high thermal conductivity. At the spinodal temperature (573 K), explosive evaporation of water has been reported to occur and heated particles begin to be cooled by vaporized liquid with low thermal conductivity.[24]

Figure 5. 5 shows the calculated temperature change of Fe_3O_4 particles in water irradiated with a single pulse and with burst pulses (20-burst and 50-burst) at a laser fluence of 100 mJ cm^{-2}. This calculation result suggests that we can control the heating process of particles via burst-pulse irradiation. The temperature of particles irradiated with a single pulse instantaneously reaches the melting point under irradiation with a picosecond pulse with a laser fluence of 100 mJ $pulse^{-1}$ cm^{-2}, although the heat distribution in the particles is inhomogeneous. In 20-burst pulse mode, particles are gradually heated by a series of 20 pulses with an average laser fluence of 5 mJ $pulse^{-1}$ cm^{-2} and a pulse interval of 13.9 ns; the particle temperature eventually reaches the melting point. In 50-burst pulse mode, particles

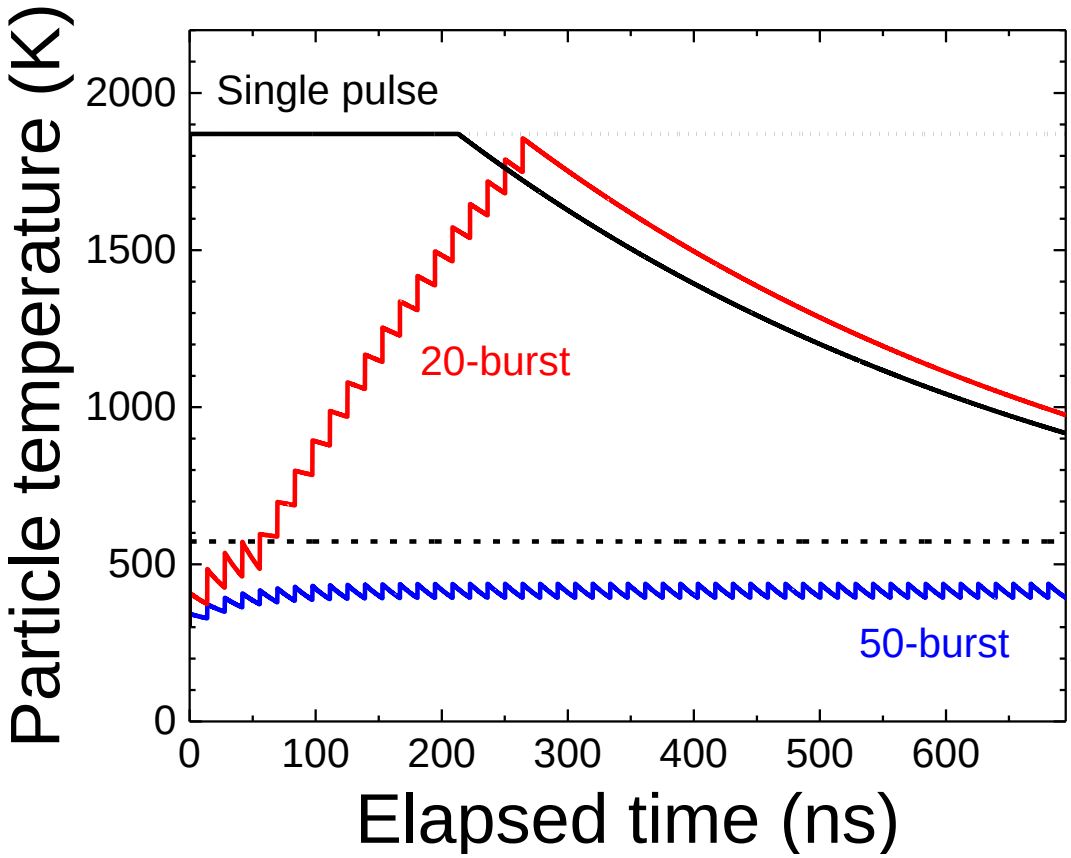

Figure 5. 5. Calculated temporal evolution of the temperature of particles irradiated with a pulsed laser using different numbers of pulses per pulse train. The dotted horizontal line represents the melting point of Fe_3O_4, the dashed horizontal line represents the spinodal temperature of water.

are not melted by irradiation with 50 burst pulses with an average laser fluence of 2 mJ pulse^{-1} cm^{-2}.

Minimum pulse interval to homogenize heat distribution in Fe_3O_4 particles irradiated with a picosecond laser is estimated as a few nanoseconds from the calculation of thermal diffusion length. However, heat dissipation from particles irradiated with burst-mode pulsed laser increases with the increase in the pulse interval of burst pulses.[11] Therefore, optimum value of the pulse interval is a few nanoseconds in this experiment. In PLML, time between two consecutive laser pulses for particle solidification and complete cooling (a microsecond time scale) is required to form spherical and crystalline submicrometer particles.[7, 25] Just utilizing high-repetition-rate laser such as 100 MHz is not suitable for synthesis of submicrometer spherical particles because cooling time of particle is insufficient. By utilizing burst-mode laser, the heat distribution within the particle is homogenized during pulse interval of burst pulses, and particles are completely cooled during time between two consecutive burst-pulse trains.

The particles dissipate thermal energy through the cooling effect of the surrounding liquid during several tens of nanoseconds of heating, and the heat loss from the particles during pulsed-laser heating increases with longer laser pulse durations.[11] The heating duration by irradiation with burst pulses increases with increasing number of pulses. Therefore, the heat loss from the particles also increases with increasing number of burst pulses. Particles irradiated with 20-burst pulses are gradually cooled by surrounding vapor at temperatures above the spinodal temperature during a pulse interval, resulting in the formation of submicrometer spherical particles. In 50-burst pulse mode, burst pulse irradiation with a laser fluence of 2 mJ pulse^{-1} cm^{-2} is insufficient to form the vapor layer surrounding the particles. Therefore, particles are rapidly cooled by surrounding liquid water with high thermal conductivity at temperatures below the spinodal temperature and maintain the shape and size of the raw Fe_3O_4 particles. Some of the particles in the suspension are melted and submicrometer spherical particles are formed by

50-burst pulsed irradiation [Fig. 5. 2(f)]. This result is caused by the influence of the high repetition rate of 0.1 MHz. The local temperature of the liquid surrounding the particles is increased by heat dissipation from the particles absorbing consecutive laser pulses.[25)] Therefore, the liquid adjacent to the particles absorbing consecutive laser pulses can easily evaporate, resulting in a reduction of the heat dissipation by the cooling effect.

In summary, byproduct formation through the partial evaporation of particles irradiated with an ultrafast laser was suppressed by control of the heating process utilizing a burst-mode laser. The formation of nanoparticles as byproducts decreased with increasing number of burst pulses because the laser fluence per burst pulse was decreased and heat distribution in the particles was homogenized during the pulse interval between burst pulses. However, as the heating duration of the burst pulse train was increased, the thermal energy of particles was dissipated by the cooling effect of the surrounding liquid during the interval between burst pulses. When the heating rate of particles irradiated with burst pulses did not sufficiently exceed the cooling rate of particles, vapor layers surrounding the particles did not form and particles were not melted.

References

[1] D. Zhang, B. Gökce, and S. Barcikowski, Chem. Rev. **117**, 3990 (2017).

[2] S. Ibrahimkutty, P. Wagener, T. D. S. Rolo, D. Karpov, A. Menzel, T. Baumbach, S. Barcikowski, and A. Plech, Sci. Rep. **5**, 16313 (2015).

[3] C. Y. Shih, C. Wu, M. V. Shugaev, and L. V. Zhigilei, J. Colloid Interface Sci. 489, 3 (2017).

[4] K. Sasaki, T. Nakano, W. Soliman, and N. Takada, Appl. Phys. Exp. **2**, 0465011 (2009).

[5] F. Mafuné, J. Kohno, Y. Takeda, T. Kondow, and H. Sawabe, J. Phys. Chem. B **104**, 9111 (2000).

[6] H. Wang, A. Pyatenko, K. Kawaguchi, X. Li, Z. Swiatkowska-Warkocka, and N. Koshizaki, Angew. Chem. Int. Ed. **49**, 6361 (2010).

[7] A. Pyatenko, H. Wang, N. Koshizaki, and T. Tsuji, Laser Photonics Rev. **7**, 596 (2013).

[8] A. Pyatenko, H. Wang, and N. Koshizaki, J. Phys. Chem. C **118**, 4495 (2014).

[9] T. Tsuji, Y. Higashi, M. Tsuji, Y. Ishikawa, and N. Koshizaki, Appl. Surf. Sci. **348**, 10 (2015).

[10] Z. Swiatkowska-Warkocka, A. Pyatenko, F. Krok, B. R. Jany, and M. Marszalek, Sci. Rep. **5**, 9849 (2015).

[11] S. Sakaki, H. Ikenoue, T. Tsuji, Y. Ishikawa, and N. Koshizaki, ChemPhysChem **18**, 1101 (2017).

[12] R. Streubel, S. Barcikowski, and B. Gökce, Opt. Lett. **41**, 1486 (2016).

[13] H. Wang, N. Koshizaki, L. Li, L. Jia, K. Kawaguchi, X. Li, A. Pyatenko, Z. Swiatkowska-Warkocka, Y. Bando, and D. Golberg, Adv. Mater. **23**, 1865 (2011).

[14] Y. Ishikawa, and N. Koshizaki, Sci. Rep. **8**, 14208 (2018).

[15] D. Zhang, M. Lau, S. Lu, S. Barcikowski, and B. Gökce, Sci. Rep. **7**, 1 (2017).

[16] S. Sakaki, K. Saitow, M. Sakamoto, H. Wada, Z. Swiatkowska-

warkocka, Y. Ishikawa, and N. Koshizaki, Appl. Phys. Exp. **11**, 035001 (2018).

[17] W. Hu, Y. C. Shin, and G. King, Appl. Phys. A Mater. Sci. Process. **98**, 407 (2010).

[18] S. Karimelahi, L. Abolghasemi, and P. R. Herman, Appl. Phys. A Mater. Sci. Process. **114**, 91 (2014).

[19] Z. Swiatkowska-Warkocka, K. Kawaguchi, H. Wang, Y. Katou, and N. Koshizaki, Nanoscale Res. Lett. **6**, 226 (2011).

[20] Y. Ishikawa, N. Koshizaki, and A. Pyatenko, Electron. Commun. Japan **99**, 37 (2016).

[21] A. G. Every, Z. N. Utegulov, and I. A. Veres, J. Appl. Phys. **114**, 203508 (2013).

[22] Thermodynamic database MALT for windows, H. Yokoyama, S. Yamauchi, and T. Matsumoto, Calphad **26**, 155 (2002).

[23] L. S. Sundar, E. Venkata Ramana, M. P. F. Graça, M. K. Singh, and A. C. M. Sousa, Int. Commun. Heat Mass Transf. **73**, 62 (2016).

[24] A. Siems, S. A. L. Weber, J. Boneberg, and A. Plech, New J. Phys. **13**, 043018 (2011).

[25] S. Sakaki, H. Ikenoue, T. Tsuji, Y. Ishikawa, and N. Koshizaki, Appl. Surf. Sci. **435**, 529 (2018).

Supplementary data

Section 1. UV–vis extinction spectra of samples.

UV–vis extinction spectra of suspensions irradiated with different numbers of burst pulses are shown in Fig. 5. S1. The suspension irradiated with a single pulse showed an increase in extinction in the UV region (<400 nm), which has been reported to be caused by nanoparticle formation [1]. With increasing number of burst pulses, the extinction in the UV region decreased. This result also shows that nanoparticle formation caused by partial evaporation of particles would be suppressed by burst pulses irradiation. The extinction spectrum of the suspension irradiated with 50-burst pulses was almost identical to that of the raw suspension. Therefore, most of the particles in the suspension maintained their shape and size.

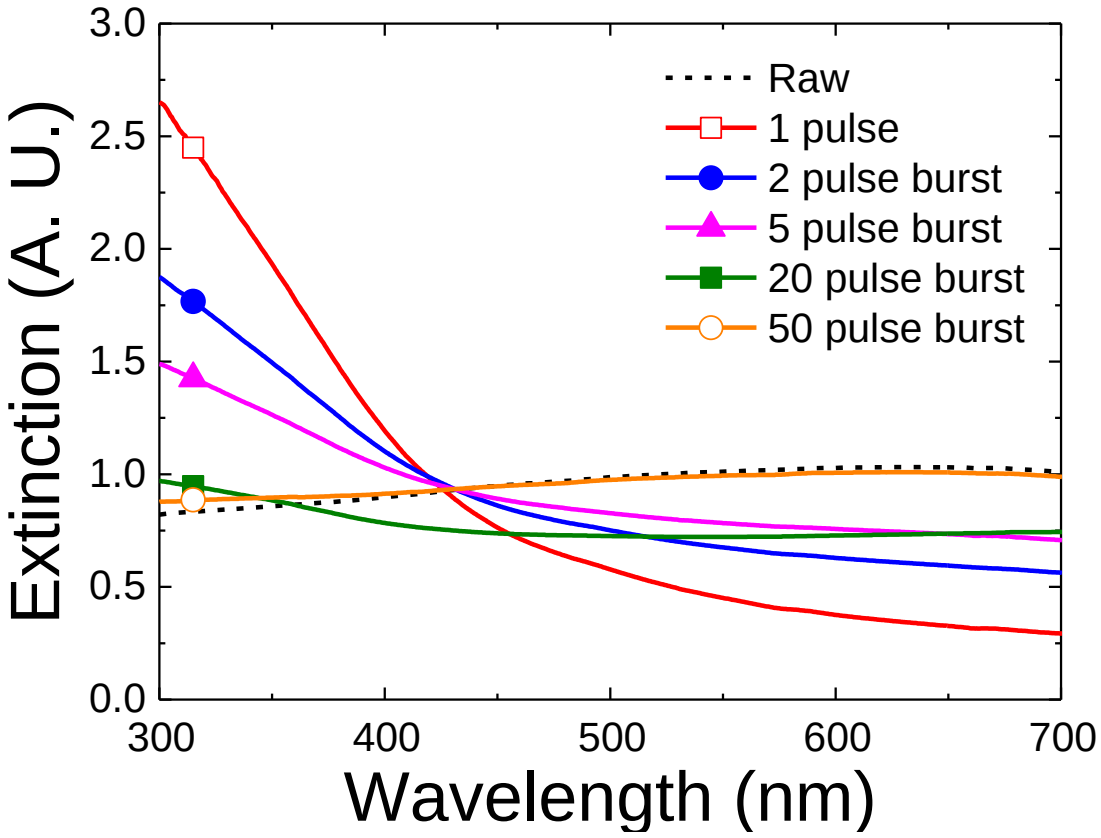

Figure 5. S1. UV–vis extinction spectra of samples obtained by laser irradiation with different numbers of pulses per pulse train.

Section 2. SEM images of samples irradiated with a single pulse mode.

SEM images of suspensions irradiated with a single pulse at a laser fluence of 33 and 50 mJ cm^{-2} are shown in Fig. 5. S2. The particles irradiated with a single pulse at a laser fluence of 33 mJ cm^{-2} are not melted and maintain their shape [Fig. 5. S2(a)]. When the laser fluence is 50 mJ cm^{-2}, submicrometer spherical particles are obtained [Fig. 5. S2(b)]. Therefore, laser fluence threshold for submicrometer spherical particles formation is 50 mJ cm^{-2}.

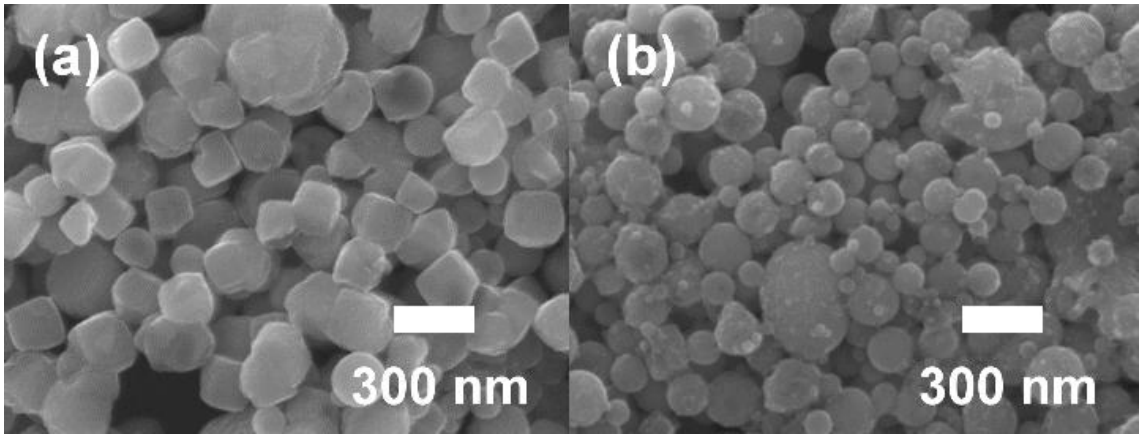

Figure 5. S2. SEM images of samples irradiated with a single pulse mode at a laser fluence of (a) 33 and (b) 50 mJ cm^{-2}.

Section 3. Particle temperature calculated using particle heating-cooling model.

Particles absorb laser energy depending on the input energy of pulsed laser. In this model, all laser energy absorbed by the particle is converted to particle heat energy.

$$\frac{dE_{abs}}{dt} = Q_{abs}^{\lambda} \cdot \frac{\pi d^2}{4} \cdot J(t)$$

Here, Q_{abs}^{λ} is the absorption efficiency based on Mie theory, $\frac{\pi d^2}{4}$ is the particle geometrical cross section, and $J(t)$ is the time-dependent laser fluence. The integral of time-dependent laser fluence corresponds to the laser fluence.

Particles dissipate the heat energy to the surrounding liquid. In this model, conductive heat transfer is defined because convection around submicrometer-scale particle is negligible.[2)]

$$\frac{dq}{dt} = h \cdot \pi d^2 \cdot \{T(t) - T_0\}$$

where $h = \frac{Nu_d \cdot k_w}{d}$

Here, h is the heat transfer coefficient, πd^2 is the particle surface area, $T(t)$ is the particle temperature, and T_0 is the temperature of the surrounding liquid. The heat transfer coefficient is proportional to the heat conductivity of the surrounding liquid, k_w, Nusselt number, Nu_d, and inversely proportional to the particle diameter, d.

In the initial heating stage, particles contact directly with the liquid and are cooled. At the spinodal temperature of 573 K, explosive evaporation of the water is reported to occur,[3–5)] and heated particles start to be cooled by vaporized liquid over 573 K with the following heat transfer coefficient value.

$$h = \frac{Nu_d \cdot k_v}{d}$$

Here, k_v is the heat conductivity of the surrounding evaporating vapor. The heat conductivity of vapor is much lower than that of liquid, and therefore, the cooling rate by vapor is much slower than by liquid. Cooling process is drastically switched by evaporation of surrounding liquid.
The Nusselt number is the ratio of convective heat transfer to conductive heat transfer. In the case of natural convection on a sphere, the Nusselt number is given as below.[6)]

$$\overline{Nu_d} = 2 + \frac{0.589 Ra_d^{1/4}}{[1 + (0.469/Pr)^{9/16}]^{4/9}}$$

Here, Ra_d is the Rayleigh number and Pr is the Prandtl number. In submicrometer scale heating, heat transfer is governed by heat conduction but not by fluid convection. In this case, the Nusselt number is constant, $Nu_d \approx 2$, because the Rayleigh number is negligibly small on the submicrometer scale.[2)]

The accumulated heat energy in a particle is the difference between the laser energy absorbed by a particle and the energy dissipated by conductive heat transfer.

$$\frac{dE}{dt} = \frac{dE_{abs}}{dt} - \frac{dq}{dt}$$

If the laser energy is not enough to melt the agglomerate of raw particles, only particle heating in the solid state is expected.

$$T(t) = T_0 + \frac{1}{\rho_p \cdot \frac{\pi d^3}{6} \cdot c_s} \cdot E(t)$$

Here, ρ_p is the density of the particle, $\frac{\pi d^3}{6}$ is the particle volume, and c_s is the particle specific heat in the solid state.

If the agglomerate absorbs more energy, particle melting occurs.

$$T(t) = T_m$$

Here, T_m is the melting point of the material. During particle melting, the particle temperature stays at the melting point.

With more absorbed energy, the particle completely melts and the temperature of the droplet increases further.

$$T(t) = T_{\mathrm{m}} + \frac{1}{\rho_p \cdot \frac{\pi d^3}{6} \cdot c_l} \cdot \left[E(t) - \rho_p \cdot \frac{\pi d^3}{6} \cdot \left(H_{T_m} - H_{T_0} + \Delta H_m\right)\right]$$

Here, $H_{T_m} - H_{T_0}$ is the relative enthalpy required for start of melting, ΔH_m is the latent enthalpy of melting, and c_l is the particle specific heat in the liquid state.

References

[1] J. M. J. Santillán, D. M. Arboleda, D. F. Coral, M. B. F. van Raap, D. Muraca, D. C. Schinca, and L. B. Scaffardi, ChemPhysChem **18**, 1192 (2017).

[2] J. S. Donner, G. Baffou, D. McCloskey, and R. Quidant, ACS Nano **5**, 5457 (2011).

[3] F. Caupin, and E. Herbert, C. R. Phys. **7**, 1000 (2006).

[4] [V. Kotaidis, C. Dahmen, G. von Plessen, F. Springer, and A. Plech, J. Chem. Phys. **124**, 184702 (2006).

[5] A. Siems, S. A. L. Weber, J. Boneberg, and A. Plech, New J. Phys. **13**, 043018 (2011).

[6] A. F. Mills, Heat Transfer, 2nd ed., Prentice Hall, New York, pp. 275–282 (1998).

Chapter 6

General Conclusion

In this dissertation, the author studied the thermal behavior of submicrometer spherical particle formation by PLML in order to understand the formation mechanism. The conclusions of the present work are summarized as follows.

In Chapters 2 and 3, the heat dissipation to the surrounding liquid from the particles in picosecond to nanosecond pulse heating is studied. Figure 6. 1 shows the pulse width dependence of the heating efficiency of PLML as estimated using the particle heating–cooling model. The heating efficiency of PLML is the ratio of the maximum heat energy within a particle considering cooling to all energy absorbed by a particle ignoring cooling (no heat loss). If the particle dissipates no heat to the surrounding liquid, all energy absorbed by the particle converts to heat energy within the particle. Heat dissipation from the particles to the surrounding liquid increases with increasing pulse width. In picosecond pulse heating, almost all of the laser energy is spent on particle heating. However, when the pulse width exceeded tens of nanoseconds, the particles drastically dissipated heat through the cooling effect of the surrounding liquid.

Another important factor for heat dissipation to the surrounding liquid is the particle size. Figure 6. 1 clearly indicates that the heating efficiency drastically decreases when the particle size becomes smaller than a threshold value, even for the same laser pulse width. This is attributable to the inverse correlation between the cooling rate of the particles and the particle's diameter. This effect culminates in the extreme difference in the attained temperature of particles with different sizes by pulsed laser heating.

Figure 6. 2 shows the temperature time profile based on the particle heating–cooling model, as calculated for the laser heating (pulse width: 7 ns) of Au nanoparticles of different sizes, 10 and 60 nm.[1)] The temperature of the Au particle with 60 nm diameter reaches the boiling point via laser heating, whereas the 10 nm particle is just slightly heated. This calculation

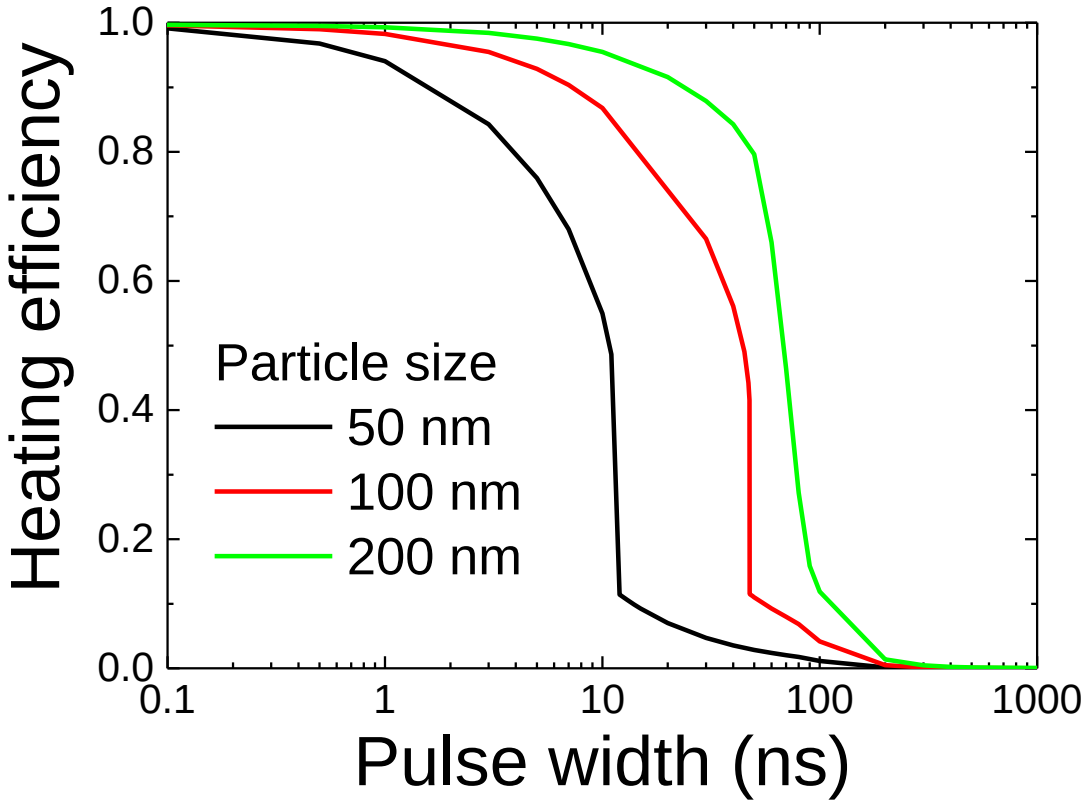

Figure 6. 1. Pulse width dependence of the heating efficiency of ZnO spherical particles irradiated with a pulsed laser at the laser fluence of 50 mJ pulse^{-1} cm^{-2}, as estimated from the particle heating–cooling model.

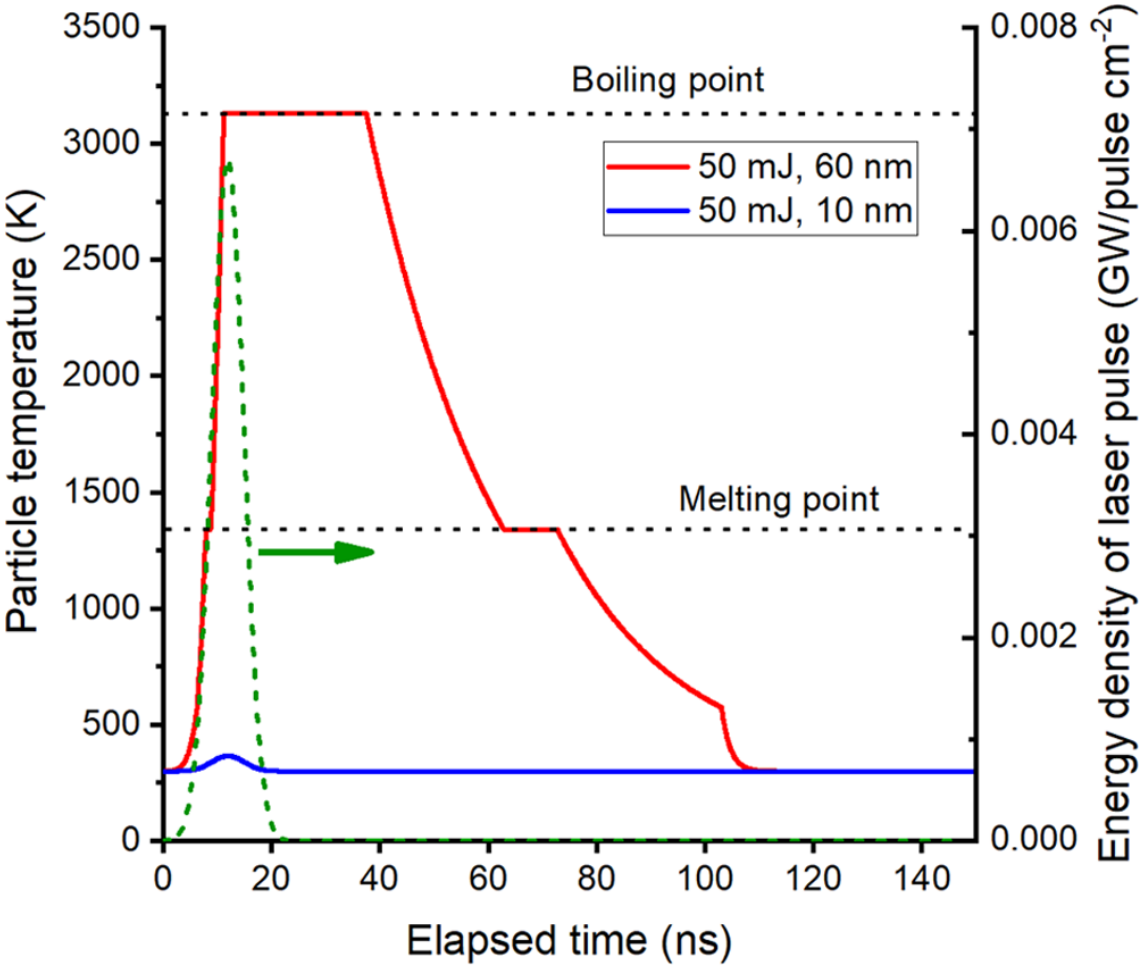

Figure 6. 2. Temporal temperature changes of an Au nanoparticle during the irradiation of a nanosecond laser pulse at 532 nm and 50 mJ cm^{-2}, as calculated for 10 and 60 nm Au nanoparticles. The dotted line shows the temporal profile of the nanosecond laser pulse used in the calculation. *Reprinted with permission from Ref 1. Copyright 2018 American Chemical Society.*

explains the experimental results after stabilizer removal and the agglomeration of the Au particles of different sizes. When Au particles stabilized by high concentration sodium citrate (approximately 60 nm diameter) are irradiated with a pulsed laser, Au nanoparticles (approximately 10 nm diameter) smaller than the original Au particles form via evaporation, and submicrometer spherical particles are created simultaneously by the melting and fusion process. The maximum temperature of the nanoparticles (10 nm) is less than the decomposition temperature of sodium citrate; the Au nanoparticles (10 nm) coated with the stabilizer are not largely modified at this laser fluence condition and are likely to remain within a high stabilizer concentration.

The calculation based on the particle heating–cooling model can explain not only the submicrometer spherical particle formation process, but also the nanoparticle formation process by evaporation and stabilizer removal process. Furthermore, an appropriate pulse width should be adopted depending on the particle's diameter to efficiently synthesize submicrometer spherical particles by PLML.

In Chapters 2 and 3, the thermal diffusion within the particle during pulsed heating on the picosecond to nanosecond timescale is also studied. Figure 6. 3 shows the thermal diffusion length during pulsed laser heating as calculated by diffusion equation. The thermal diffusion length increases with increasing pulse width. If the thermal diffusion length is smaller than the particle size, the particle will be inhomogeneously heated around the space where the laser energy is selectively charged because of the electromagnetic interaction between the laser light and the particle. Inhomogeneous heating causes partial evaporation around the space of the laser absorption, resulting in nanoparticle formation. Therefore, time is required for thermal diffusion within the particles to heat the particle homogeneously. For materials with high heat conductivity, such as metals and semiconductors, the time for homogeneous heating is on the picosecond timescale. In comparison, materials with low heat conductivity, such as oxides and nitrides, require nanoseconds to achieve homogeneous heating. Therefore, an appropriate pulse width that depends on the particle's diameter and the material should be adopted, such that the submicrometer spherical particles are heated homogeneously. The size of the obtained submicrometer spherical particles decreases with decreasing thermal diffusion length, which depends on the

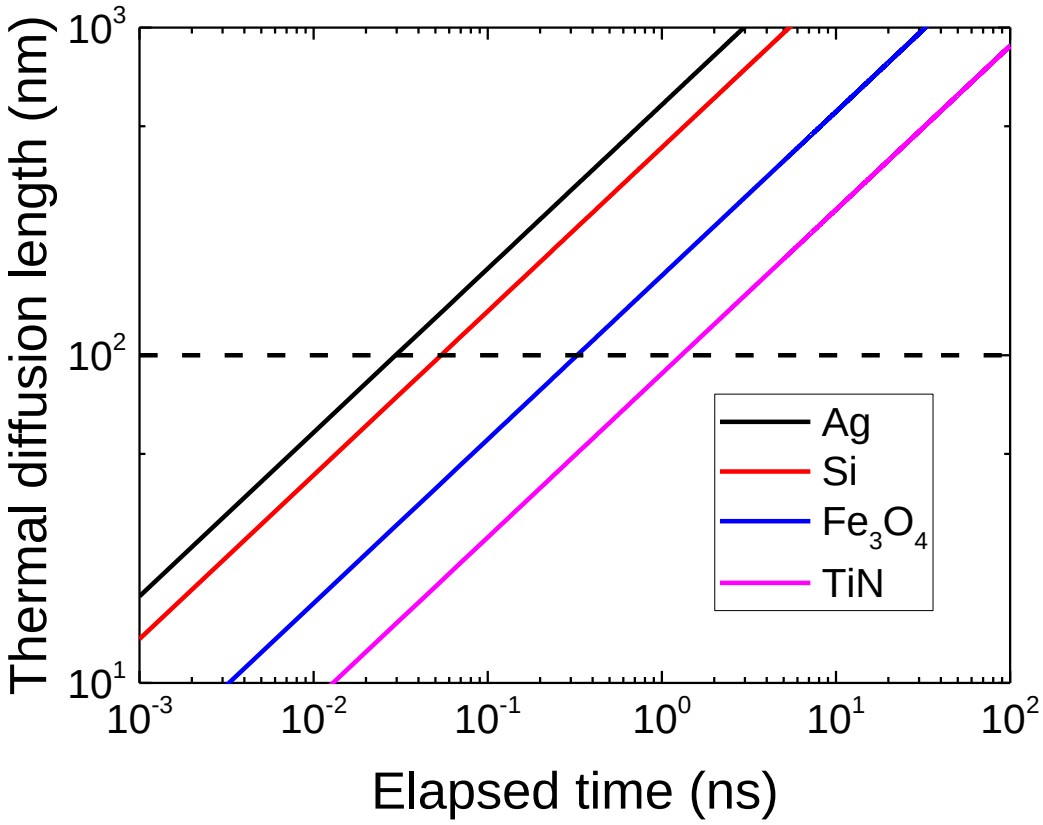

Figure 6. 3. Pulse width dependence of the thermal diffusion length for different materials estimated from the calculation using diffusion equation.

pulse width. Pulse width control could become a new approach for controlling the size of submicrometer spherical particles.

In Chapter 4, the influence of pulse frequency and liquid temperature on the synthesis of submicrometer spherical particles is studied. The total laser irradiation time for the synthesis can be reduced using a high-frequency pulsed laser. However, nanoparticles and submicrometer spherical particles form simultaneously at pulse frequencies above the threshold. The time required to cool down the particles from the melting point to ambient temperature is much shorter than the pulse interval between the consecutive laser pulses. Therefore, nanoparticle formation can be attributed to an increase in the suspension temperature. The suspension temperature is elevated during laser irradiation by the heat diffusion from the particles absorbing the laser energy. The liquid temperature adjacent to the particles is higher than the total suspension temperature because of the temperature gradient from the heat-source particle heated by pulsed laser irradiation. Calculations suggest that the highest attained temperature of the particles increases by a few hundred kelvins through heat accumulation in the adjacent liquid because of the initial particle temperature increase and reduction in heat dissipation. The liquid temperature influences the heat transfer from the particles to the liquid.

In Chapter 5, a burst-mode laser is utilized to control the formation process of submicrometer spherical particles. Although ultrafast laser systems are commercially available as high-power laser sources, ultrafast laser irradiation to the particles dispersed in a liquid causes byproduct (nanoparticles) formation derived from the insufficiency of the thermal diffusion length within the particle. In the burst mode, the laser produces a series of pulse trains, each consisting of an adjustable number of burst pulses with a nanosecond-scale pulse interval. The formation of nanoparticles as a byproduct is suppressed by burst-pulse irradiation because the heat distribution in the particles is homogenized during the interval between burst pulses. However, the heating duration of burst-pulse train irradiation increases with the number of burst pulses, thus resulting in large heat dissipation from the particles to the surrounding liquid. Controlling the heating process by adjusting the number of burst pulses leads to the homogeneous and efficient heating of submicrometer spherical particles when utilizing an ultrafast high-power laser source.

In this study, the thermal characteristics of submicrometer spherical particle formation by PLML were presented (Figure 6. 4). The time-resolved particle temperature for particles irradiated with a pulsed laser was estimated on the basis of the new model developed by the author. This result enables the control of the nanosecond-scale particle heating and cooling process of PLML depending on the material's characteristics, such as the size and composition of the particle. However, no method for directly observing the submicrometer spherical particle formation process by PLML has yet been established. Observing the temporal lattice expansion of particles fabricated by PLML using time-resolved X-ray diffraction is a promising approach for measuring time-resolved particle temperature profiles of particles irradiated with a pulsed laser in a liquid.[2, 3)] In addition, monitoring the time-resolved absorbance of a suspension irradiated with a pulsed laser suggests a particle heating and cooling process since nanobubbles are generated around the particles by the thermal diffusion from the heated particles.[4, 5)] In order to measure the time-resolved X-ray diffraction and absorbance, the timescale of the particle heating and cooling process should be estimated. Calculating the particle temperature using the new model on the formation process of submicrometer spherical particles by PLML allows appropriate conditions for the time-resolved study to be set.

The formation process of submicrometer spherical particles by PLML, which represents the fastest temperature change in material processing, is in a thermal nonequilibrium. Owing to the fast formation process, thermal nonequilibrium materials such as the AuCo alloy, which is immiscible under equilibrium, are synthesized.[6)] Controlling the formation process of submicrometer spherical particles under a nonequilibrium condition leads to the synthesis of new functional materials.

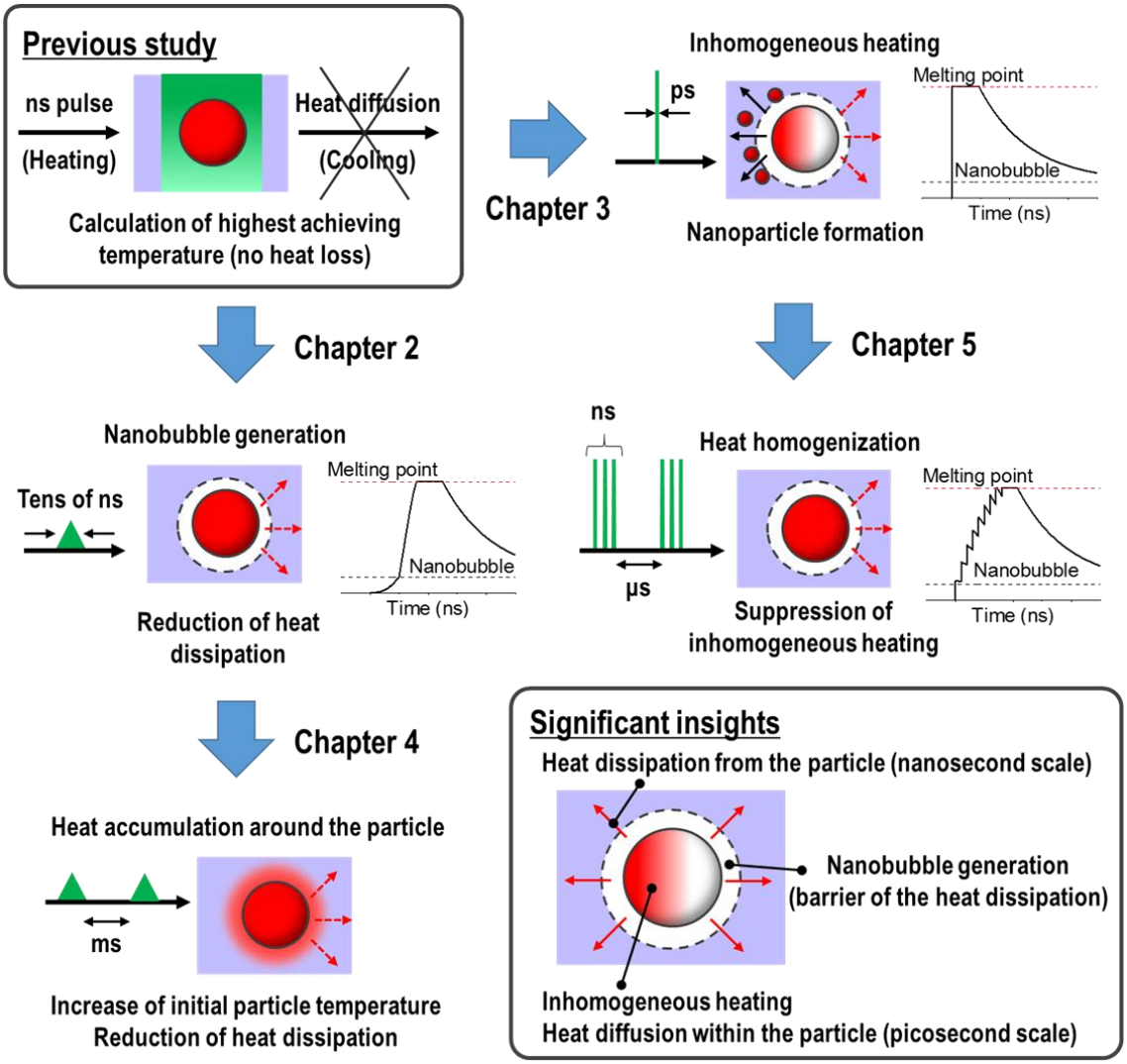

Figure 6. 4. Schematic overview of the content per chapter.

References

[1] T. Tsuji, S. Sakaki, H. Fujiwara, H. Kikuchi, M. Tsuji, Y. Ishikawa, and N. Koshizaki, J. Phys. Chem. C **122**, 21659 (2018).

[2] K. Ichiyanagi, H. Sekiguchi, T. Sato, S. Nozawa, A. Tomita, M. Hoshino, S. Adachi, and Y. C. Sasaki, J. Synchrotron Rad. **22**, 29 (2015).

[3] A. Plech, V. Kotaidis, M. Lorenc, M. Wulff, Chem. Phy. Let. **401**, 565 (2005).

[4] E. Lukianova-Hleb, Y. Hu, L. Latterini, L. Tarpani, S. Lee, R. A. Drezek, J. H. Hafner, and D. O. Lapotko, ACS Nano **4**, 2109 (2010).

[5] E. Y. Lukianova-Hleb, A. N. Volkov, and D. O. Lapotko, Langmuir **30**, 7425 (2014).

[6] Z. Swiatkowska-Warkocka, K. Koga, K. Kawaguchi, H. Wang, A. Pyatenko, and N. Koshizaki, RSC Adv. **3**, 79 (2013).

List of Publications

Chapter 2
Shota Sakaki, Hiroshi Ikenoue, Takeshi Tsuji, Yoshie Ishikawa, and Naoto Koshizaki,
Pulse-width dependence of cooling effect on submicrometer ZnO spherical particle formation by pulsed laser melting in liquid,
ChemPhysChem **18**, 1101-1107 (2017).

Chapter 3
Shota Sakaki, Ken-ichi Saitow, Masanori Sakamoto, Hiroyuki Wada, Zaneta Swiatkowska-Warkocka, Yoshie Ishikawa, and Naoto Koshizaki,
Comparison of picosecond and nanosecond lasers for the synthesis of TiN sub-micrometer spherical particles by pulsed laser melting in liquid,
Applied Physics Express **11**, 035001 (2018).

Chapter 4
Shota Sakaki, Hiroshi Ikenoue, Takeshi Tsuji, Yoshie Ishikawa, and Naoto Koshizaki,
Influence of pulse frequency on synthesis of nano and submicrometer spherical particles by pulsed laser melting in liquid,
Applied Surface Science **435**, 529–534 (2018).

Chapter 5
Shota Sakaki, Yoshie Ishikawa, and Naoto Koshizaki,
Heating process control of pulsed-laser melting in liquid via a burst-mode laser,
Applied Physics Express **12**, 015002 (2019).

The following publication is not included in this thesis

Takeshi Tsuji, Shota Sakaki, Hideki Fujiwara, Hirotsugu Kikuchi, Masaharu Tsuji, Yoshie Ishikawa, and Naoto Koshizaki,
Stabilizer-Concentration Effects on the Size of Gold Submicrometer-Sized Spherical Particles Prepared Using Laser-Induced Agglomeration and Melting of Colloidal Nanoparticles,
The Journal of Physical Chemistry C **122**, 21659−21666 (2018)

Acknowledgements

This thesis is based on the study carried out under the direction and supervision of Professor Naoto Koshizaki, Division of Quantum Science and Engineering, Faculty of Engineering in Hokkaido University. The author would like to express his deepest gratitude to Professor Naoto Koshizaki's generous guidance and invaluable suggestions.

The author is also grateful to Professor Koichi Sasaki, Professor Masato Ohnuma, and Professor Satoshi Tomioka, Division of Quantum Science and Engineering, Faculty of Engineering in Hokkaido University, who provided invaluable advices on the doctoral dissertation as sub-chief examiners.

Special thanks are due to Dr. Yoshie Ishikawa from Nanomaterials Research Institute, Department of Materials and Chemistry in National Institute of Advanced Industrial Science and Technology (AIST), Professor Hiroshi Ikenoue from Department of Gigaphoton Next GLP, Graduate School of Information Science and Electrical Engineering in Kyushu University, and Professor Ken-ichi Saitow from Department of Chemistry, Graduate School of Science in Hiroshima University for their kind help with the experiments in this paper.

The author would like to express his appreciation to Associate Professor Takeshi Tsuji from Department of Chemistry, Interdisciplinary Graduate School of Science and Engineering in Shimane University, Associate Professor Takahiro Nakamura from Polymer Hybrid Materials Research Center, Institute of Multidisciplinary Research for Advanced Materials in Tohoku University, and Dr. Zaneta Swiatkowska-Warkocka from Department of Materials Science, Institute of Nuclear Physics, Polish Academy of Sciences for the invaluable discussion and helpful advice.

The author appreciates the great help and warm encouragement of all the members of Professor Koshizaki's laboratory. The author thanks the Ministry of Education, Culture, Sports, Science, and Technology through the Program for Leading Graduate Schools. Finally, the author wishes to thank his family for their continuous encouragement.